長岡技術科学大学
Nagaoka University of Technology

DEVELOPMENT OF RIGID PLASTIC CONSTITUTIVE EQUATION USING NON-LINEAR SHEAR STRENGTH PROPERTY ON SANDY SOIL TO ESTIMATE ULTIMATE BEARING CAPACITY OF FOOTING

(砂質地盤の非線形剛塑性構成式の開発と基礎の極限支持力解析への応用)

環 境 防 災 研 究 室

Environmental and Disaster Prevention Laboratory

NGUYEN LE DU

平成 28 年 03 月

March 2016

長岡技術科学大学
Nagaoka University of Technology

Development of Rigid Plastic constitutive equation using non-linear shear strength property of sandy soil to estimate ultimate bearing capacity of footing

(砂質地盤の非線形剛塑性構成式の開発と基礎の極限支持力解析への応用)

- by -

Nguyen Le Du

Bachelor degree in Civil Engineering, Ho Chi Minh University of Technology, 2009
Master degree in Geotechnical Engineering, Ho Chi Minh University of Technology, 2011

A dissertation submitted in partial fulfillment of the requirements for the degree of
Doctor of Engineering

in
Energy and Environment Science

Examination committees:
Professor Dr. Eng. Ohtsuka Satoru (Chairman)
Professor Dr. Eng. Sugimoto Mitsutaka
Professor Dr. Eng. Iwasaki Eiji
Assoc. Professor Dr. Eng. Kobayashi Shunichi
Assoc. Professor Dr. Eng. Toyota Hirofumi

Department of Civil and Environmental Engineering
Nagaoka University of Technology
Niigata, Japan

平成 28 年 03 月

March 2016

ABSTRACT

Currently, there are many formulas used to calculate the ultimate bearing capacity such as Terzaghi (1943) and others (e.g. Meyerhof, 1951, 1963). However, the formula has disadvantages in application to practice since it is only applied in calculating simple footing shape and uniform grounds. Most formulas don't take into account the size effect of footing on ultimate bearing capacity except for the formula by Architectural Institute of Japan. The advantage of finite element method is the application to non-uniform grounds, which are for example multi-layered ground and improved ground, and complicated footing shape in three dimensional condition. It greatly improves the accuracy in estimating ultimate bearing capacity. Moreover, limit state analysis is possible to be conducted without the assumption on potential failure modes. The objective of this study is proposing a rigid plastic constitutive equation using non-linear shear strength property against the confining pressure. The constitutive equation was built based on the experiment regarding non-linear shear strength property against confining pressure reported by Tatsuoka and other researchers. The obtained results from experiment on Toyoura sand and various kinds of sands indicated that although internal friction angle differs among sandy soils, the normalized internal friction angle decreased with the increase in the normalized first stress invariant for various sands despite of dispersion in data. This property always holds irrespective of the reference value of the confining pressure in normalization of internal friction angle. This equation is expressed by the higher order parabolic function and easily applied to RPFEM. Applicability of proposed rigid plastic equation was proved by comparing with the ultimate bearing capacity formula by Architectural Institute of Japan (AIJ, 1998, 2001) which is an experimental formula to take into account the size effect of footing.

Size effect of footing is observed in ultimate bearing capacity, but basically not accounted in the ultimate bearing capacity formulas. In this study two discussions on the size effect were conducted. One is the size effect in case of a uniform sandy ground and the other is in case of a multi-layered ground. The results of RPFEM with the proposed constitutive equation were obtained similar to the results by Architectural Institute of Japan. It is clear that RPFEM with

the use of non-linear shear strength against the confining pressure provides good estimations to the ultimate bearing capacity of footing by taking account of size effect of footing. RPFEM was clearly shown to be effective for the complicated problems in material properties and footing shape than the conventional ultimate bearing capacity analysis.

Moreover, ultimate bearing of footing related to inclined loads or combined loads (vertical, horizontal and moment loads combination) is an important aspect in geotechnical engineering. Meyerhof and others (e.g. Hansen, 1970, Vesic, 1975) conducted empirical generalizations of the simpler cases without examining in detail and the size effect of footing does not consider in the previous research. This is a major topic of this study. The obtained results show that the normalized vertical load decreases with the increase in the normalized horizontal load and/or moment load. The normalized moment load is obtained greater than that of linear shear strength property and therefore effect of non-linear shear strength property on the normalized limit load space in vertical, horizontal and moment loads is clearly indicated.

ACKNOWLEDGEMENT

I would like to express my deep gratitude and appreciation to my supervisor, Professor OHTSUKA Satoru at Environmental and Disaster prevention laboratory, Nagaoka University of technology, for welcoming me in his laboratory to work on this challenging research topic, and for his warm encouragement and thoughtful guidance, and were always accessible with friendly support throughout my time in Japan. I would like to thank the ministry of education, culture, sports, science & technology (MEXT) for awarding scholarship during my PhD course at Nagaoka University of technology, Japan.

I also wish to thank Professor Sugimoto Mitsutaka, A/ Professor Toyota Hirofumi, Professor Iwasaki Eiji, and A/Professor Kobayashi Shunichi (Kanazawa University), for their critical review of the manuscript and constructive suggestions and active discussions as committee members of my doctoral degree. I would like to express my appreciation to Dr. Hoshina Takashi (Sato Kogyo Ltd. Company), Dr. Kaneda Kazuhiro (Takenaka Corporation) and Assos. Professor. Dr. Isobe Koichi (Hokkaido University) for their comments for my research.

I would like to thank the members of Environment Disaster and Prevention lab for their support and friendship. Thanks to my friends who had made my time in Nagaoka, Japan such an unforgettable memory. I received a lot of help and advice from them.

Many thanks are reserved for the staffs from Division of International Affairs and Division of Academic Affairs, the persons who had always supported me and my family during my study time and stay in Nagaoka.

I wish to dedicate this thesis to my FATHER, my MOTHER and my younger SISTER whose life times have been devoted to my education.

I thank my beloved wife, HIEN, who had to withstand time and long distance in over three long years in beautiful Nagaoka. Our love means so much to me.

Especially, thanks to my little daughter, NGUYEN NGOC QUYNH CHAU and my son, NGUYEN BAO LONG, they always motivated for me to finish my research.

Thank you so much for all. Love JAPAN.

Sincerely, **NGUYEN LE DU**

LIST OF SYMBOLS

Material parameters

c	Cohesion of soil
ϕ	Shear resistance angle of soil
γ	Unit weight of soil
a, b	The material constants

Bearing capacity parameters

q_{ult}	Ultimate bearing capacity
i_q, i_c, i_γ	Inclination load factor
s_c, s_q, s_γ	Shape factors
d_c, d_q, d_γ	Depth factors
m_L, m_B, m	Empirical parameters involving the footing shape factor
ρ	Load factor
σ_2	Lateral stress
θ	Inclined angle
ϕ_0	Shear resistance angle for the specific lateral stress σ_{20}
η	The size effect factor
γ_{st}	Density of building
h	Building height
α, β	Shape coefficient of AIJ bearing capacity
N_c	Cohesion factor
N_q	Overburden factor
N_γ	Self-weight factor

Footing parameters

A	Plan area of footing
A'	Effective plan area of footing under eccentric load
B	Footing width
B_0	Reference value in footing width
e	Eccentricity
L	Length of footing
L'	Effective length of footing
q_{v_0}	Vertical force from the weight of building
q_{h_0}	horizontal force
k_h	Seismic coefficient

Load parameters

V	Vertical load
H	Horizontal load
M	Moment load
X_i	Body force
T_i	Surface force
$\boldsymbol{F}$	vector of all nodal forces
V_0	the ultimate vertical load
e	The eccentricity of the load

Hyperplasticity parameters

$\dot{\boldsymbol{\varepsilon}}$	Vector of total strain
$\dot{\boldsymbol{\varepsilon}}^{e}$	Elastic strain
$\dot{\boldsymbol{\varepsilon}}^{p}$	Plastic strain
$\dot{\boldsymbol{\varepsilon}}_{ij}$	Strain rate (second-order tensor)
$\boldsymbol{\varepsilon}_{ij}$	The diagonal strain components
$\boldsymbol{\varepsilon}_{ij}$	Shear strain
$\gamma_{12}, \gamma_{13}, \gamma_{23}$	Engineering shear strain
$\dot{\mathbf{u}}$	Vector of all nodal velocities
$\dot{\mathbf{u}}_{i}$	Displacement vector
$\dot{\mathbf{u}}_{i,j}$	Second-order tensor
$\overline{K}$	Stiffness matrix
I_1	First invariant of stress
J_2	Second invariant of deviator stress
$\dot{e}$	The norm of strain rate
$\dot{\mathbf{v}}$	Vector of rates of volume change of all element
$\boldsymbol{\sigma}_{i}$	Stress
$\boldsymbol{\sigma}_{ij}^{*}$	An arbitrary stress
$\boldsymbol{\sigma}_{0}$	Initial stress
λ	The plastic multiplier
$d\boldsymbol{\varepsilon}_{ij}^{p}$	Plastic strain rate
$D(\boldsymbol{\varepsilon}_{ij}^{p})$	Plastic energy dissipation

$\mathbf{s}$	Vector of deviatoric stress s_{ij} of all elements
S_σ	Stress boundary condition
$\boldsymbol{B}$	Matrix defined such as $\dot{\boldsymbol{\varepsilon}} = \mathrm{B}\dot{\mathbf{u}}$
$\boldsymbol{L}$	Matrix defined such as $\dot{\mathbf{v}} = \mathrm{L}\dot{\mathbf{u}}$
$\boldsymbol{N}$	The shape function matrix
$\boldsymbol{m}$	Transfer vector
$\boldsymbol{X}$	The total nodal force vector
x	The unit node weight
$\boldsymbol{I}$	Unit tensor
t	Surface force applied at nodes
P	Mean stress
(k_1, μ_1)	Lagrange multiplier
(μ, κ)	Penalty multiplier

TABLE OF CONTENTS

LIST OF FIGURES

LIST OF TABLES

CHAPTER 1

INTRODUCTION

1.1 Background

In design of buildings, three main design criteria, namely the ultimate bearing capacity of the footings; the total and differential settlements and the economic feasibility of the footing are required to satisfy. This study mainly focuses on the first of these criteria; the assessment for ultimate bearing capacity of footing is an important task in order to examine the stability of building - ground system. Bearing capacity failure occurs as the soil supporting the foundation fails in shear, which may involve either a general, local or punching shear failure mechanism (Bowles, 1988). Estimation and prediction of the ultimate bearing capacity of the footing is one of the significant and complicated problems in geotechnical engineering (Poulos et al., 2001). Currently, there are many formulas used to calculate the ultimate bearing capacity. A list of principal contributions to the study of this subject may be found, for example, in Terzaghi (1943), Hansen (1970), Meyerhof (1963) and Tani and Craig (1995). These studies focuses on the estimation of the ultimate bearing capacity of the footing under combination of vertical, horizontal and moment loading, as well as the effect of soil rigidity, load inclination and the depth of the foundation on the ultimate bearing capacity of footings. However, the formula has disadvantages in application to practice since it is only applied in calculating simple footing shape and uniform grounds. Most formulas don't take into account the size effect of footing on ultimate bearing capacity except for the formula by Architectural Institute of Japan. The advantage of finite element method is the application to non-uniform grounds, which are, for example, multi-layered ground and improved ground, and complicated footing shape in three dimensional conditions. It greatly improves the accuracy of estimating ultimate bearing capacity. The objective of this study is proposing a rigid plastic constitutive equation using non-linear shear strength property against the confining pressure. The constitutive equation was built based on the experiment regarding non-linear shear strength property against confining pressure

reported by Tatsuoka and other researchers. The obtained results from experiment on Toyoura sand and various kinds of sands indicated that although internal friction angle differs among sandy soils, the normalized internal friction angle decreased with the increase in the normalized first stress invariant for various sands despite of dispersion in data. It was shown no matter how to select the standard value of confining stress in normalization of internal friction angle. Applicability of proposed rigid plastic equation was proved by comparing with the ultimate bearing capacity formula by Architectural Institute of Japan which is an experimental formula to take into account the size effect of footing. The results of RPFEM with the proposed constitutive equation were obtained similar to the results by Architectural Institute of Japan. It is clear that RPFEM with the use of non-linear shear strength against the confining pressure provides good estimations to the ultimate bearing capacity of footing by taking account of size effect of footing. This study discussed the size effect of footing in ultimate bearing capacity in case of multi-layered ground

Moreover, in previous geotechnical research, the combined vertical and horizontal load is referred as the inclined loads. Their results showed that the vertical bearing capacity significantly decreased when the inclined angle $\theta = \text{atan}(H/V)$ increased. Many researchers provide procedures for a general case; however they only conduct empirical generalizations of the simpler cases without examining in detail.

Recently, the numerical methods are efficient techniques for solving problems related to geotechnical engineering. The rigid-plastic finite element method (RPFEM) was applied in geotechnical engineering by Tamura (1991). In this process, the limit load is calculated without the assumption about the potential failure mode. The method is effective in calculating the ultimate bearing capacity of footing against the three-dimensional boundary value problems. Although RPFEM was originally developed based on the upper bound theorem in plasticity, Tamura proved that it could be derived directly by using the rigid plastic constitutive equation.

This research investigated the ultimate bearing capacity of footing on sandy soils against the combined load of vertical, horizontal and moment loads. This research applied rigid plastic finite element method which employs the rigid plastic constitutive equation in which non-linear shear

strength properties against confining pressure in case the internal friction angle of 30 and 40 deg. The vertical load V, horizontal load H and moment M, which were applied at the center of the footing, were subjects in this study. The analytical method provides the reliable computational results. The relation in normalization form of H/V_0 vs V/V_0 and V/V_0 vs M/BV_0 were acquired and then were compared with the relationship by Meyerhof (1956), Architectural Institute of Japan (1988, 2001) and Loukidis et al. (2008).

RPFEM was clearly shown to be effective for the complicated problems in material property and footing shape than the conventional ultimate bearing capacity analysis.

1.2 Scope and Objective of the study

The objective of this study is proposing a rigid plastic constitutive equation using non-linear shear strength property against the confining pressure; the obtained results provide good estimations to the ultimate bearing capacity of footing by taking account of size effect of footing in case of multi-layered ground and also the ultimate bearing capacity of the footing under combination of vertical, horizontal and moment loading

1.3 Thesis outline

Chapter 1 gives the general background of ultimate bearing capacity and scope and objective of research work.

Chapter 2 review ultimate bearing capacity of footing under vertical load condition; combined loading and also review on rigid plastic finite element method (RPFEM).

Chapter 3 describes numerical formulation on rigid plastic finite element method. In this chapter, strength tests of Toyoura sand by Tatsuoka et al. was shown and rigid plastic constitutive equation for non-linear shear strength property are proposed

Chapter 4 simulate finite element model to estimate ultimate bearing capacity of footing under plane strain condition using rigid Plastic constitutive equation for Drucker –Prager yield

function and non-linear shear strength property

Chapter 5 is a chapter for a discussion on size effect of footing on ultimate bearing capacity. The discussions on result comparison are also written.

Chapter 6 is a chapter for ultimate bearing capacity of footing against combined loading (Vertical, horizontal and moment loads combination).

Finally, *chapter 7* summarizes the general conclusion of this study and gives some suggests some area requiring further work.

As an overview, the research presented in this thesis can be divided into three principal areas;

(1) Proposing a rigid plastic constitutive equation using non-linear shear strength property against the confining pressure

(2) The development of the ultimate bearing capacity for strip footing on a multi-layered, homogeneous soil profile.

(3) The development of the ultimate bearing capacity for strip footing under combination of vertical, horizontal and moment loading.

The structure of this thesis reflects the three main topics listed above. The obtained numerical results are presented on chapter 5 to chapter 6. Many cases and problems are separated and discussed.

Chapter 7 presented a summary and conclusion of this study, including recommendations for future research.

References

[1] AIJ (1988, 2001), Architectural Institute of Japan. Recommendations for design of building foundations, 430p.

[2] Aysen, A., 2002. Soil Mechanics – Basic Concepts and Engineering Applications. Balkema AA Publisher, 413–419.

[3] Du, N. L., Ohtsuka, S., Hoshina, T., Isobe, K. and Kaneda, K., 2013. Ultimate bearing capacity analysis of ground against inclined load by taking account of non-linear property of shear strength", Int. J. GEOMATE **5** (2), 678–684.

[4] Drucker D.C., Greenberg H.J., Lee E.H., Prager, W., 1951. On plastic rigid solutions and limit design theorems for elastic plastic bodies. 1st US NCAM, pp. 533–538.

[5] De Beer, E. E., 1970. Experimental determination of the shape factors and the ultimate bearing capacity factors of sand, Geotechnique, **20**(4), 387 – 411.

[6] Hanna, A., M., and Meyerhof, G. G., 1981. Experimental evaluation of ultimate bearing capacity of footings subjected to inclined loads, Can. Geotech. J. **18**(4): 599-603.

[7] Meyerhof, G. G., 1951. Ultimate bearing capacity of foundations, Geotechnique, **2**(4), 301-332

[8] Meyerhof, G. G. 1963. Some recent research on the ultimate bearing capacity of foundations, Can. Geotech. J., **1**(1), 243-256

CHAPTER 2

LITERATURE REVIEW ON ULTIMATE BEARING CAPACITY AND RIGID PLASTIC FINITE ELEMENT METHOD

In order to facilitate the discussion in later chapters, a number of definitions which will be used in this thesis are presented below.

Bearing capacity is the ability of a soil to safely carry the pressure placed on it from any engineered structure without suffering a shear failure with accompanying large settlements. Applying a bearing pressure which is safe with admiration to failure does not ensure that settlement of the foundation will be within acceptable limits. Therefore, settlement analysis should mostly be performed since most structures are sensitive to excessive settlement (Merifield (2005)).

Ultimate bearing capacity is the intensity of bearing pressure at which the associate ground is estimated to fail in shear, i.e. a collapse will take place (Whitlow (1995)).

2.1 Literature on ultimate bearing capacity

2.1.1 Review of the ultimate bearing capacity of footing theories - centric vertical loading

In design of buildings, the assessment for ultimate bearing capacity of footing is a key task in order to observe the stability of building - ground system. The value of the bearing capacity of footing depends not only on the mechanical property of the soil but also on the size of the loaded range, its shape, and its location with reference to the surface of the soil. The term "strip footing" is practical to a footing whose length is very long in comparison with its width. In most parts of this chapter, the soil is supposed to be an isotropic, homogeneous and elastic-perfectly plastic material which follows the Coulomb yield condition and the associated flow rule. A plane strain condition is assumed in this chapter. The effect of non-homogeneity on the bearing capacity of footings will be conversed later.

Limit analysis is concerned with the development and applications of such methods. Although the limit analysis methods were established firmly less than twenty years ago, there have been an enormous number of applications in a wide variety of fields from metal deformation

processing to the design of reinforced concrete structures. Applications to beams and frames are the most highly developed aspect of limit analysis and design so that the basic techniques are given in several texts. Reference to the work of many investigators is given also in the ASCE Manual 41 (ASCE-WRC, 1971) on plastic design in steel. Applications of limit analysis to plates and shells for both metal and reinforced concrete materials are given in the recent book by Save and Massonnet (1972). A great deal of attention has been paid recently to soil mechanics in addition to concrete and rock. An appreciable amount of practical information is now available as the result of this and allied work. Perhaps the most striking feature of the limit analysis method is that no matter how complex the geometry of a problem or loading condition, it is always possible to obtain a realistic value of the collapse load. When this is coupled with its other merits, namely, that it is relatively simple to apply, that it provides engineers with a clear physical picture of the mode of failure, and that many of the solutions obtained by the method have been substantiated numerically by comparing with the existing results for which satisfactory solutions already exist, it can be appreciated that it is a working tool with which every engineer should be conversant. Limit analysis is not the only method of assessing the collapse load of a stability problem in soil mechanics. The other standard and widely known techniques used in the solutions of soil mechanics problems may be divided into two principal groups - the slip-line method and the limit equilibrium method

The limit analysis method employed herein does not consider the deformation of the soil and the solutions obtained are essentially the same as that assuming the soil to be rigid-perfectly plastic material. This chapter is also primarily concerned with complete failure of the footing, or its ultimate bearing capacity. This type of failure is referred to here as a general shear failure.

Kötter (1903) was the first to derive these slip-line equations for the case of plane deformations. Prandtl (1920) was the first to obtain an analytical closed form solution to these equations for a footing on a weightless soil. In the analysis, he developed the solution with a singular point with a pencil of straight slip-lines passing through it. These results were subsequently applied by Reissner (1924) and Novotortsev (1938) to certain particular problems on the bearing capacity of footings on a weightless soil, when the slip-lines of at least one family are straight and the solutions have closed form.

The so-called limit equilibrium method has traditionally been used to obtain approximate

solutions for the stability problems in soil mechanics. Examples of this approach are the solutions presented in the book by Terzaghi (1943). The method can probably best be described as an approximate approach to the construction of a slip-line field and generally entails an assumed failure surface of various simple shapes-planes, circular or log-spiral. With this assumption, each of the stability problems is now reduced to one of finding the most dangerous position for the failure or slip surface of the shape chosen which may not be particularly well founded, but quite often gives acceptable results. In this method, it is also necessary to make sufficient assumptions regarding the stress distribution along the failure surface such that an overall equation of equilibrium, in terms of stress resultants, may be written for a given problem. Therefore, this simplified approach makes it possible to solve various problems by simple statics. Various solutions obtained by this method are summarized in graphical or tabular form in the texts by Terzaghi (1943) and by Taylor (1948) and are now quite widely used in practice. It is worth mentioning here that none of the equations of solid mechanics is explicitly satisfied everywhere inside or outside of the failure surface. Since the stress distribution is not precisely defined anywhere inside and outside of the assumed failure surface, one cannot say definitely that an acceptable stress distribution which satisfies equilibrium, stress boundary conditions and the yield criterion, exists such that the solution meets the requirements of the lower-bound rules of limit analysis. Although the limit equilibrium technique utilizes the basic philosophy of the upper-bound rules of limit analysis, that is, a failure surface is assumed and a least answer is sought, it does not meet the precise requirements of the upper-bound rules so that it is not an upper bound. The method basically gives no consideration to soil kinematics, and equilibrium conditions are satisfied only in a limited sense. It is clear than that a solution obtained using the limit equilibrium method is not necessarily an upper or a lower bound. However, any upper-bound limit analysis solution will obviously be a limit equilibrium solution.

Studies of the bearing capacity of foundations under conditions of plane strain have been made by Terzaghi (1943), by Meyerhof (1951) using limit equilibrium method, by Sokolovskii (1965), by Brinch Hansen (1961) using slip-line method, by Shield (1954b), by Chen and Davidson (1973) using limit analysis method, and many others.

The ultimate bearing capacity formula of footing by Terzaghi (1943) has been widely employed in practice. It takes account of the effects of cohesion, surcharge and soil weight. This theory

determine the ultimate bearing capacity of a shallow, rough, rigid, continuous (strip) foundation supported by a homogeneous soil layer extending to a great depth. The failure surface in soil at ultimate load (that is, q_u per unit area of the foundation) assumed by Terzaghi is shown in Figure 2.1. Referring to Figure 2.1, the failure area in the soil under the foundation can be divided into three major zones:

1. Zone abc. This is a triangular elastic zone located immediately below the bottom of the foundation. The inclination of sides' ac and bc of the wedge with the horizontal is $\alpha = \phi$ (soil friction angle).

2. Zone bcf. This zone is the Prandtl's radial shear zone.

3. Zone bfg. This zone is the Rankine passive zone. The slip lines in this zone make angles of $\pm\left(45 - \phi/2\right)$ with the horizontal.

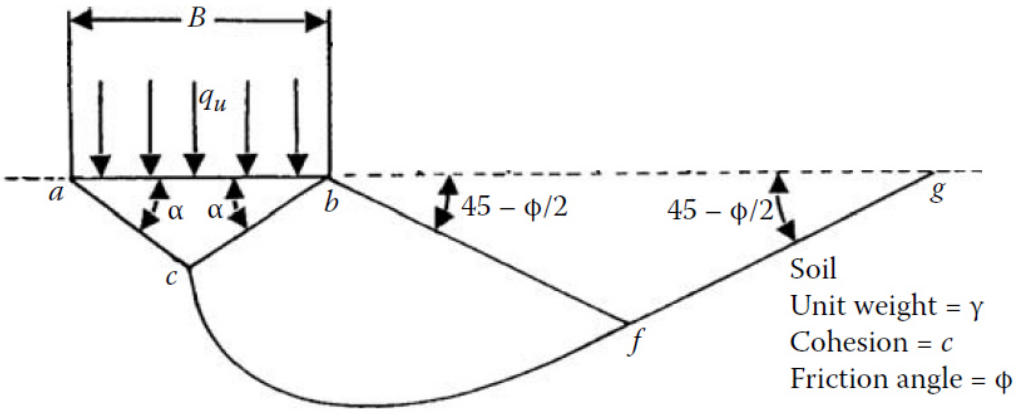

Figure 2.1 Failure surface in soil at ultimate load for a continuous rough rigid foundation as assumed by Terzaghi.

Since Terzaghi's founding work, numerous experimental studies to estimate the ultimate bearing capacity of shallow foundations have been conducted. Based on these studies, it appears that Terzaghi's assumption of the failure surface in soil at ultimate load is essentially correct. However, the angle α that sides ac and bc of the wedge (Figure 2.1) make with the horizontal is closer to $\left(45 + \phi/2\right)$ and not ϕ, as assumed by Terzaghi. In that case, the nature of the soil failure surface would be as shown in Figure 2.2.

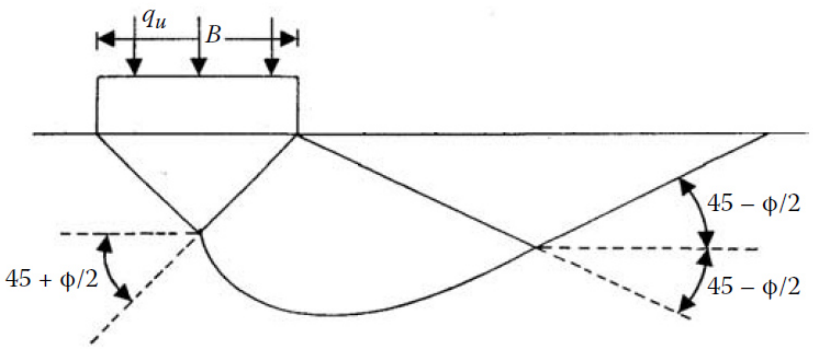

Figure 2.2 Modified failure surface in soil supporting a shallow foundation at ultimate load.

The ultimate bearing capacity formulas typically expressed as below:

$$q = cN_c + \frac{1}{2}\gamma B N_\gamma + \gamma D_f N_q \tag{2.1}$$

where N_c, N_γ, N_q are the bearing capacity factors, which are functions of internal friction angle of the soil, ϕ. The other indexes are as follows.

γ: unit weight of soil $(\mathrm{kN/m^3})$

D_f : depth of footing (m)

B: footing width (m)

Since this approach has been proposed, various studies regarding bearing capacity factors have been conducted. Precisely mathematical expressions for bearing capacity factors N_q and N_c were provided by Prandtl (1921) and Reissner (1924) as follows:

$$N_q = e^{\pi \tan\phi} \tan^2\left(\frac{\pi}{4} + \frac{\phi}{2}\right) \tag{2.2}$$

$$N_c = (N_q - 1)\cot\phi \tag{2.3}$$

With regards to N_γ factor, several formulations have been proposed but no formula is totally accurate, and also many proposed estimation methods. This has become one of the main reasons for disagreement between methods used to estimate q_{ult}, as the value of N_γ for equation values of ϕ can produce large differences, depend on the estimation method used. The task of categorically validating a method for calculating N_γ is complex due to the difficulty in obtaining q_{ult} experimentally. A clearly defined value of q_{ult} is not always obtained in a load test; this is mainly due to the limitations of test procedures or because the progressive failure effect leads to repositioning of

soil particles beneath the foundation, and the highest load levels are not reached (Elhakim 2005). For this reason, to determine q_{ult}, and in turn N_γ, experimentally it is necessary to use methods such as those proposed by de Beer (1970); Vesic (1973); Briaud and Jeanjean (1994); Amar et al. (1998); Decourt (1999). However, these methods vary widely as they define q_{ult} based on selection criteria from a point on the load–settlement curve that can be very subjective (Lutenegger and Adams 1998; Elhakim 2005). Table 2.1 shows the methods for estimating N_γ in term of ϕ, along with the author of each method and the theory on which it is based.

Table 2.1 Expression for the estimation of the N_γ factor [11].

Terzaghi (1943); fitted expression; limit equilibrium	$N_\gamma = \left[\tan^2\left(\frac{\pi}{4}+\frac{\phi}{2}\right)\exp(\pi\tan\phi)+3.0\right]\tan(1.34\phi)$
Caquot and Kérisel(1953); fitted from *Ukritchon et al. (2003)*: method of characteristics	$N_\gamma = \left[1.413\tan^2\left(\frac{\pi}{4}+\frac{\phi}{2}\right)\exp(\pi\tan\phi)+1.794\right]\tan(1.27\phi)$
Meyerhof (1963); semi-empirical based on limit equilibrium	$N_\gamma = \left[\tan^2\left(\frac{\pi}{4}+\frac{\phi}{2}\right)\exp(\pi\tan\phi)-1.0\right]\tan(1.4\phi)$
Muhs and Weiss (1969); (Euro-code 7); semi-empirical expression	$N_\gamma = 2\left[\tan^2\left(\frac{\pi}{4}+\frac{\phi}{2}\right)\exp(\pi\tan\phi)-1.0\right]\tan(\phi)$
Brich-Hansen (1970); semi-empirical based on *Lundgren-Mortensen(1953)*; failure mechanics	$N_\gamma = 1.5\left[\tan^2\left(\frac{\pi}{4}+\frac{\phi}{2}\right)\exp(\pi\tan\phi)-1.0\right]\tan(\phi)$
Vesis (1973); approximation based on *Caquot and Kérisel(1953)*; analysis using the method of characteristics	$N_\gamma = 2\left[\tan^2\left(\frac{\pi}{4}+\frac{\phi}{2}\right)\exp(\pi\tan\phi)+1.0\right]\tan(\phi)$
Hettler and Gudehus (1988); empirical	$N_\gamma = \left[5.71(\tan\phi)^{1.15}\right]-1.0$
Zadroga (1994); empirical expression	$N_\gamma = 0.657\exp(0.141\phi)$ ϕ in degree
Michalowski (1997); upper bound limit analysis	$N_\gamma = \exp(0.66+5.11\tan\phi)\tan\phi$
Poulos et al. (2001); solution based on	$N_\gamma = 0.1054\exp(9.6\phi)$

Davis and Brooker (1971)	
Lyamin et al. (2007); lower and upper bound analysis	$N_\gamma = \left[\tan^2\left(\frac{\pi}{4}+\frac{\phi}{2}\right)\exp(\pi\tan\phi)-0.6\right]\tan(1.33\phi)$
Kumar and Khatri (2011); fitted expression; lower bound with finite element and linear programming	$N_\gamma = \left[\tan^2\left(\frac{\pi}{4}+\frac{\phi}{2}\right)\exp(\pi\tan\phi)-5.115\right]\tan(1.577\phi)$

The numerical solution of characteristic equations is described in detail by Sokolovskii (1965). If an associated flow rule is used, and there sulting stress-strain rate equations can be integrated to yield a kinematically admissible velocity field, the slip-line solution is an upper bound solution. If, in addition, the slip-line stress field can be extended over the entire soil domain such that the equilibrium equations, the stress boundary conditions and the yield condition are satisfied, the slip-line solution is also a lower bound, and is hence the exact solution. Although the slip-line method may be used to compute a partial plastic stress field, there is no guarantee that this stress field can be associated with a kinematically admissible velocity field or extended satisfactorily throughout the body (Bishop, 1953). Although the slip-line method can generally be expected to give a good estimate of the correct solution, its accuracy is difficult to ascertain once either of the bounding property is lost. Due to the complexities that are associated with the introduction of self-weight, a great variety of approximate solutions for the bearing capacity factor N_γ have appeared in the literature (Chen, 1975).The differences among these solutions are often very substantial, particularly for friction angles greater than about 30^0. Unfortunately, experimental research on the ultimate bearing capacity of footings on sand has not shed much light on the question of which values of N_γ are theoretically correct. This is partly because of the difficulty in selecting an appropriate friction angle for the bearing capacity calculations when comparing the theoretical predictions with test results. Scale effects are also another complication. Existing theoretical solutions suggest that the factor increases very rapidly with the angle of friction. In view of this strong dependence, it seems unlikely that footing experiments alone can resolve the question of which values of N_γ are correct. More recently,

Michałowski (1997) and Soubra (1998), among others, have used rigid-block mechanisms to estimate the bearing capacity factor N_γ. Their results show some improvement on Chen's solutions but are still fairly conservative. The last three decades has witnessed a growing use of the finite element method in almost all areas of geotechnical engineering, including shallow foundation stability. However, only a few authors have attempted to apply this method to predict the bearing capacity of strip footings on cohesionless soils (Sloan and Randolph, 1982; Griffiths, 1982; Frydman and Burd, 1997). This is largely due to the difficulty in developing finite element formulations that are capable of providing precise estimates of the limit load.

A long-term research program has been undertaken at the University of Tokyo (Tatsuoka et al., 1991, 1994b, 1997; Siddiquee et al., 1999). The research consists of: i) Physical model tests with different footing shapes, load inclinations and footing depths under the gravitational force (i.e., in 1g) and in a centrifuge, using three types of granular materials having different particle sizes; ii) A series of stress-strain tests to evaluate thoroughly the strength and deformation property of the test materials; iii) Their constitutive modelling; iv) Numerical simulation by FEM analysis of the model tests. The two dimensional constitutive model of one of the test materials (i.e., Toyoura sand) that has been developed for plane strain analyses (Tatsuoka et al., 1994a) was implemented into the FEM analysis as a generalized elasto-plastic, isotropic strain-hardening and softening one with a non-associated flow rule using Mohr-Coulomb type yield surface.

Meyerhof (1951, 1963) introduced the other factors such as semi - empirical inclination factors i_c, i_γ, i_q. The ultimate bearing capacity formula is described as follows:

$$q = \mathrm{i}_c c N_c + \tfrac{1}{2} i_\gamma \gamma_1 B N_\gamma + i_q \gamma_2 D_f N_q \qquad (2.4)$$

The effects of inclination factor have been investigated both theoretically and experimentally by a number as researchers as table 2.2.

Table 2.2 Inclination factors found in the literature

Author	i_c	i_q	i_γ
Meyerhof (1953) Meyerhof and Koumoto (1986)	$\left(1-\frac{\theta^0}{90^0}\right)^2$ for any ϕ	i_γ for any ϕ	$\left(1-\frac{\theta^0}{\phi^0}\right)^2$ for $\phi>0$ $i_\gamma = 0$ for $\phi = 0$
Brich Hansen (1970)	$i_q - \frac{1-i_q}{V\tan\phi}$ for $\phi>0$ $0.5\left(1-\frac{H}{A_f c_a}\right)^{1/2}$ for $\phi=0$	$\left(1-\frac{H}{V+A_f c_a\cot\phi}\right)^5$	$\left(1-\frac{H}{V+A_f c_a\cot\phi^0}\right)^5$
Vesic (1975)	$i_q - \frac{1-i_q}{V\tan\phi}$ for $\phi>0$ $1-\frac{mH}{A_f c_a N_c}$ for $\phi=0$	$\left(1-\frac{H}{V+A_f c_a\cot\phi}\right)^m$	$\left(1-\frac{H}{V+A_f c_a\cot\phi^0}\right)^{m+1}$

where θ: the inclination angle of load with respect to the vertical plane.

$m = m_B = \frac{\left(2+B/L\right)}{\left(1+B/L\right)}$ with the horizontal load H is in parallel to the footing width *B*

$m = m_L = \frac{\left(2+L/B\right)}{\left(1+L/B\right)}$ with the horizontal load H is in parallel to the footing length *L*

$m = \sqrt{m_L^2 + m_B^2}$ with the direction of *H* is in between the directions of footing width and length.

A_f: effective contact area of the footing.

H: horizontal component of the inclined load.

V: Vertical component of the inclined load.

c_a: unit adhesion on the base of the footing.

Architectural Institute of Japan (AIJ, 1988, 2001) developed the ultimate bearing capacity formula and now is widely used in Japan. By using factors N_c, N_q given by Prandtl and N_γ described by Meyerhof, the ultimate bearing capacity formula is expressed as follows:

$$q = i_c \alpha c N_c + i_\gamma \gamma_1 \beta B \eta N_\gamma + i_q \gamma_2 D_f N_q \qquad (2.5)$$

In the above equation, α and β express the shape coefficient and $\alpha = 1$ and $\beta = 0.5$ are recommended by De Beer [8], respectively. There, η is the size effect factor defined in the following.

$$\eta = \left(\frac{B}{B_o} \right)^m \tag{2.6}$$

where,

B_0: reference value in footing width

m: coefficient determined from the experiment, m = -1/3 is recommended in practice.

The ultimate bearing capacity formula by AIJ successfully takes into account of the size effect of footing which has not been considered in the past formulae employing the Mohr-Coulomb criteria for soils strength. Since the past formulae overestimate the ultimate bearing capacity with the increase in footing width, this effect needs to be examined for intensive practical request. Ueno et al. [42] expressed that the size effect on ultimate bearing capacity was mainly attributed to the stress level effect on shear strength of soils. Their research indicated that the mean stress ranged from $2\gamma B$ to $10\gamma B$ beneath the footing and it caused the change in internal friction angle of ground widely due to the mean stress. This study attempts to discuss the size effect on ultimate bearing capacity by using the finite element analysis with the rigid plastic constitutive equation which simulates the non-linear shear strength property of sandy soil against the confining pressure.

2.1.2 Review of ultimate bearing capacity against combined load of vertical, horizontal and moment loads

Due to bending moments and horizontal thrusts transferred from the superstructure, shallow foundations are often subjected to eccentric and inclined loads. Under such circumstances the ultimate bearing capacity theories presented about need some modification, and this is the subject of discussion in this chapter.

This chapter starts with a review of commonly-used solutions applicable to the problem of bearing capacity of footings under combined loading. This includes several well-known semi-empirical bearing capacity formulae (such as Meyerhof (1953), Hansen (1971), Vesic (1975)) and some experimental research. Several techniques which can be used to determine the bearing capacity envelope are also reviewed. These procedures are then used in a number of

finite element analyses to compare the efficiency and accuracy of each technique in determining the envelope. After that a series of analyses is conducted to construct the envelope, and the results are then compared with the methods previewed.

2.1.2.1 Vertical bearing capacity

From the theory of plasticity, the exact solution for a strip footing on sandy soil (based on Prandtl 1920) [26] can be derived

$$V_0 = (\pi + 2)c.B \tag{2.7}$$

where B is the footing width; c is the cohesion of soil.

2.1.2.2 Bearing capacity between vertical load and moment load

Under combined vertical loads and moment loads, bearing capacity is usually showed as the equivalent problem of an eccentric vertical load (Fig. 2.3).

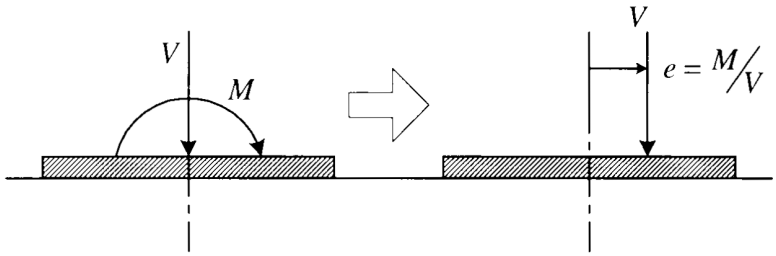

Fig.2.3. Equivalent eccentric load

The eccentric vertical load is assumed to act on a reduced area on which the load acts centrally. For a strip footing, the effective width is $B' = B - 2e$ (Fig. 2.4).

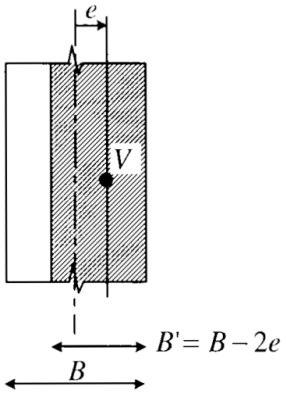

Fig.2.4. Effective area concept

This leads to a (V, M) bearing capacity interaction diagram defined as a simple parabola as follow:

$$\frac{M}{M_0} = 4\frac{V}{V_0}\left(1 - \frac{V}{V_0}\right) \tag{2.8}$$

where V_0 is the vertical ultimate load and $M_0 = BV_0/8$ is the maximum moment capacity.

In Fig. 2.5, (V/V_0, M/BV_0) interaction of Meyerhof method for strip footings is plotted given that V_0 is determined by equation (2.8).

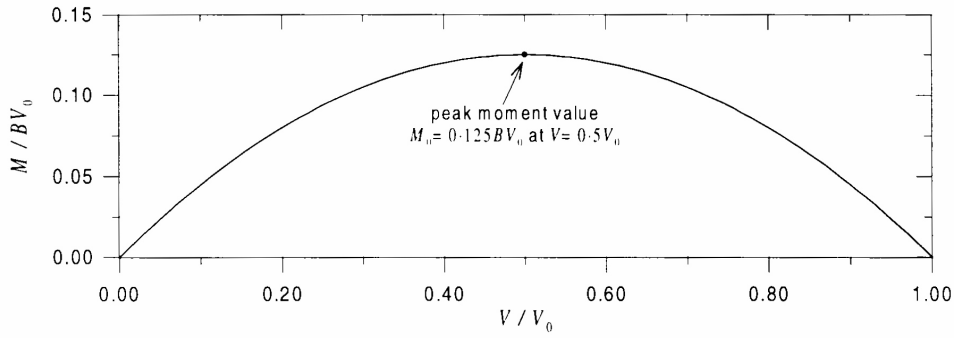

Fig.2.5 (M, V) interaction chart of a strip footing

2.1.2.3 Bearing capacity between vertical load and horizontal load

In early geotechnical papers combined vertical and horizontal loading is referred to as inclined loading. Having found that the vertical bearing capacity significantly reduced as the inclined angle $\theta = \tan^{-1}(H/V)$ increased. Meyerhof (1956) introduced 'inclination factors', the (V, H) failure envelope is defined as follows:

$$\frac{V}{V_0} = \left(1 - \frac{\theta^0}{90^0}\right)^2 \tag{2.9}$$

where V_0 is the ultimate vertical load. Interaction diagrams of H/V_0 vs. V/V_0 are obtained and compared with the failure surface of Meyerhof.

2.1.2.4 Bearing capacity between vertical, horizontal and moment loads

Meyerhof (1956) also proposed ultimate bearing capacity interaction between vertical loads,

horizontal loads and moment loads: an inclined load of magnitude $\sqrt{V^2 + H^2}$ is assumed to act centrally on a reduced footing area determined by the eccentricity $e = M/V$ as depicted in Fig. 2.3. The methods by Meyerhof (1956) can be used to define the following (V, H, M) failure envelopes:

$$\frac{V}{V_0} = \left(1 - \frac{\theta^0}{90^0}\right)\frac{A'}{A} \tag{2.10}$$

This paper investigate the ultimate bearing capacity of footing on sandy soils against the combined load of vertical, horizontal and moment loads, using rigid plastic finite element method employing the rigid plastic constitutive equation, which considers non-linear shear strength property against confining pressure.

On the other hand, the general bearing capacity equation has been proposed by Meyerhof (1963):

$$q'_u = cN_c.s_c.i_c.d_c + \gamma.D_f.N_q.s_q.d_q.i_q + 0.5.\gamma.B.N_\gamma.s_\gamma.d_\gamma.i_\gamma \tag{2.11}$$

where

s_c, s_q, s_γ : shape factors

i_c, i_q, i_γ : inclination factors

d_c, d_q, d_γ : depth factors

c : cohesion of soil

N_c, N_q, N_γ : bearing capacity factors which are only functions of soil friction angle ϕ

$$Q_{ult} = q'_u.A' \tag{2.12}$$

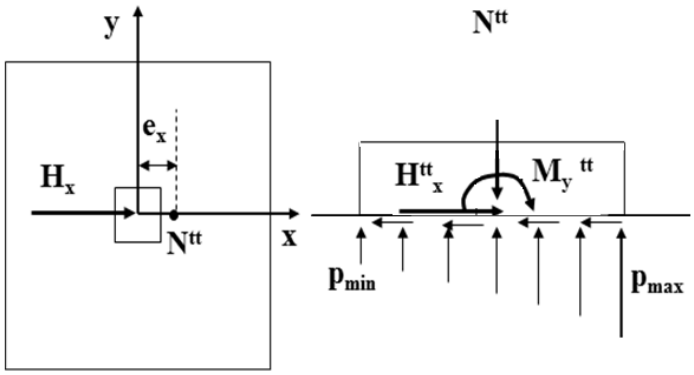

Figure 2.6: Vertical, Horizontal and eccentric loads applied to footing

A. Footings with Vertical, horizontal and eccentric loads combined - One way Eccentricity problem

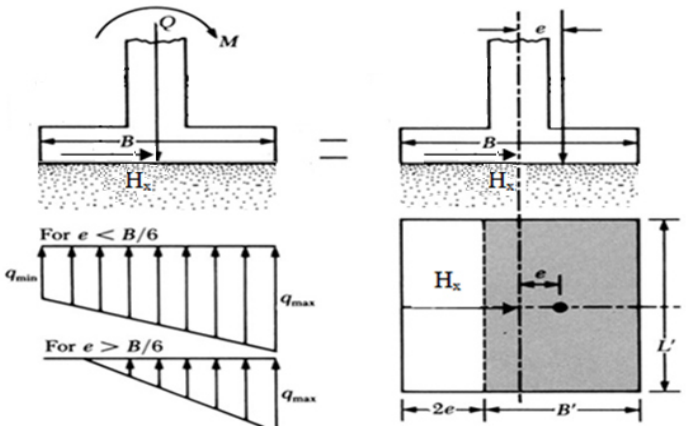

Figure 2.7: Footings with one way eccentricity

The effective width now: $B' = B - 2e$. Whereas the effective length is still $L' = L$

The distribution of the nominal pressure is:

$$q_{\max} = \frac{Q}{BL} + \frac{6M}{B^2 L} \tag{2.13}$$

$$q_{\min} = \frac{Q}{BL} - \frac{6M}{B^2 L} \tag{2.14}$$

where Q is the load vertical load and M is the moment on the footing in one axis

The distance e is the eccentricity of the load, or

$$e = \frac{M}{Q} \tag{2.15}$$

Substituting:

$$q_{\max} = \frac{Q}{BL}\left(1 + \frac{6e}{B}\right) \tag{2.16}$$

and

$$q_{\min} = \frac{Q}{BL}\left(1 - \frac{6e}{B}\right) \tag{2.17}$$

- Note that in these equations, when the eccentricity e becomes B/6, q_{min} is zero.

- For e > B/6, q_{min} will be negative, which means that tension will develop.

- Because soils can sustain very little tension, there will be a separation between the footing and the soil under it.

- Also note that the eccentricity tends to decrease the load bearing capacity of a foundation.

- In such cases, placing foundation column off-center, as shown in Figure is probably advantageous.

- Doing so in effect, produces a centrally loaded foundation with a uniformly distributed pressure.

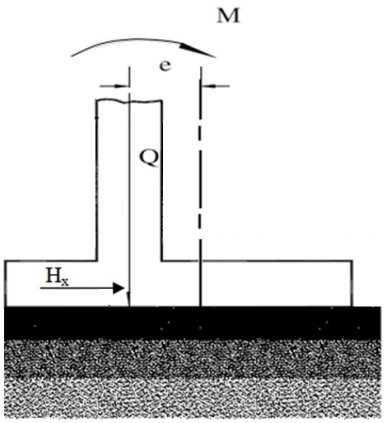

Figure 2.8: A footing with the column off - center to preserve a uniform pressure on the soil

The general bearing capacity equation is therefore modified to,

$$q'_u = c' N_c . s_c . i_c . d_c + \gamma . D_f . N_q . s_q . d_q . i_q + 0.5 . \gamma . B . N_\gamma . s_\gamma . d_\gamma . i_\gamma \qquad (2.18)$$

and $Q_u = q'_u . B' . L'$ (2.19)

B. Footings with Vertical, horizontal and eccentric loads combined - Twoway Eccentricitys problem

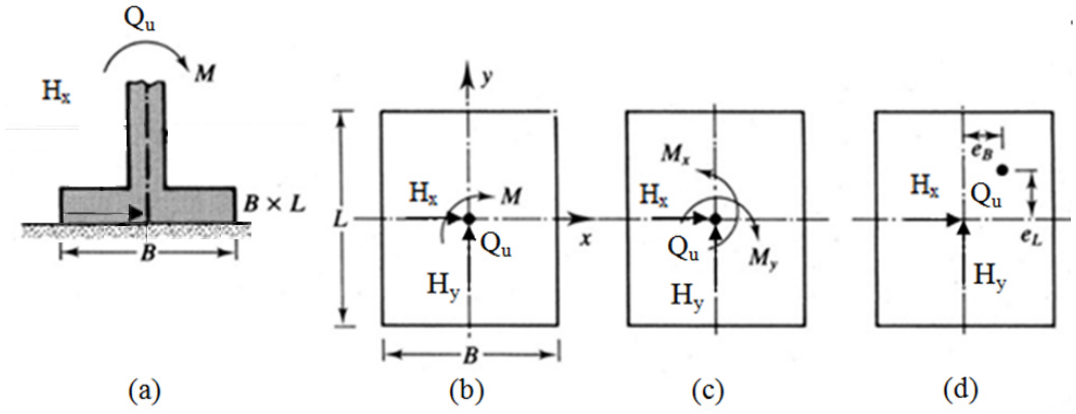

Figure 2.9: Footings with two way eccentricities

If Q_{ult} is needed, it can be obtained as $Q_{ult} = q_u^{'}.A'$ (2.20)

where $$q_u^{'} = c'N_c.s_c.i_c.d_c + \gamma.D_f.N_q.s_q.d_q.i_q + 0.5.\gamma.B.N_\gamma.s_\gamma.d_\gamma.i_\gamma \quad (2.21)$$

and A' is the effective area $B'.L'$: $A' = B'.L'$ (2.22)

Finally $Q_{ult} = q'_u.A'$ (2.23)

As before, to evaluate s_c, s_q, s_γ, use the effective length (L') and the effective width (B') dimensions instead of L and B, respectively. To calculate d_c, d_q, d_γ, do not replace B with B'. In determining the effective area (A'), effective width (B'), and the effective (L'), four possible cases may arise (Highter and Anders, 1985).

Case 1: $e_L/L \geq 1/6$ and $e_B/B \geq 1/6$

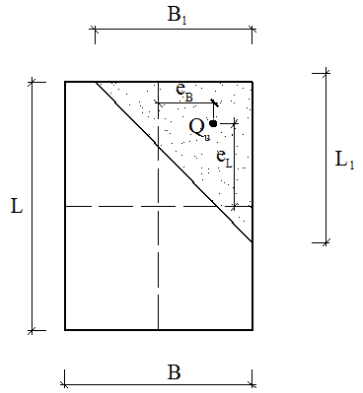

Figure 2.10: Effective area in Case $e_L/L \geq 1/6$ and $e_B/B \geq 1/6$

Effective area shown in Figure 2.5:

$$A' = \frac{1}{2}B_1.L_1 \quad (2.24)$$

where

$$B_1 = B.\left(1.5 - \frac{3e_B}{B}\right) \quad (2.25)$$

$$L_1 = L.\left(1.5 - \frac{3e_L}{L}\right) \quad (2.26)$$

Chose effective length $L' = \max(L_1, B_1)$

and B':

$$B' = \frac{A'}{L'} \quad (2.27)$$

Case 2: $e_L/L < 0.5$ and $e_B/B < 1/6$

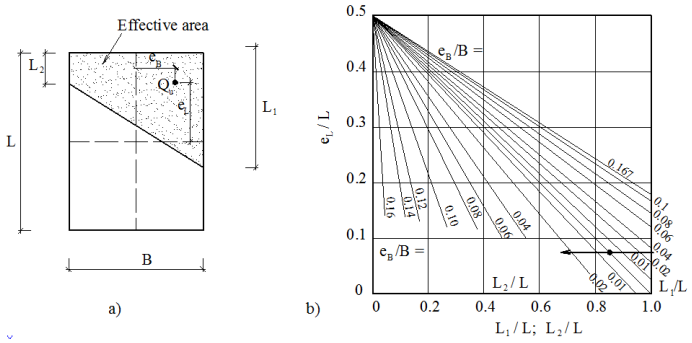

Figure 2.11: Effective area in Case $e_L/L < 0.5$ and $e_B/B < 1/6$

Effective area shown in Figure 2.6a:

$$A' = \frac{1}{2}(L_1 + L_2).B \tag{2.28}$$

L_1 and L_2 value are defined from the figure 2.6b. The effective width:

$$B' = \frac{A'}{\max(L_1, L_2)} \tag{2.29}$$

and effective length $L' = \max(L_1, L_2)$

Case 3: $e_L/L < 1.6$ and $0 < e_B/B < 0.5$

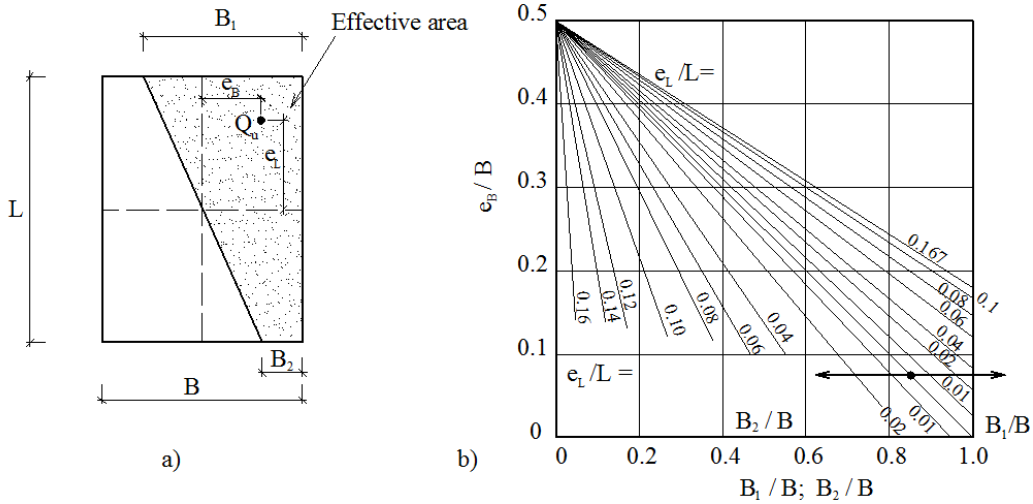

Figure 2.12: Effective area in Case $e_L/L < 1.6$ and $0 < e_B/B < 0.5$

Effective area shown in Figure 2.7a:

$$A' = \frac{1}{2}(B_1 + B_2).L \tag{2.30}$$

The effective width:

$$B' = \frac{A'}{L} \tag{2.31}$$

and effective length $L' = L$

B_1 and B_2 value are defined from the figure 2.12b.

Case 4: $e_L/L < 1.6$ and $e_B/B < 1.6$

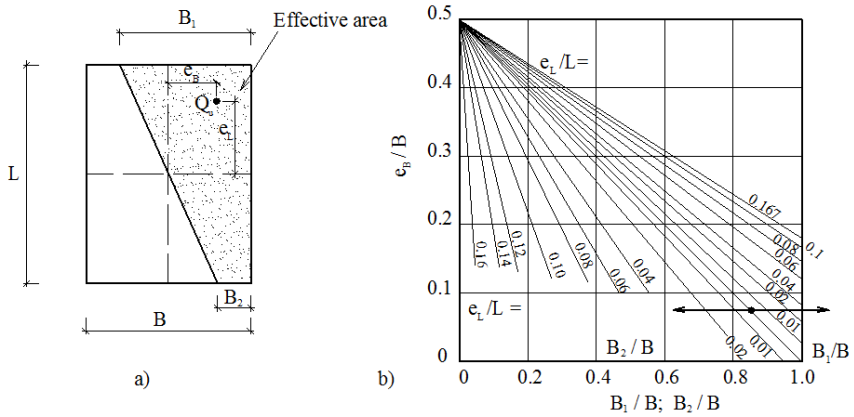

Figure 2.13: Effective area in Case $e_L/L < 1.6$ and $e_B/B < 1.6$

Effective area shown in Figure 2.13a

B_2 value defined when known B_2/B and B_2/B defined from the figure 2.8 based on diagrams has a line e_L/L going up.

The same L_2 value defined when known L_2/L and L_2/L defined from the figure 2.8 based on diagrams has a line e_L/L going down. Now Effective area:

$$A' = L_2.B + \frac{1}{2}(B + B_2).(L - L_2) \tag{2.32}$$

The effective width:

$$B' = \frac{A'}{L} \tag{2.33}$$

and effective length $L' = L$

2.1.3 Review of ultimate bearing capacity on multi-layered ground system

Button (1953) analyzed the bearing capacity of a strip footing resting on two layers of clay. He assumed that the cohesive soils in both layers are consolidated approximately to the same degree. In order to determine the ultimate bearing capacity of the footing, he assumed that the failure surface at the ultimate load is cylindrical, where the curve lies at the edge of the footing. The bearing capacity factor used depends on the upper soil layer and on the ratio of the cohesions of the lower/upper clay layers.

Brown and Meyerhof (1969) investigated foundations resting on a stiff clay layer overlying a soft clay layer deposit, and the case of a soft layer overlying a stiff layer. They assumed that the footing fails by punching through the top layer for the first case, and with full development of the bearing capacity of the lower layer in the second case. Equations and charts giving the appropriate modified bearing capacity factors were given, derived from the empirical relationships obtained based on the experimental results. The results of the investigation are summarized in charts, which may be used in evaluating the bearing capacity of layered clay foundations, but these results are essentially experimental, and therefore are strongly affected by the characteristics of the clay tested. The purpose of this paper is to present the results of a series of model footing tests carried out on twolayered clay soils, and the models have many limitations. First, they are limited to one type of clay, although the strength of the clay was varied, the deformation property remained constant. Second, studies were limited to surface loading only, using rigid strip and circular footings with rough bases. Third, all studies were made in terms of the undrained shear strength of the clay, using the $\Phi = 0$ analyses. They also conducted a series of tests on footings in homogeneous clay. They observed that the pattern of failure beneath a footing is a function of the physical mode of rupture of the clay, which is strongly dependent on the structure of the clay. The failure mechanism of the structure of the clay is not adequately defined by conventional Mohr-Coulomb concepts of cohesion and friction.

Meyerhof (1974) investigated the case of sand layer overlying clay: dense sand on soft clay and

loose sand on stiff clay. The analyses of different modes of failure were compared with the results of model test results on circular and strip footings and field data. In the case of dense sand overlying a soft clay deposit, the failure mechanism was assumed as an approximately truncated pyramidal shape, pushed into the clay so that, in the case of general shear failure, the friction angle Φ of the sand and the undrained cohesion C of the clay are mobilized in the combined failure zones. Based on this theory, semi-empirical formulae were developed to calculate the bearing capacity of strip and circular footings resting on dense sand overlying soft clay. He conducted model tests on strip and circular footings on the surface and at shallow depths in the dense sand layer overlying clay. The results of these tests, and the filed observations were found to agree with the theory developed. In the case of loose sand on stiff clay, the sand mass beneath the footing failed laterally by squeezing at an ultimate load. Formulae for the ultimate bearing capacity of strip and circular footings were developed.

Model tests were carried out on strip and circular footings, and the results also agreed with the theory developed. Theory and test results showed that the influence of the sand layer thickness beneath the footing depends mainly on the bearing capacity ratio of the clay to the sand, the friction angle Φ of the sand, the shape and depth of the foundation. The paper is limited to vertically loaded footings, and does not include eccentric or inclined loads, it is also limited to sand over clay, and has no solution for clay over sand. In the case of dense sand on soft clay, the theory considers simultaneous failure of the sand layer by punching, and general shear failure in the clay layer, which is not always the case.

Meyerhof and Hanna (1978) considered the case of footings resting in a strong layer overlying weak deposit and a weak layer overlying strong deposit. The analyses of different soil failure were compared with the results of model tests on circular and strip footings on layered sand and clay. They developed theories to predict the bearing capacity of layered soils under vertical load and inclined loading conditions. In the case of a strong layer overlying a weak deposit, considering the failure as an inverted uplift problem, an approximate theory of the ultimate bearing capacity was developed. At failure, a soil mass, roughly shaped like a truncated pyramid, of the upper layer is pushed into the underlying deposit in the approximate direction of the applied load. The forces developed on the actual punching failure surface in the upper layer are

the total adhesion force and total passive earth pressure inclined at an average angle δ acting upwards on an assumed plane inclined at an angle α to the vertical. The analysis for strip footings was extended to circular and rectangular footings, and approximate formulae for the bearing capacity of strip, rectangular, and circular footings were developed, taking into consideration the case of eccentric and inclined loading as well. Model tests on rough strip and circular footings under central inclined loads at varying angles α were made on the surface and at shallow depth in different cases of two layered soils of sand and clay, where good agreement was found between the theoretical and experimental results.

In the case of a weak layer overlying a strong deposit, considering the weak soil mass beneath the footing may fail laterally by squeezing, which is the same theory as from the previous paper developed the theory of the ultimate bearing capacity. The bearing capacity can be estimated by the approximate semi-empirical formulae. Model tests were also carried out on strip and circular footings under vertical and inclined loads, and the results of the tests were compared to the theoretical ones. The authors concluded that the ultimate bearing capacity of footings on a dense layer overlying a weak layer can be expressed by inclination factors in conjunction with punching shear coefficients, which depend on the shear strength parameters and bearing capacity ratio of the layers under vertical loads. Formulae and design charts were developed and introduced in this paper. This paper is a development of the previous theory (Meyerhof 1974), taking into consideration all possible cases of two different layers of subsoil, and also including the effect of inclined and eccentric loading on the ultimate bearing capacity of strip, rectangular and circular footings. This theory and the failure mechanism considered are approximations of the real failure mechanism, which depends on many factors. Hanna and Meyerhof (1979) extended their previous theory of the ultimate bearing capacity of two-layer soils to the case of three-layer soils. The analysis compared well with the results of model tests of strip and circular footings on a three-layer soil. Only one case was considered in this paper, that for footings subjected to vertical loads and resting on subsoil consisting of two strong layers overlying a weak deposit.

The same theoretical failure mechanism was assumed by considering a soil mass of the upper two layers is pushed into the lower layer, and the same forces acting on the failure surface was

assumed as well. Formulae and charts were developed and can be used in designing foundations having the same conditions. Model tests on rough strip and circular footings under central vertical loads were made on the surface of three-layer sand consisting of two dense upper layers and a loose lower one. By comparing the results of the model tests with the results of the punching theory, good agreement was found. Briefly, this paper is an extension of the previous theory in order to include the case of the three-layer soil. But, it is restricted to only one case of three-layer soil, and it needs more development to include all possible cases of three-layer soils. **Pfeifle and Das (1979)** presented laboratory model tests results for the case of rough rectangular footings in sand with a rigid rough base located at a limited depth. The results were compared to the predicted results of Mandel and Salencon (1972) and Meyerhof (1974). The authors concluded that the critical depth of location of the rough rigid base beyond which it has no effect on the value of the ultimate bearing capacity is about 50% - 75% higher than that predicted by the theory. And the previous theories do not predict correctly the bearing capacity for the case when the rigid base is located at shallow depth. This experimental investigation is very limited to one case of layered soils, and the friction angle Φ of the sand used varies in a small range (42° - 45°), and the conclusion may be valid only for this range of Φ. Hanna and **Meyerhof (1981)** investigated experimentally the ultimate bearing capacity of footings subjected to axially inclined loads by conducting tests on model strip and circular footings on homogeneous sand and clay. The results were analyzed to determine the inclination factors, depth factors and the shape factors incorporated in the general bearing capacity equation for shallow foundations. These values were compared with the recommended values given in the Canada Foundation Engineering Manual. The values of these factors given in the manual agree reasonably well with the experimental ones, except for the depth and shape factors, for which the theoretical values are on the conservative side when applied to inclined loads. Hanna (1981) extended his previous theory to cover the case of footings resting on subsoil consisting of a strong sand layer overlying a weak sand deposit. Applying the same theory that at ultimate load, a soil mass of the upper layer is pushed to the lower sand layer, and by calculating the forces on the assumed vertical punching failure surface, the ultimate bearing capacity can be calculated theoretically. Charts are presented in this paper and can be used in the design of footings. In order to verify the theory presented, model tests on strip and circular footings resting on a dense

sand layer overlying loose sand layer were done, and the results of the tests agreed well with the theory presented. 19 Hanna (1981) conducted an experimental investigation on the ultimate bearing capacity of strip and circular model footings on a two-layered soil in order to verify the validity of the empirical method proposed by Satyanarayana and Garg (1980) to predict numerically the ultimate bearing capacity of footings on layered soils. Summary of the results was presented in the form of comparative charts in order to compare the experimental and theoretical results. The author concluded that by extensive comparisons between the observed ultimate bearing capacity values and those calculated by the method reveal discrepancies ranging between70% to 85%. Thus, the method needs more refinement and further investigation before it can be recommended for practical applications. Hanna (1982) investigated the case of footings resting on subsoil consisting of a weak sand layer overlying a dense sand deposit. Based on model tests of strip and circular footings, the author extended the classical equation of bearing capacity to cover cases of these footings in layered sand; consisting of weak sand layer overlying a dense sand deposit. In order to calculate the ultimate bearing capacity of these footings, the author proposed to use the classical equation of homogeneous sand in conjunction with the modified bearing capacity factors. These factors depend on the relative strength of the upper and lower layers and the thickness of the upper weak sand layer, and are calculated from the model tests results conducted on similar soil profiles. Design charts were presented as an aid in design. According to the theory presented in this paper, the failure mechanism of the upper layer is the same as if the footing was in a homogeneous deep sand layer, and the influence of the layered soil is restricted to the difference in the bearing capacity factors, which were calculated experimentally from model tests. It is a simple method to overcome the complexity of finding the real failure mechanism, and it gives fairly accurate results. But the values of the bearing capacity factors depend on the kind of sand used in the tests, and they may change by using different kind of sands taken from different places.

Das (1988) presented a technique to improve the ultimate bearing capacity and settlement conditions of shallow foundations on soft clay soil, which consists of placing the footings over a compact granular fill, lay over the clay layer. Placing geotextile at the interface of the clay layer and the sand layer can further increase the bearing capacity. The purpose of placing the granular layer is to distribute the load on a larger area of the clay layer, and the purpose of placing the

geotextile mesh is to reduce the depth of the sand layer required to distribute the load. The objective of this research was primarily to present the results of model tests conducted on a strip foundation resting on a sand layer overlying a weak clay layer, and compares the results with the theory of Meyerhof and Hanna (1978). Secondly, to compare results of the bearing capacity of footings on layered soil with and without the use of the geotextile mesh at the interface of the two layers in order to evaluate any advantage derived from the inclusion of the geotextile. A number of laboratory model tests results for the ultimate bearing capacity of strip footings resting on a sand layer underlain by a weak clay layer with and without the inclusion of geotextile at the interface of the two layers have been presented in this paper. Based on the experimental results; first, without the inclusion of geotextile, the results were consistent with the theory of Meyerhof and Hanna (1978). Second, the inclusion of geotextile at the interface of the layers increases the bearing capacity, and at the same time, reduces the depth of the sand layer to be placed over the clay layer. Third, the most economical width of the geotextile layer to be used as determined from the study is about four times the width of the strip footing. This paper is experimental and the conclusions deduced are strictly related to the model tests done, so the results may vary with the type of geotextile mesh used, its strength, dimensions, and the depth at which the geotextile is placed. More investigation and experiments are needed regarding the use of geotextile for increasing the bearing capacity of shallow foundations on weak soils.

Michalowski and Shi (1995) considered the bearing capacity of strip footing over a two-layer foundation soil. The kinematics approach of limit analysis is used to calculate the average limit pressure under footing. The method is applicable to any combination of parameters of the two layers, but the results are presented only for a specific case when a footing placed on a layer of a granular soil resting on clay. The depth of a collapse mechanism is found to be very much dependent on the strength of the clay. Very weak clay can attract the mechanism even at great depths. The results are presented as limit pressures rather than traditional bearing capacity coefficients. The latter are strongly dependent not only on the internal friction angle of the sand, but also on the thickness of the sand layer, cohesion of the clay, and surcharge pressure. Results are presented in the form of dimensionless charts for different internal friction angle of sand. It was found that linear interpolation within 5 increments is acceptable in the range of ϕ from 30°

to 45°.

Merifield and Sloan (1999) studied the ultimate bearing capacity of surface strip footings resting on a horizontally layered clay profile. Many empirical and semi-empirical formulae can be used, which give approximate solutions to the problem. More recently, Florkiewicz (1989) presented an upper bound method proposing a kinematically admissible failure mechanism. Although this method is useful, but limited results were produced. The upper bound method has been widely used to estimate the bearing capacity of layered clays, but it may lead to a lower factor of safety for design that the real one. A more desirable solution is a lower bound estimate, as it results in a safe design and, if used in conjunction with an upper bound solution, serves to bracket the actual collapse load from above and below. The purpose of this paper is to take advantage of the ability of the limit theorems to bracket the actual collapse load by computing both types of solution for the bearing capacity of footings on a two-layered clay profile. These solutions are obtained using the numerical techniques developed by Sloan (1988) and Sloan **Ming Zhu and Radoslaw L. Michalowski (2005)** examined earlier proposals for shape factors used in calculations of bearing capacity of square and rectangular footings. These proposals are based on empirical data for small footings, whereas a new suggestion for these factors presented in this study is based on the elasto-plastic model of the soil and finite element analysis. The earlier factors modifying the contribution of cohesion and overburden were found to be conservative, but acceptable in design. However, bearing Capacity Factor N_c*27 proposals for the shape factor that affects the contribution of the soil weight to the bearing capacity indicate contradictory trends, and the factor calculated in this paper is suggested as an alternative. ZenonSzypcio and KatarzynaDolzyk (2006) analyzed various methods for calculation of the bearing capacity of layered subsoil. The values obtained are compared with the values calculated by means of PLAXIS Version 8, the latter being considered the correct ones. It is shown that Polish Standards and proposition modified by the authors are admissible to use only in the case of subsoil with a weak cohesionless lower layer, with small angle of friction. From the engineering point of view only the layer thickness H = 2B influences the subsoil bearing capacity. Accordingly to the Polish Standards the substitute foundation can be laid only on the top of a very weak cohesionless lower layer. The simpler authors' modification of the Polish Standards proposition for that case is also correct. The most general, simple and correct

calculation of the bearing capacity of layered subsoil is done based on the Terzaghi formula with average parameters of homogeneous subsoil. There is no big difference in the bearing capacity if we use a direct formula for calculating the average angle of friction or indirect formula. In this paper, the investigation was carried out only for strip and square foundations of the width B =1.0 m loaded symmetrically and vertically. In authors' opinion, similar conclusions are correct for other loaded foundations of different size and shape. Ming Zhu and Radoslaw L. Michalowski (2010) presented a finite element analysis of square and rectangular footings over two-layer clay foundation soil. Bearing capacity results are shown for a limited range of parameters. While the bearing capacity is distinctly affected by both the ratio of the strengths of the two layers and the depth of the weak layer, the shape factors are only dependent on the depth ratio. The bearing capacity of clay is reduced if a weaker layer of clay is present below a stronger crust. The limit load is affected by both the depth of the weaker layer and the ratio of the strengths of the two layers. However, the shape factor appears to be only weakly dependent on the depth, whereas it varies distinctly with a change in the strength ratio of the two layers.

Ming Zhu and Radoslaw L. Michalowski (2010) presented a finite element analysis of square and rectangular footings over two-layer clay foundation soil. Bearing capacity results are shown for a limited range of parameters. While the bearing capacity is distinctly affected by both the ratio of the strengths of the two layers and the depth of the weak layer, the shape factors are only dependent on the depth ratio. The bearing capacity of clay is reduced if a weaker layer of clay is present below a stronger crust. The limit load is affected by both the depth of the weaker layer and the ratio of the strengths of the two layers. However, the shape factor appears to be only weakly dependent on the depth, whereas it varies distinctly with a change in the strength ratio of the two layers.

2.2 Literature on Rigid plastic finite element method

2.2.1 Limit analysis and application to finite element method

In contrast to slip-line and limit equilibrium methods, the limit analysis method considers the stress-strain relationship of a soil in an idealized manner. This idealization, termed normality (or

the flow rule), establishes the limit theorems on which limit analysis is based. Within the framework of this assumption, the approach is rigorous and the techniques are competitive with those of limit equilibrium, in some instances being much simpler. The plastic limit theorems of Drucker et al. (1952) may conveniently be employed to obtain upper and lower bounds of the collapse load for stability problems, such as the critical heights of unsupported vertical cuts, or the bearing capacity of nonhomogeneous soils.

One of the most important problems in Geomechanics is to analysis the limit state of soil structures such as foundations and slopes. There are many methods applied to this problem. A large number of material constants, however, must be specified before-hand and an elaborate step by step calculation is necessary to pursue along the loading history from the initial state. Although such an approach is accepted to some extend from a practical point of view, no exact information is offered concerning the limit state itself since the usual calculation procedure breaks down and becomes meaningless at this stage.

Slip line theory is a well-known method to analyze the limit state, in which the characteristics of hyperbolic type of equations are composed in several ways. Many closed form solutions are obtained for typical problems by this method. However, skillful techniques are required to get solutions with a good accuracy and it difficult to use the slip line theory as an approach for general boundary conditions.

Hill (1951) and Drucker (1951, 1952) published their ground breaking lower and upper bound theorems of plasticity theory, on which limit analysis is based. It is apparent that limit analysis would be an effective tool to provide important insights into the bearing capacity problem. The complete formulation of these theorems is easy for numerical analysis since it can be converted into the primal and dual linear programming problems (Charnes, Lemke and Zienkiewicz, 1959; Martin, 1975; Sloan et al., 2005; Sloan et al., 2009).

For instance, the elasto-plastic finite element method is considered to be a typical one. But it is often said that it suffers from some numerical difficulty in the stress range close to the limit state. Therefore different techniques for this problem are required to be established. Tamura et al. (1984) developed the rigid plastic finite element method with Drucker-Prager yield criterion which is only to analyze limit state of structures. First, they derive stress-strain rate relations with the concept of indeterminate stress. Second, substituting these into the equation of

equilibrium, the formulated the rigid plastic finite element method in a simple way. Equations to be solved consist of the condition of equilibrium, the constraint condition of volumetric change and a relation to normalize the magnitude of displacement velocity.

2.2.2 The fundamental of the rigid plastic finite element method

The most widely used theory is to assume that the plastic strain rate (or increment) can be determined by the following formula (Von Mises, 1928; Melan, 1938; Hill, 1950):

$$d(\varepsilon_{ij}^{p}) = d\lambda \frac{\partial f}{\partial \sigma_{ij}} \tag{2.34}$$

where $d\lambda$ is a positive scalar, and

$$f = f(\sigma_{ij}) = f(I_1, I_2, I_3) = 0 \tag{2.35}$$

If the plastic potential is the same as the yield surface, then the plastic flow rule equation (2.34) is called the associated flow (or normality) rule. Otherwise it is called non-associated flow rule.

If the unit normal to the plastic potential approaches a finite number of linearly independent limiting values as the stress point approaches the singular point in question. Koiter (1953) proposes the following generalized flow rule:

$$d(\varepsilon_{ij}^{p}) = \sum_{i=1}^{n} d\lambda_i \frac{\partial f_i}{\partial \sigma_{ij}} \tag{2.36}$$

where $d\lambda_i$ are nonnegative and $\frac{\partial f_i}{\partial \sigma_{ij}}$ are the linearly independent gradients.

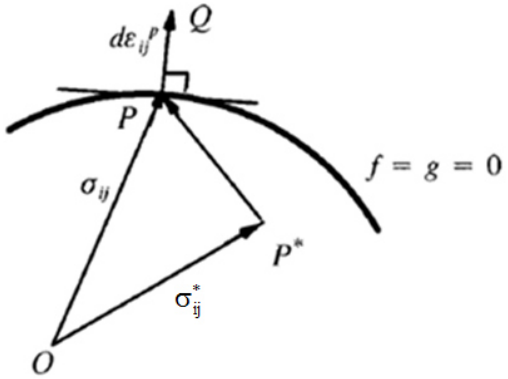

Fig.2.14Maximum plastic work principle

Suppose the plastic strain rate $d\varepsilon_{ij}^{p}$ is given and the corresponding stress state, σ_{ij}, determined from the normality rule and the yield criterion, is represented by a point P in the stress path in Fig 2.14. If σ_{ij}^{*} is an arbitrary allowable stress represented by a point P^{*} on or inside the yield surface, then the difference between the incremental plastic works done by the two stress states on the actual plastic strain rate is

$$dW = \left(\sigma_{ij} - \sigma_{ij}^{*}\right)d\varepsilon_{ij}^{p} \tag{2.37}$$

Eq. 2.37 represents the scalar product of the vector $P^{*}P$ and PQ. If the yield surface is strictly convex, the angle between these vectors is acute and the scalar product is positive. Therefore

$$\left(\sigma_{ij} - \sigma_{ij}^{*}\right)d\varepsilon_{ij}^{p} > 0 \tag{2.38}$$

This condition, due to Von Mises (1928) and Hill (1948, 1950), is known as the maximum plastic work principle or theorem. Equation (2.38) is the basic for a number of important theorems concerning elastic-plastic solids. The maximum plastic work principle is always unique. It is a mathematical statement of the important idea that the plastic strain rate (or increment) is normal to the yield surface.

To obtain definitions applicable to general stress states, we will adopt the proposal of Drucker (1951, 1964). Hypothesis of Drucker is maximum plastic work principle $\left(\sigma_{ij} - \sigma_{0}\right)d\varepsilon_{ij}^{p} \geq 0$.

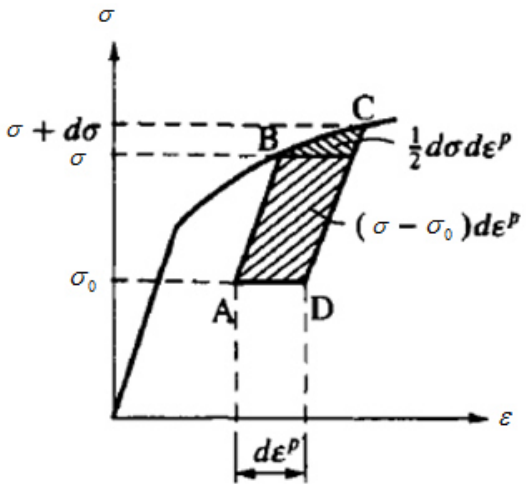

Fig.2.15 Stress cycle when the starting point A is below the current yield stress

Drucker's postulate makes use of a stress cycle and to illustrate this concept as in Fig 2.15. First the material had been load to point B and then unloaded elastically to point A. the state indicated by point A with the stress σ_0 is now considered as the existing state of the material. We now image that an additional load is the first applied to the material; this brings us to point B with the stress σ. The additional load is now increased by the infinitesimal amount $d\sigma$ and this brings us to point C with the stress $\sigma + d\sigma$. Then the entire additional load is removed and the material therefore unloads elastically to point D with the stress σ_0 equal to the stress at point A. It appears that the additional load has carried the material through a complete stress cycle is occasionally called an external agency.

Letting W denote the work per unit volume performed by the external agency during a complete stress cycle:

$$W = \int_{ABCD} (\sigma - \sigma_0) d\varepsilon \tag{2.39}$$

The strain increment $d\varepsilon$ consists of its elastic and plastic component $d\varepsilon = d\varepsilon^v + d\varepsilon^p$ and plastic strains only develop during load path BC.

$$\begin{aligned} W &= \int_A^B (\sigma - \sigma_0) d\varepsilon^e + \int_B^C (\sigma - \sigma_0)(d\varepsilon^e + d\varepsilon^p) + \int_C^D (\sigma - \sigma_0) d\varepsilon^e \\ &= \int_A^B (\sigma - \sigma_0) d\varepsilon^e + \int_B^C (\sigma - \sigma_0) d\varepsilon^e + \int_B^C (\sigma - \sigma_0) d\varepsilon^p + \int_C^D (\sigma - \sigma_0) d\varepsilon^e \quad (2.16) \\ &= \int_A^D (\sigma - \sigma_0) d\varepsilon^e + \int_B^C (\sigma - \sigma_0) d\varepsilon^p \geq 0 \end{aligned}$$

The first integral express the change of elastic strain energy over the stress cycle considered and therefore this integral evidently becomes equal to zero. This implies that the second term also become equal to zero.

$$W = \int_B^C (\sigma - \sigma_0) d\varepsilon^p \geq 0 \tag{2.40}$$

In this expression are illustrated in Fig. 2.15, where $\sigma > \sigma_0$, the second order becomes:

$$(\sigma - \sigma_0) d\varepsilon^p \geq 0 \tag{2.41}$$

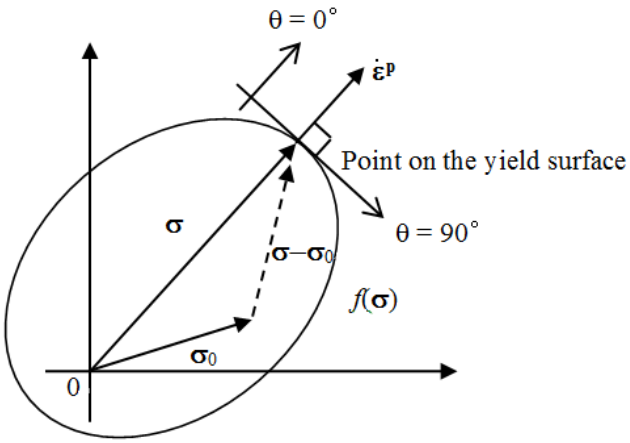

Fig.2.16 Convexity of yield surface in the stress space

It is assumed that the plastic work principle in the stress cycle is non-negative and monotonous loading is also non-negative. It will turn out that this postulate leads to the associated flow rule as well as to the convexity of the yield surface. Drucker's postulate for hardening plasticity implies the two important points: convexity of the yield surface as well as the normality principle $d(\varepsilon_{ij}^p) = d\lambda \frac{\partial f}{\partial \sigma_{ij}}$ and also ensures the uniqueness of the elasto-plastic boundary value problem.

For a given plastic strain rate $\dot{\varepsilon}_{ij}^p$, we can define the rate of specific plastic energy dissipation $D(\dot{\varepsilon}_{ij}^p)$:

$$D(\dot{\varepsilon}_{ij}) = \boldsymbol{\sigma}_{ij}\dot{\varepsilon}_{ij} \tag{2.42}$$

where $\boldsymbol{\sigma}_{ij}$ is a stress on the yield surface associated with $\dot{\varepsilon}_{ij}$ through the normality rule.

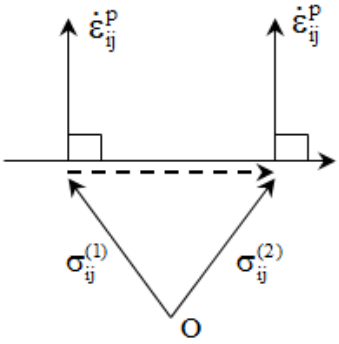

Fig.2.17 Two states of stress corresponding to a plastic strain rate

On the other hand, more than one stress state, say $\sigma_{ij}^{(1)}$ and $\sigma_{ij}^{(2)}$, may correspond to give ε_{ij}^{p} when the yield surface contains a flat face or a line as some portion of it. But $D(\varepsilon_{ij}^{p})$ can be regarded as a single valued function of ε_{ij}^{p} since the difference $\left(\sigma_{ij}^{(1)} - \sigma_{ij}^{(2)}\right)$ is always perpendicular to ε_{ij}^{p} as Fig 2.17.

The property of $D(\varepsilon_{ij}^{p})$ was shown as bellows:

i) $D(\varepsilon_{ij}^{p}) = \sigma_{ij}\varepsilon_{ij}^{p}$ is homogeneous of degree one in ε_{ij}^{p} since σ_{ij} is independent of the magnitude of ε_{ij}^{p}.

ii) The variation of D, denoted by δD, is calculated as

$$\delta D = \sigma_{ij}\delta\varepsilon_{ij}^{p} \tag{2.43}$$

iii) $D(\varepsilon_{ij}^{p})$ is convex in ε_{ij}^{p} if it is continuously differentiable.

We consider a rigid plastic material subjected to a body force X_i in a region V and a surface traction T_i on the stress boundary S_σ. This steady state of flow invariably obeys the equation of equilibrium.

$$\sigma_{ij,j} + X_i = 0 \qquad \text{(in V)} \tag{2.44}$$

and the stress boundary condition on S_σ

$$\sigma_{ij} n_j = T_i \qquad (\text{in } S_\sigma) \tag{2.45}$$

where n_j is the outward normal on the boundary of the region. In equation (2.44), "j" means the differentiation with respect to the j-th coordinate. It should be noted that the stress σ_{ij} is homogeneous of degree zero in $\dot{\varepsilon}_{ij}$.

In the other words, the magnitude of the velocity field $\dot{u}_i$ or the strain rate $\dot{\varepsilon}_{ij}$ in immaterial but the only proportional distribution of these values is crucial to determine the stress state in the

plastic flow. Here the relation between the velocity and the strain rate is assumed to be

$$\dot{\varepsilon}_{ij}^{p} = \frac{1}{2}\left(\frac{\partial u_{i,j}}{\partial x_i} + \frac{\partial u_{j,i}}{\partial x_j} \right) \qquad \text{(in V)} \tag{2.46}$$

The displacement prescribed on the displacement boundary S_σ:

$$\dot{u}_i = \dot{u}_0 \qquad (\text{in } S_\sigma) \tag{2.47}$$

The plastic collapse (at the limit load) occurs under constant the external forces $\dot{\sigma}_{ij} = 0$. Since

$\dot{\varepsilon}_{ij}^{e} = 0$ when $\dot{\sigma}_{ij} = 0$ we find that $\dot{\varepsilon}_{ij} = \dot{\varepsilon}_{ij}^{p}$ applies at the limit load.

For a complete solid body, the principle of virtual work is mathematically given by the following basic energy equation

$$\int_V \boldsymbol{\sigma}.d\dot{\varepsilon}dV = \int_{S_u} \mathbf{T}.\delta\mathbf{u}dS + \int_V \mathbf{X}.\delta\mathbf{u}dV \tag{2.48}$$

We summarize the basic equation of the rigid plastic flow as follow:

1) Equation of equilibrium equation (2.44)

2) Compatibility equation (2.46)

3) Boundary condition equation (2.45) and equation (2.47)

4) Stress-strain rate relation as constitutive equation as equation (2.49)

$$\dot{\boldsymbol{\varepsilon}} = \dot{\boldsymbol{\varepsilon}}^{e} + \dot{\boldsymbol{\varepsilon}}^{p} = A\dot{\boldsymbol{\sigma}} + \lambda \frac{\partial f(\boldsymbol{\sigma})}{\partial \dot{\boldsymbol{\sigma}}} \tag{2.49}$$

When the plastic collapse occurs, the virtual work can obtain constant the external forces $\rho\mathbf{T}$, the stress $\boldsymbol{\sigma}$ and $\boldsymbol{\sigma} + \dot{\boldsymbol{\sigma}}dt$ can be expressed as follows:

$$\int_V \boldsymbol{\sigma}.\delta\dot{\varepsilon}dV = \rho\int_{S_u} \mathbf{T}.\delta\mathbf{u}dS + \int_V \mathbf{X}.\delta\mathbf{u}dV \tag{2.50}$$

$$\int_V (\boldsymbol{\sigma} + \dot{\boldsymbol{\sigma}}dt).\delta\dot{\varepsilon}dV = \rho\int_{S_u} \mathbf{T}.\delta\mathbf{u}dS + \int_V \mathbf{X}.\delta\mathbf{u}dV \tag{2.51}$$

Therefore, the difference between equation (2.50) and equation (2.51) can be shown as equation (2.52)

$$\int_V \boldsymbol{\sigma}.\delta\dot{\varepsilon}dV - \rho\int_{S_u} \mathbf{T}.\delta\mathbf{u}dS + \int_V \mathbf{X}.\delta\mathbf{u}dV - \left(\int_V (\boldsymbol{\sigma} + \dot{\boldsymbol{\sigma}}dt).\delta\dot{\varepsilon}dV - \rho\int_{S_u} \mathbf{T}.\delta\mathbf{u}dS + \int_V \mathbf{X}.\delta\mathbf{u}dV \right) = 0$$

$$\Rightarrow \int_V \dot{\boldsymbol{\sigma}}dt.\delta\dot{\varepsilon}dV = \int_V \boldsymbol{\sigma}.\delta\dot{\varepsilon}dV \tag{2.52}$$

To the above equation is satisfied

$$\boldsymbol{\sigma}.\delta\dot{\varepsilon} = 0 \tag{2.53}$$

Based on the hypothesis of Drucker $\sigma\varepsilon^{p} \geq 0$, this condition becomes:

$$\boldsymbol{\sigma}.\delta\dot{\varepsilon} = \boldsymbol{\sigma}.\delta\dot{\varepsilon}^{e} + \boldsymbol{\sigma}.\delta\dot{\varepsilon}^{p} = 0 \tag{2.54}$$

It is useful to know if the consistent distribution of stresses produced by applied surface displacement is unique, or if it depends upon the state of stress beforehand. Two answer this question, Hill (1948, 1950) proved that for a rigid-plastic solid there is not more than one consistent stress solution for which the hole mass deforms plastically. Suppose that $\left(\boldsymbol{\sigma}(1),\dot{\varepsilon}^{p}(1)\right)$ and $\left(\boldsymbol{\sigma}(2),\dot{\varepsilon}^{p}(2)\right)$ could be two consistent solutions corresponding to the same boundary conditions. It can be show that

$$\int_{V}\left\{\left(\boldsymbol{\sigma}(1)-\boldsymbol{\sigma}(2)\right)\left(\delta\dot{\varepsilon}(1)-\delta\dot{\varepsilon}(2)\right)\right\}=0 \tag{2.55}$$

This condition is satisfied when either the surface displacements or the external forces are prescribed. The whole masses are possible in the plastic state. It is obvious that as long as the yield surface is convex they are all positive unless the two solutions for the stresses are the same $\boldsymbol{\sigma}(1)=\boldsymbol{\sigma}(2)$. We have therefore proved that in a rigid plastic material, there cannot be two distinct plastic stress solutions that satisfy the same boundary conditions.

2.2.3 Rigid plastic finite element method based on the upper bound theorem

Load factor ρ of external forces

Let T_i be the surface force and X_i be the body force in V and the traction on the traction boundary S_σ, respectively. A proportional increase or decrease of external forces is expressed as ρT_i . $\dot{\mathbf{u}}$ is some velocity field defined over the whole region V.

When the plastic collapse occurs, the virtual work can obtain constant the external forces $\rho\mathbf{T}$, the stress $\boldsymbol{\sigma}$ can be expressed as follows:

$$\int_{V}\boldsymbol{\sigma}:\dot{\varepsilon}dV = \rho\int_{S_\sigma}\mathbf{T}.\dot{\mathbf{u}}dS + \int_{V}\mathbf{X}.\dot{\mathbf{u}}dV \tag{2.56}$$

The stress strain rate relationships obtained here replace the stress by strain rate $\dot{\varepsilon}$ and λ . The

strain rate is related to the velocity by

$$\dot{\boldsymbol{\varepsilon}} = \dot{\boldsymbol{\varepsilon}}^{p} = \frac{1}{2}\left(\frac{\partial \mathbf{u}}{\partial \mathbf{x}} + \frac{\partial \mathbf{u}^{T}}{\partial \mathbf{x}} \right) \tag{2.57}$$

To prove the upper bound theorem, we consider

$$\int_{V} (\boldsymbol{\sigma} - \boldsymbol{\sigma}_{0}) : \dot{\varepsilon} dV \tag{2.58}$$

In general this stress field will not be in equilibrium. From the principle of maximum plastic work, it is obvious that the expression is non-negative, namely

$$\int_{V} (\boldsymbol{\sigma} - \boldsymbol{\sigma}_{0}) : \dot{\varepsilon} dV \geq 0 \tag{2.59}$$

which leads to

$$\int_{V} \boldsymbol{\sigma} : \dot{\varepsilon} dV \geq \int_{V} \boldsymbol{\sigma}_{0} : \dot{\varepsilon} dV \tag{2.60}$$

The correct stress field determined from the principle of virtual work from the right-hand side of the above equation, and substituting external force work rate in equation (2.56)

$$\int_{V} \boldsymbol{\sigma} : \dot{\varepsilon} dV \geq \rho \int_{S\sigma} \mathbf{T}.\dot{\mathbf{u}} dS + \int_{V} \mathbf{X}.\dot{\mathbf{u}} dV \tag{2.61}$$

Therefore, load factor ρ can be defined:

$$\rho \leq \frac{\int_{V} \boldsymbol{\sigma} : \dot{\varepsilon} dV - \int_{V} \mathbf{X}.\dot{\mathbf{u}} dV}{\int_{S\sigma} \mathbf{T}.\dot{\mathbf{u}} dS} \tag{2.62}$$

According to the mathematical programming theory, equation (2.62) can be formulated as follows in the absence of body force:

$$\rho = \min \int_{V} \boldsymbol{\sigma} : \dot{\varepsilon} dV \tag{2.63}$$

Subjected to $$\int_{S\sigma} \mathbf{T}.\dot{\mathbf{u}} dS = 1 \tag{2.64}$$

2.2.4 Rigid plastic finite element method with the Mises yield criterion

Mises criterion

$$f = \frac{1}{2}\left(\mathbf{s} : \mathbf{s} - \sigma_{0}^{2} \right) = 0 \tag{2.65}$$

When we apply a flow rule to yield function equation (2.63), strain rate is finally determined as in equation (2.66). Here, P is the mean stress.

$$\begin{aligned}\dot{\boldsymbol{\varepsilon}} &= \lambda\frac{\partial f(\boldsymbol{\sigma})}{\partial\boldsymbol{\sigma}} = \lambda\frac{\partial f}{\partial\boldsymbol{\sigma}}\left(\frac{1}{2}\left(\mathbf{s}:\mathbf{s}-\sigma_0^2\right)\right) = \frac{1}{2}\lambda\left(\frac{\partial(\mathbf{s}:\mathbf{s})}{\partial\boldsymbol{\sigma}}-\frac{\partial\left(\sigma_0^2\right)}{\partial\boldsymbol{\sigma}}\right)\\ &= \frac{1}{2}\lambda\left(\frac{\partial(\mathbf{s})}{\partial\boldsymbol{\sigma}}:\mathbf{s}+\mathbf{s}:\frac{\partial(\mathbf{s})}{\partial\boldsymbol{\sigma}}-\frac{\partial\left(\sigma_0^2\right)}{\partial\boldsymbol{\sigma}}\right) = \frac{1}{2}\lambda\left(2\frac{\partial(\mathbf{s})}{\partial\boldsymbol{\sigma}}:\mathbf{s}-2\sigma_0\frac{\partial\left(\sigma_0^2\right)}{\partial\boldsymbol{\sigma}}\right)\\ &= \lambda\left(\frac{\partial(\mathbf{s})}{\partial\boldsymbol{\sigma}}:\mathbf{s}\right) = \lambda\left(\frac{\partial(\boldsymbol{\sigma}-\mathrm{P}\mathbf{I})}{\partial\boldsymbol{\sigma}}:\mathbf{s}\right) = \lambda\left(\frac{\partial(\boldsymbol{\sigma})}{\partial\boldsymbol{\sigma}}-\mathrm{P}\frac{\partial(\mathbf{I})}{\partial\boldsymbol{\sigma}}\right):\mathbf{s}\\ &= \lambda\left(\frac{\partial(\boldsymbol{\sigma})}{\partial\boldsymbol{\sigma}}:\mathbf{s}\right) = \lambda\mathbf{s}\end{aligned} \tag{2.66}$$

Here

$$\frac{\partial(\boldsymbol{\sigma})}{\partial\boldsymbol{\sigma}} = \frac{\partial\begin{bmatrix}\sigma_{11} & \sigma_{12} & \sigma_{13}\\ \sigma_{21} & \sigma_{22} & \sigma_{23}\\ \sigma_{31} & \sigma_{32} & \sigma_{33}\end{bmatrix}}{\partial\boldsymbol{\sigma}} = \begin{bmatrix}\frac{\partial\sigma_{11}}{\partial\boldsymbol{\sigma}} & \frac{\partial\sigma_{12}}{\partial\boldsymbol{\sigma}} & \frac{\partial\sigma_{13}}{\partial\boldsymbol{\sigma}}\\ \frac{\partial\sigma_{21}}{\partial\boldsymbol{\sigma}} & \frac{\partial\sigma_{22}}{\partial\boldsymbol{\sigma}} & \frac{\partial\sigma_{23}}{\partial\boldsymbol{\sigma}}\\ \frac{\partial\sigma_{31}}{\partial\boldsymbol{\sigma}} & \frac{\partial\sigma_{32}}{\partial\boldsymbol{\sigma}} & \frac{\partial\sigma_{33}}{\partial\boldsymbol{\sigma}}\end{bmatrix}$$

where

$$\frac{\partial\sigma_{11}}{\partial\boldsymbol{\sigma}} = \frac{\partial\sigma_{11}}{\partial\begin{bmatrix}\sigma_{11} & \sigma_{12} & \sigma_{13}\\ \sigma_{21} & \sigma_{22} & \sigma_{23}\\ \sigma_{31} & \sigma_{32} & \sigma_{33}\end{bmatrix}} = \begin{bmatrix}\frac{\partial\sigma_{11}}{\partial\sigma_{11}} & \frac{\partial\sigma_{11}}{\partial\sigma_{12}} & \frac{\partial\sigma_{11}}{\partial\sigma_{13}}\\ \frac{\partial\sigma_{11}}{\partial\sigma_{21}} & \frac{\partial\sigma_{11}}{\partial\sigma_{22}} & \frac{\partial\sigma_{11}}{\partial\sigma_{23}}\\ \frac{\partial\sigma_{11}}{\partial\sigma_{31}} & \frac{\partial\sigma_{11}}{\partial\sigma_{32}} & \frac{\partial\sigma_{11}}{\partial\sigma_{33}}\end{bmatrix} = \begin{bmatrix}1 & 0 & 0\\ 0 & 0 & 0\\ 0 & 0 & 0\end{bmatrix}$$

$$\frac{\partial\sigma_{12}}{\partial\boldsymbol{\sigma}} = \frac{\partial\sigma_{12}}{\partial\begin{bmatrix}\sigma_{11} & \sigma_{12} & \sigma_{13}\\ \sigma_{21} & \sigma_{22} & \sigma_{23}\\ \sigma_{31} & \sigma_{32} & \sigma_{33}\end{bmatrix}} = \begin{bmatrix}\frac{\partial\sigma_{12}}{\partial\sigma_{11}} & \frac{\partial\sigma_{12}}{\partial\sigma_{12}} & \frac{\partial\sigma_{12}}{\partial\sigma_{13}}\\ \frac{\partial\sigma_{12}}{\partial\sigma_{21}} & \frac{\partial\sigma_{12}}{\partial\sigma_{22}} & \frac{\partial\sigma_{12}}{\partial\sigma_{23}}\\ \frac{\partial\sigma_{12}}{\partial\sigma_{31}} & \frac{\partial\sigma_{12}}{\partial\sigma_{32}} & \frac{\partial\sigma_{12}}{\partial\sigma_{33}}\end{bmatrix} = \begin{bmatrix}0 & 1 & 0\\ 0 & 0 & 0\\ 0 & 0 & 0\end{bmatrix}$$

Therefore,

$$\frac{\partial(\boldsymbol{\sigma})}{\partial\boldsymbol{\sigma}}=\begin{bmatrix}\frac{\partial\sigma_{11}}{\partial\boldsymbol{\sigma}} & \frac{\partial\sigma_{12}}{\partial\boldsymbol{\sigma}} & \frac{\partial\sigma_{13}}{\partial\boldsymbol{\sigma}}\\ \frac{\partial\sigma_{21}}{\partial\boldsymbol{\sigma}} & \frac{\partial\sigma_{22}}{\partial\boldsymbol{\sigma}} & \frac{\partial\sigma_{23}}{\partial\boldsymbol{\sigma}}\\ \frac{\partial\sigma_{31}}{\partial\boldsymbol{\sigma}} & \frac{\partial\sigma_{32}}{\partial\boldsymbol{\sigma}} & \frac{\partial\sigma_{33}}{\partial\boldsymbol{\sigma}}\end{bmatrix}=\begin{bmatrix}\begin{bmatrix}1&0&0\\0&0&0\\0&0&0\end{bmatrix} & \begin{bmatrix}0&1&0\\0&0&0\\0&0&0\end{bmatrix} & \begin{bmatrix}0&0&1\\0&0&0\\0&0&0\end{bmatrix}\\ \cdots\cdots\cdots\cdots & \cdots\cdots\cdots\cdots & \cdots\cdots\cdots\cdots\\ \begin{bmatrix}0&0&0\\0&0&0\\1&0&0\end{bmatrix} & \begin{bmatrix}0&0&0\\0&0&0\\0&1&0\end{bmatrix} & \begin{bmatrix}0&0&0\\0&0&0\\0&0&1\end{bmatrix}\end{bmatrix}$$

$$\frac{\partial(\mathbf{s})}{\partial\boldsymbol{\sigma}}:\mathbf{s}=\begin{bmatrix}\begin{bmatrix}1&0&0\\0&0&0\\0&0&0\end{bmatrix} & \begin{bmatrix}0&1&0\\0&0&0\\0&0&0\end{bmatrix} & \begin{bmatrix}0&0&1\\0&0&0\\0&0&0\end{bmatrix}\\ \cdots\cdots\cdots\cdots & \cdots\cdots\cdots\cdots & \cdots\cdots\cdots\cdots\\ \begin{bmatrix}0&0&0\\0&0&0\\1&0&0\end{bmatrix} & \begin{bmatrix}0&0&0\\0&0&0\\0&1&0\end{bmatrix} & \begin{bmatrix}0&0&0\\0&0&0\\0&0&1\end{bmatrix}\end{bmatrix}:\begin{bmatrix}s_{11}&s_{12}&s_{13}\\s_{21}&s_{22}&s_{23}\\s_{31}&s_{32}&s_{33}\end{bmatrix}$$

and

$$=\left\{\begin{bmatrix}1&0&0\\0&0&0\\0&0&0\end{bmatrix}*s_{11}\right\}+\left\{\begin{bmatrix}0&1&0\\0&0&0\\0&0&0\end{bmatrix}*s_{12}\right\}+\ldots+\left\{\begin{bmatrix}0&0&0\\0&0&0\\0&0&1\end{bmatrix}*s_{33}\right\}$$

$$=\begin{bmatrix}s_{11}&s_{12}&s_{13}\\s_{21}&s_{22}&s_{23}\\s_{31}&s_{32}&s_{33}\end{bmatrix}=\mathbf{s}$$

Equivalent plastic strain rate

$$\begin{aligned}\dot{\mathbf{e}}&=\sqrt{\dot{\boldsymbol{\varepsilon}}:\dot{\boldsymbol{\varepsilon}}}=\sqrt{\lambda\mathbf{s}:\lambda\mathbf{s}}\\&=\lambda\sqrt{(\mathbf{s}:\mathbf{s})}\\&=\lambda\sqrt{\sigma_0^2}=\lambda\sigma_0\end{aligned}\tag{2.67}$$

Plastic multiplier

$$\lambda=\frac{\dot{\mathbf{e}}}{\sigma_0}\tag{2.68}$$

Therefore,

$$\dot{\boldsymbol{\varepsilon}}=\left(\frac{\dot{\mathbf{e}}}{\sigma_0}\right)\mathbf{s}\tag{2.69}$$

Meanwhile, Mises yield criterion assumed that no volumetric plastic strain rate occur under the

limit state. Here, V_l is a small area obtained by dividing a region V.

$$\int_{V_l} \dot{\varepsilon}_v dV = 0 \qquad (l = 1,2,3...n) \tag{2.70}$$

The internal dissipation rate is eventually expressed by the equation (2.71). Here, I_1 is the first invariant of the Cauchy stress tensor and $\mathbf{I}$ is the unit tensor.

$$\begin{aligned} \boldsymbol{\sigma} : \dot{\boldsymbol{\varepsilon}} &= (\mathbf{s} + P\mathbf{I}) : \dot{\boldsymbol{\varepsilon}} = \mathbf{s} : \dot{\boldsymbol{\varepsilon}} + P(\mathbf{I} : \dot{\boldsymbol{\varepsilon}}) \\ &= \mathbf{s} : \dot{\boldsymbol{\varepsilon}} + \left(\frac{1}{3} I_1\right)(\mathbf{I} : \dot{\boldsymbol{\varepsilon}}) = \mathbf{s} : \dot{\boldsymbol{\varepsilon}} + \left(\frac{1}{3}(0)\right)(\mathbf{I} : \dot{\boldsymbol{\varepsilon}}) \\ &= \mathbf{s} : \dot{\boldsymbol{\varepsilon}} \end{aligned} \tag{2.71}$$

Based on the upper bound theorem, to satisfy the boundary condition on equation (2.64), load factor ρ is equal to the minimum value from equation (2.62). Moreover, the internal dissipation rate from the flow rule is a linear function of strain rate; objective function is also a linear function on $(\dot{\mathbf{u}}, \dot{\boldsymbol{\varepsilon}})$. It is permitted, through the above explanation, to state that the limit analysis by the finite element method is formulated as the problem of finding out the saddle point $(\dot{\mathbf{u}}, k_1, \mu_1)$ of the following function:

$$\Phi(\dot{\mathbf{u}}, k_1, \mu) = \int_V \boldsymbol{\sigma} : \dot{\boldsymbol{\varepsilon}} dV - \int_V \mathbf{X}.\dot{\mathbf{u}} dV + k_1 \int_{V_l} \dot{\varepsilon}_v dV + \mu_1 \int_{S\sigma} \mathbf{T}.\dot{\mathbf{u}} dS \tag{2.72}$$

in which k_1 and μ_1 are called the Lagrange multiplier.

In addition, from the stationary condition (the value of the function does not change), the following simultaneous equations are obtained:

$$\Phi(\dot{\mathbf{u}}, k_1, \lambda) = \int_V \boldsymbol{\sigma} : \dot{\boldsymbol{\varepsilon}} dV - \int_V \mathbf{X}.\dot{\mathbf{u}} dV + k_1 \int_{V_l} \dot{\varepsilon}_v dV + \mu_1 \int_{S\sigma} \mathbf{T}.\dot{\mathbf{u}} dS \text{ for } \forall \delta\dot{\mathbf{u}} \tag{2.73}$$

Subjected to

$$\sum_{V_l \in V} \delta k_1 \int_{V_l} \delta\dot{\varepsilon}_v dV = 0 \qquad \text{for } \forall \delta k_1 \tag{2.74}$$

$$\delta\mu_1 \left(\int_{S\sigma} \mathbf{T}.\delta\dot{\mathbf{u}} dS - 1 \right) = 0 \qquad \text{for } \forall \delta\mu_1 \tag{2.75}$$

The expression (2.73) and substituting internal dissipation rate equation (2.71), finally equation (2.76) is satisfied

$$\Phi(\dot{\mathbf{u}}, k_1, \lambda) = \int_V \boldsymbol{\sigma} : \delta\dot{\boldsymbol{\varepsilon}} dV - \int_V \mathbf{X}.\delta\dot{\mathbf{u}} dV + \sum_{V_l \in V} k_1 \int_{V_l} \delta\dot{\varepsilon}_v dV + \mu_1 \int_{S\sigma} \mathbf{T}.\delta\dot{\mathbf{u}} dS = 0$$

$$\Rightarrow \int_V \boldsymbol{\sigma} : \delta\dot{\boldsymbol{\varepsilon}} dV + \sum_{V_l \in V} k_1 \int_{V_l} \delta\dot{\varepsilon}_v dV = -\mu_1 \int_{S\sigma} \mathbf{T}.\delta\dot{\mathbf{u}} dS + \int_V \mathbf{X}.\delta\dot{\mathbf{u}} dV$$

$$\Rightarrow \int_V \boldsymbol{\sigma} : \delta\dot{\boldsymbol{\varepsilon}} dV + \sum_{V_1 \in V} k_1 \int_{V_1} (\mathbf{I} : \delta\dot{\boldsymbol{\varepsilon}}) dV = -\mu_1 \int_{S\sigma} \mathbf{T}.\delta\dot{\mathbf{u}} dS + \int_V \mathbf{X}.\delta\dot{\mathbf{u}} dV$$

$$\Rightarrow \int_V (\boldsymbol{\sigma} + k_1\mathbf{I}) : \delta\dot{\boldsymbol{\varepsilon}} dV = -\mu_1 \int_{S\sigma} \mathbf{T}.\delta\dot{\mathbf{u}} dS + \int_V \mathbf{X}.\delta\dot{\mathbf{u}} dV$$

$$\Rightarrow \int_V (\mathbf{s} + k_1\mathbf{I}) : \delta\dot{\boldsymbol{\varepsilon}} dV = -\mu_1 \int_{S\sigma} \mathbf{T}.\delta\dot{\mathbf{u}} dS + \int_V \mathbf{X}.\delta\dot{\mathbf{u}} dV$$

Therefore,

$$\int_V (\mathbf{s} + k_1\mathbf{I}) : \delta\dot{\boldsymbol{\varepsilon}} dV = -\mu_1 \int_{S\sigma} \mathbf{T}.\delta\dot{\mathbf{u}} dS + \int_V \mathbf{X}.\delta\dot{\mathbf{u}} dV \quad (2.76)$$

In the above equation, undetermined coefficients of Lagrange $(-\mu_1 = \rho)$, it is regarded as the average stress P with k_1 on the area V; it has become the virtual work equation and the equivalent in extreme conditions. Equation (2.76) is based on the maximum plastic work principle; the stress is calculated in accordance with the setting of the strain rate. Therefore, any $\dot{\boldsymbol{\varepsilon}} = 0$ will satisfy $f(\boldsymbol{\sigma}) = 0$.

Finite element method is a method for dividing up a very complicated area into small areas that can be solved in relation to each other. From equation (2.73), (2.74) and (2.75) for all area, we can divide in the small areas as the spatial discretization as bellows:

$$\int_V (\mathbf{s} + k_1\mathbf{I}) : \delta\dot{\boldsymbol{\varepsilon}} dV = -\mu \int_{S\sigma} \mathbf{T}.\delta\dot{\mathbf{u}} dS + \int_V \mathbf{X}.\delta\dot{\mathbf{u}} dV$$

$$\Rightarrow \int_V (\mathbf{s} + k_1\mathbf{m}) : (\mathbf{B}\delta\dot{\mathbf{U}}) dV = -\mu \int_{S\sigma} (\mathbf{NT}).(\mathbf{N}\delta\dot{\mathbf{U}}) dS + \int_V (\mathbf{NX}).(\mathbf{N}\delta\dot{\mathbf{U}}) dV$$

$$\Rightarrow \int_V (\mathbf{B}\delta\dot{\mathbf{U}})^T (\mathbf{s} + k_1\mathbf{m}) dV = -\mu \int_{S\sigma} (\mathbf{N}\delta\dot{\mathbf{U}})^T (\mathbf{NC}) dS + \int_V (\mathbf{N}\delta\dot{\mathbf{U}})^T (\mathbf{NX}) dV$$

$$\Rightarrow \int_V (\mathbf{B}\delta\dot{\mathbf{U}})^T (\mathbf{s} + k_1\mathbf{m}) dV = -\mu \int_{S\sigma} (\mathbf{N}\delta\dot{\mathbf{U}})^T (\mathbf{NT}) dS + \int_V (\mathbf{N}\delta\dot{\mathbf{U}})^T (\mathbf{NX}) dV$$

$$\Rightarrow \int_V \delta\dot{\mathbf{U}}^T \mathbf{B}^T (\mathbf{s} + k_1\mathbf{m}) dV = -\mu\delta\dot{\mathbf{U}}^T \int_{S\sigma} \mathbf{N}^T (\mathbf{NT}) dS + \delta\dot{\mathbf{U}}^T \int_V \mathbf{N}^T (\mathbf{NX}) dV$$

$$\Rightarrow \delta\dot{\mathbf{U}}^T \int_V \mathbf{B}^T (\mathbf{s} + k_1\mathbf{m}) dV = -\mu\delta\dot{\mathbf{U}}^T \int_{S\sigma} \mathbf{N}^T (\mathbf{NT}) dS + \delta\dot{\mathbf{U}}^T \int_V \mathbf{N}^T (\mathbf{NX}) dV$$

$$\Rightarrow \delta\dot{\mathbf{U}}^T \int_V \mathbf{B}^T (\mathbf{s}) dV + \delta\dot{\mathbf{U}}^T \int_V \mathbf{B}^T (k_1\mathbf{m}) dV = -\mu\delta\dot{\mathbf{U}}^T \int_{S\sigma} \mathbf{N}^T (\mathbf{NT}) dS + \delta\dot{\mathbf{U}}^T \int_V \mathbf{N}^T (\mathbf{NX}) dV$$

$$\Rightarrow \delta\dot{\mathbf{U}}^T \int_V \mathbf{B}^T (\mathbf{s}) dV + \delta\dot{\mathbf{U}}^T \int_V \mathbf{B}^T (k_1\mathbf{m}) dV + \mu\delta\dot{\mathbf{U}}^T \int_{S\sigma} \mathbf{N}^T (\mathbf{NT}) dS - \delta\dot{\mathbf{U}}^T \int_V \mathbf{N}^T (\mathbf{NX}) dV = 0$$

$$\Rightarrow \delta\dot{\mathbf{U}}^T \left(\int_V \mathbf{B}^T (\mathbf{s}) dV + \int_V \mathbf{B}^T (k_1\mathbf{m}) dV + \mu \int_{S\sigma} \mathbf{N}^T (\mathbf{NT}) dS - \int_V \mathbf{N}^T (\mathbf{NX}) dV \right) = 0$$

$$\Rightarrow \int_V \mathbf{B}^T(\mathbf{s})dV + \int_V \mathbf{B}^T(k_I\mathbf{m})dV + \mu\int_{S\sigma} \mathbf{N}^T(\mathbf{NT})dS - \int_V \mathbf{N}^T(\mathbf{NX})dV = 0$$

Therefore,

$$\int_V \mathbf{B}^T(\mathbf{s})dV + \int_V \mathbf{B}^T(k_I\mathbf{m})dV = -\mu\int_{S\sigma} \mathbf{N}^T(\mathbf{NT})dS + \int_V \mathbf{N}^T(\mathbf{NX})dV \quad (2.77)$$

From equation (2.74),

$$\sum_{V_I \in V} \delta k_I \int_{V_I} \delta\dot{\varepsilon}_v dV = 0$$

$$\Rightarrow \sum_{V_I \in V} \delta k_I \int_{V_I} (\mathbf{I} : \boldsymbol{\varepsilon})dV = 0$$

$$\Rightarrow \sum_{V_I \in V} \delta k_I \int_{V_I} (\mathbf{m} : (\mathbf{B}\dot{\mathbf{U}}))dV = 0$$

$$\Rightarrow \sum_{V_I \in V} \delta k_I \int_{V_I} (\mathbf{m}^T(\mathbf{B}\dot{\mathbf{U}}))dV = 0$$

$$\Rightarrow \sum_{V_I \in V} \delta k_I \left\{\int_{V_I} (\mathbf{m}^T\mathbf{B}\dot{\mathbf{U}})dV\right\} = 0$$

Therefore,

$$\int_{V_I} (\mathbf{m}^T\mathbf{B}\dot{\mathbf{U}})dV = 0 \quad (2.78)$$

From equation (2.75),

$$\delta\mu\left(\int_{S\sigma} \mathbf{T}.\delta\dot{\mathbf{u}}dS - 1\right) = 0$$

$$\Rightarrow \delta\mu\left(\int_{S\sigma} (\mathbf{NT}).(\mathbf{N}\dot{\mathbf{U}})dS - 1\right) = 0$$

$$\Rightarrow \delta\mu\left(\int_{S\sigma} (\mathbf{NT})^T(\mathbf{N}\dot{\mathbf{U}})dS - 1\right) = 0$$

$$\Rightarrow \delta\mu\left(\int_{S\sigma} \mathbf{T}^T\mathbf{N}^T(\mathbf{N}\dot{\mathbf{U}})dS - 1\right) = 0$$

$$\Rightarrow \int_{S\sigma} \mathbf{T}^T\mathbf{N}^T(\mathbf{N}\dot{\mathbf{U}})dS - 1 = 0$$

Therefore,

$$\int_{S\sigma} \mathbf{T}^T\mathbf{N}^T(\mathbf{N}\dot{\mathbf{U}})dS = 1 \quad (2.79)$$

where

B: kinematic matrix (3x8 sizes) defined such as $\dot{\boldsymbol{\varepsilon}} = \mathrm{B}\dot{\mathbf{u}}$

N: the shape function matrix (2x8 sizes)

m: transfer vector.

$\dot{\mathbf{U}}$: vector of all nodal velocities

t: surface force applied at nodes

x: the unit node weight.

In addition, we can show equation (2.78) and (2.79) as following manner:

$$\int_{V_1}\left(\mathbf{m}^T\mathbf{B}\dot{\mathbf{U}}\right)dV = 0 \Rightarrow \int_{V_1}\left(\mathbf{m}^T\mathbf{B}\right)dV\dot{\mathbf{U}} = 0 \Rightarrow \mathbf{L}\dot{\mathbf{U}} = 0$$

$$\int_{S\sigma} T^T\mathbf{N}^T\left(\mathbf{N}\dot{\mathbf{U}}\right)dS = 1 \Rightarrow \int_{S\sigma} T^T\mathbf{N}^T\mathbf{N}dS\dot{\mathbf{U}} = 1 \Rightarrow \mathbf{F}^T\dot{\mathbf{U}} = 1$$

and

$$\int_V \mathbf{N}^T\left(\mathbf{N}X\right)dV = \mathbf{X}$$

Equation (2.77), (2.78) and (2.79) can describe into a form:

$$\begin{cases} \int_V \mathbf{B}^T\mathbf{s}dV + k_1\mathbf{L}^T = -\mu\mathbf{F} + \mathbf{X} \\ \mathbf{L}\dot{\mathbf{U}} = 0 \\ \mathbf{F}^T\dot{\mathbf{U}} = 1 \end{cases} \tag{2.80}$$

where

F: vector of all nodal forces

S_σ : stress boundary

X: the total nodal force vector

On the other hand, the stress-strain rate relationship of Mises yield function from the equation (2.69):

$$\dot{\boldsymbol{\varepsilon}} = \lambda\mathbf{s} = \left(\frac{\dot{\mathbf{e}}}{\sigma_0}\right)\mathbf{s}$$

$$\Rightarrow \mathbf{s} = \frac{\sigma_0}{\dot{\mathbf{e}}}\dot{\boldsymbol{\varepsilon}} \tag{2.81}$$

For a general strain tensor, the diagonal strain components $\varepsilon_{11}, \varepsilon_{22}, \varepsilon_{33}$ are known as “direct”

strains, while the off diagonal terms $\varepsilon_{12}=\varepsilon_{21},\varepsilon_{13}=\varepsilon_{31},\varepsilon_{23}=\varepsilon_{32}$ are known as "shear strain". The shear strains are sometimes reported as "Engineering shear strain" which are related to the formal definition by a factor of 2.

$$\gamma_{12}=2\varepsilon_{12},\gamma_{13}=2\varepsilon_{13},\gamma_{23}=2\varepsilon_{23}$$

Strain tensor (two-dimensional) $\dot{\boldsymbol{\varepsilon}}=\begin{bmatrix}\dot{\varepsilon}_{11} & \dot{\varepsilon}_{12}\\ \dot{\varepsilon}_{21} & \dot{\varepsilon}_{22}\end{bmatrix}$

Strain vector (two-dimensional) $\dot{\boldsymbol{\varepsilon}}=\begin{Bmatrix}\dot{\varepsilon}_{11}\\ \dot{\varepsilon}_{22}\\ 2\dot{\varepsilon}_{12}\end{Bmatrix}$

Engineering shear strain vector (two-dimensional) $\hat{\dot{\boldsymbol{\varepsilon}}}=\begin{Bmatrix}\dot{\varepsilon}_{11}\\ \dot{\varepsilon}_{22}\\ \dot{\gamma}_{12}\end{Bmatrix}$

Therefore, to converts the engineering shear strain to the shear strain, the matrix Q is provided:

$$\mathbf{Q}=\begin{bmatrix}1 & 0 & 0\\ 0 & 1 & 0\\ 0 & 0 & 1/2\end{bmatrix} \tag{2.82}$$

and

$$\dot{\boldsymbol{\varepsilon}}=\mathbf{Q}\hat{\dot{\boldsymbol{\varepsilon}}} \tag{2.83}$$

Therefore, equation (2.69) can be shown:

$$\mathbf{s}=\frac{\sigma_0}{\dot{\mathbf{e}}}\dot{\boldsymbol{\varepsilon}}=\frac{\sigma_0}{\dot{\mathbf{e}}}\left(\mathbf{Q}\hat{\dot{\boldsymbol{\varepsilon}}}\right) \tag{2.84}$$

Next, substituting the above equation to the system of equations (4.80), we have equations (2.85):

$$\begin{cases}\int_V \mathbf{B}^T\left(\frac{\sigma_0}{\dot{\mathbf{e}}}\right)(\mathbf{QB})\mathrm{d}V\dot{\mathbf{U}}+k_l\mathbf{L}^T=-\mu_l\mathbf{F}+\mathbf{X}\\ \mathbf{L}\dot{\mathbf{U}}=0\\ \mathbf{F}^T\dot{\mathbf{U}}=1\end{cases} \tag{2.85}$$

Here $$\int_V \mathbf{B}^T \mathbf{s} dV = \int_V \mathbf{B}^T \left(\frac{\sigma_0}{\dot{\mathbf{e}}} \left(\mathbf{Q} \hat{\dot{\boldsymbol{\varepsilon}}} \right) \right) dV = \int_V \mathbf{B}^T \left(\frac{\sigma_0}{\dot{\mathbf{e}}} \right) \left(\mathbf{QB} \dot{\mathbf{U}} \right) dV = \int_V \mathbf{B}^T \left(\frac{\sigma_0}{\dot{\mathbf{e}}} \right) \left(\mathbf{QB} \right) dV \dot{\mathbf{U}}$$

In the above equation, undetermined coefficients of Lagrange $(-\mu = \rho)$, it is regarded as the average stress P with k_l on the area V, equation (2.85) can be expressed as:

$$\begin{cases} \int_V \mathbf{B}^T \left(\frac{\sigma_0}{\dot{\mathbf{e}}} \right) \left(\mathbf{QB} \right) dV \dot{\mathbf{U}} + k_1 \mathbf{L}^T = \rho \mathbf{F} + \mathbf{X} \\ \mathbf{L} \dot{\mathbf{U}} = 0 \\ \mathbf{F}^T \dot{\mathbf{U}} = 1 \end{cases} \tag{2.86}$$

Equation (2.85) is a system of non-linear equation for $(\dot{\mathbf{u}}, k_1, \mu_1)$. So we can solve this equation iteratively by the Newton-Raphson method.

2.2.5 Rigid plastic constitutive equation on the rigid plastic finite element method

The rigid-plastic finite element method (RPFEM) has been developed for geotechnical engineering by Tamura et al. (1984, 1987). In this process, the limit load is calculated without the assumption on the potential failure mode. The method is effective in calculating the ultimate bearing capacity of footing against the three dimensional boundary value problems where the soil condition is varied as multi-layered ground. Although RPFEM is originally developed based on the upper bound theorem in plasticity, Tamura et al. proved that it could be derived directly using the rigid plastic constitutive equation. The advantage of rigid plastic constitutive equation is the scalability for considering the material property of soils as the non-associated flow rule. This study improves RPFEM by using the non-linear shear strength property of soils and introduces the rigid plastic constitutive equation of parabolic yield function regarding the confining pressure.

Tamura (1991) developed the rigid plastic constitutive equation for frictional material. The Drucker-Prager's yield function is expressed as follows:

$$f(\sigma) = aI_1 + \sqrt{J_2} - b = 0 \tag{2.87}$$

where I_1 : first invariant of stress

J_2 : second invariant of deviator stress

The coefficients a, b express the soil constants corresponding to the internal friction

angle and cohesion, respectively

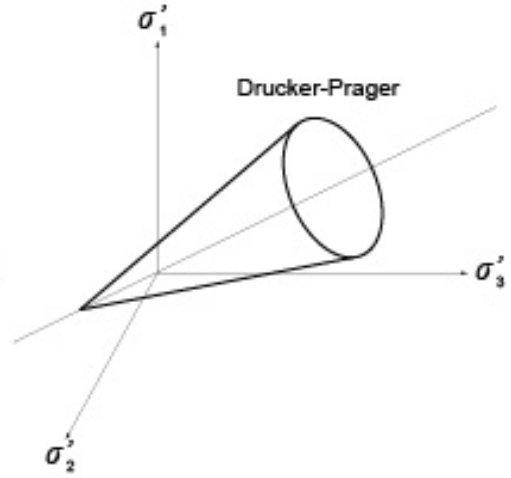

Fig.2.18 Yield surface of Drucker-Prager criterion

Following the non-associated flow rule, the strain rate $\dot{\boldsymbol{\varepsilon}} = \dot{\boldsymbol{\varepsilon}}^{p}$ could be written as follow:

$$\begin{aligned}\dot{\boldsymbol{\varepsilon}} &= \lambda \frac{\partial f(\boldsymbol{\sigma})}{\partial \boldsymbol{\sigma}} = \lambda \frac{\partial}{\partial \boldsymbol{\sigma}} \left(aI_1 + \sqrt{J_2} - b\right) = \lambda \left(\frac{\partial (aI_1)}{\partial \boldsymbol{\sigma}} + \frac{\partial \left(\sqrt{J_2}\right)}{\partial \boldsymbol{\sigma}} - \frac{\partial (b)}{\partial \boldsymbol{\sigma}} \right) \\ &= \lambda \left(\left(\frac{\partial (a)}{\partial \boldsymbol{\sigma}} I_1 + a \frac{\partial (I_1)}{\partial \boldsymbol{\sigma}} \right) + \frac{\partial \left(\sqrt{J_2}\right)}{\partial \boldsymbol{\sigma}} - \frac{\partial (b)}{\partial \boldsymbol{\sigma}} \right) \\ &= \lambda \left(\left(\frac{\partial (a)}{\partial \boldsymbol{\sigma}} I_1 + a \frac{\partial (tr\{\boldsymbol{\sigma}\})}{\partial \boldsymbol{\sigma}} \right) + \frac{\partial (J_2)^{1/2}}{\partial \boldsymbol{\sigma}} - \frac{\partial (b)}{\partial \boldsymbol{\sigma}} \right) \\ &= \lambda \left(a\mathbf{I} + \frac{\mathbf{s}}{2\sqrt{J_2}} \right)\end{aligned} \tag{2.88}$$

where

$$\frac{\partial (\mathrm{tr}\{\boldsymbol{\sigma}\})}{\partial \boldsymbol{\sigma}} \mathrm{a} = \left(\frac{\{\sigma_{11} + \sigma_{22} + \sigma_{33}\}}{\partial \begin{bmatrix} \sigma_{11} & \sigma_{12} & \sigma_{13} \\ \sigma_{21} & \sigma_{22} & \sigma_{23} \\ \sigma_{31} & \sigma_{32} & \sigma_{33} \end{bmatrix}} \right) \mathrm{a}$$

$$= tr \begin{bmatrix} \dfrac{\partial \{\sigma_{11} + \sigma_{22} + \sigma_{33}\}}{\partial \sigma_{11}} & \sigma_{12} & \sigma_{13} \\ \sigma_{21} & \dfrac{\partial \{\sigma_{11} + \sigma_{22} + \sigma_{33}\}}{\partial \sigma_{22}} & \sigma_{23} \\ \sigma_{31} & \sigma_{32} & \dfrac{\partial \{\sigma_{11} + \sigma_{22} + \sigma_{33}\}}{\partial \sigma_{33}} \end{bmatrix}$$

$$\frac{\partial(\mathrm{tr}\{\boldsymbol{\sigma}\})}{\partial\boldsymbol{\sigma}}\mathrm{a}=\begin{bmatrix}1&0&0\\0&1&0\\0&0&1\end{bmatrix}\mathrm{a}=\mathrm{a}\mathbf{I} \tag{2.89}$$

$$\begin{aligned}\frac{\partial(\mathrm{J}_2)^{1/2}}{\partial\boldsymbol{\sigma}}&=\frac{1}{2}(\mathrm{J}_2)^{-1/2}\frac{\partial(\mathrm{J}_2)}{\partial\boldsymbol{\sigma}}=\frac{1}{2\sqrt{\mathrm{J}_2}}\frac{\partial\left(\frac{1}{2}\mathbf{s}:\mathbf{s}\right)}{\partial\boldsymbol{\sigma}}=\frac{1}{2\sqrt{\mathrm{J}_2}}\left(\frac{1}{2}\frac{\partial(\mathbf{s})}{\partial\boldsymbol{\sigma}}:\mathbf{s}+\frac{1}{2}\mathbf{s}:\frac{\partial(\mathbf{s})}{\partial\boldsymbol{\sigma}}\right)\\&=\frac{1}{2\sqrt{\mathrm{J}_2}}\left(\frac{\partial(\mathbf{s})}{\partial\boldsymbol{\sigma}}:\mathbf{s}\right)=\frac{1}{2\sqrt{\mathrm{J}_2}}\left(\frac{\partial(\boldsymbol{\sigma}-\mathrm{P}\mathbf{I})}{\partial\boldsymbol{\sigma}}:\mathbf{s}\right)=\frac{1}{2\sqrt{\mathrm{J}_2}}(\mathbf{I}:\mathbf{s})\\&=\frac{\mathbf{s}}{2\sqrt{\mathrm{J}_2}}\end{aligned} \tag{2.90}$$

$$\begin{aligned}\dot{\mathbf{e}}=\sqrt{\dot{\boldsymbol{\varepsilon}}:\dot{\boldsymbol{\varepsilon}}}&=\sqrt{\lambda\left(\mathrm{a}\mathbf{I}+\frac{\mathbf{s}}{2\sqrt{\mathrm{J}_2}}:\lambda\left(\mathrm{a}\mathbf{I}+\frac{\mathbf{s}}{2\sqrt{\mathrm{J}_2}}\right)\right)}\\&=\lambda\sqrt{\mathrm{a}^2(\mathbf{I}:\mathbf{I})+2\left(\frac{\mathrm{a}}{2\sqrt{\mathrm{J}_2}}(0)+\frac{1}{4\left(\frac{1}{2}\mathbf{s}:\mathbf{s}\right)}(\mathbf{s}:\mathbf{s})\right)}\\&=\lambda\sqrt{3\mathrm{a}^2+\frac{1}{2}}\end{aligned} \tag{2.91}$$

$$\Rightarrow\lambda=\frac{\dot{\mathrm{e}}}{\sqrt{3\mathrm{a}^2+\frac{1}{2}}} \tag{2.92}$$

$$\mathbf{I}:\mathbf{I}=\mathbf{I}^{\mathrm{T}}\mathbf{I}=\begin{bmatrix}1&0&0\\0&1&0\\0&0&1\end{bmatrix}^{\mathrm{T}}\begin{bmatrix}1&0&0\\0&1&0\\0&0&1\end{bmatrix}=3 \tag{2.93}$$

$$\mathbf{s}:\mathbf{I}=\begin{bmatrix}\mathrm{s}_{11}&\mathrm{s}_{12}&\mathrm{s}_{13}\\\mathrm{s}_{21}&\mathrm{s}_{22}&\mathrm{s}_{23}\\\mathrm{s}_{31}&\mathrm{s}_{32}&\mathrm{s}_{33}\end{bmatrix}:\begin{bmatrix}1&0&0\\0&1&0\\0&0&1\end{bmatrix}=\mathrm{s}_{11}+\mathrm{s}_{22}+\mathrm{s}_{33}=\mathrm{J}_1=0 \tag{2.94}$$

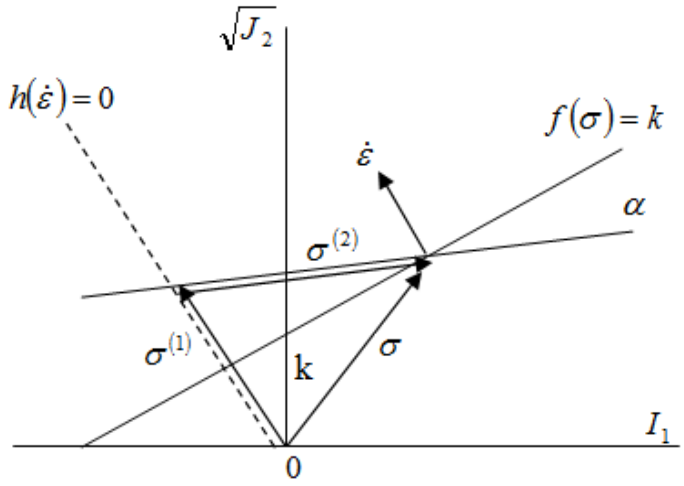

Fig.2.19 Stress decomposition for non-associated flow rule

The volumetric strain rate is expressed as follows:

$$\dot{\varepsilon}_v = \mathrm{tr}(\dot{\boldsymbol{\varepsilon}}) = \mathrm{tr}\left(\lambda\frac{\partial f(\boldsymbol{\sigma})}{\partial \boldsymbol{\sigma}}\right) = \mathrm{tr}\left(\lambda\left(a\mathbf{I}+\frac{\mathbf{s}}{2\sqrt{J_2}}\right)\right)$$

$$= \lambda\left(aI_{11}+\frac{s_{11}}{2\sqrt{J_2}}\right)+\lambda\left(aI_{22}+\frac{s_{22}}{2\sqrt{J_2}}\right)+\lambda\left(aI_{33}+\frac{s_{33}}{2\sqrt{J_2}}\right)$$

$$= \lambda\left\{a(I_{11}+I_{22}+I_{33})+\frac{1}{2\sqrt{J_2}}(s_{11}+s_{22}+s_{33})\right\}$$

$$\dot{\varepsilon}_v = \lambda(3a)$$

$$= \frac{3a}{\sqrt{3a^2+1/2}}\dot{e} \qquad (2.95)$$

No volumetric plastic strain rate occurs under the limit state. Here, V_l is a small area obtained by dividing a region V.

$$\sum_{V_l \in V}\int_{V_l}\left(\dot{\varepsilon}_v - \frac{3a}{\sqrt{3a^2+1/2}}\dot{e}\right)dV = 0 \qquad (l=1,2,3...n) \qquad (2.96)$$

where λ: the plastic multiplier, and $\dot{e}$, the norm of strain rate. **I** and **s** express the unit and the deviatoric stress tensors. The strain rate $\dot{\boldsymbol{\varepsilon}}$, which is purely plastic component, should satisfy the volumetric constraint condition which is derived by equation (2.96) as follows:

$$h(\dot{\boldsymbol{\varepsilon}}) = \dot{\varepsilon}_v - \frac{3a}{\sqrt{3a^2 + 1/2}}\dot{e} = \dot{\varepsilon}_v - \hat{\eta}\dot{e} = 0 \tag{2.97}$$

The internal dissipation rate is eventually expressed by the equation (2.98). Here, I_1 is the first invariant of the Cauchy stress tensor and $\mathbf{I}$ is the unit tensor.

$$\begin{aligned}\boldsymbol{\sigma} : \dot{\boldsymbol{\varepsilon}} &= \boldsymbol{\sigma} : \left(\lambda \left(a\mathbf{I} + \frac{\mathbf{s}}{2\sqrt{J_2}} \right) \right) = \lambda \left(a(\boldsymbol{\sigma} : \mathbf{I}) + \frac{\boldsymbol{\sigma} : \mathbf{s}}{2\sqrt{J_2}} \right) \\ &= \lambda \left(a(\boldsymbol{\sigma} : \mathbf{I}) + \frac{(\mathbf{s} + P\mathbf{I}) : \mathbf{s}}{2\sqrt{J_2}} \right) = \lambda \left(a(\boldsymbol{\sigma} : \mathbf{I}) + \frac{(\mathbf{s} : \mathbf{s} + P(\mathbf{I} : \mathbf{s}))}{2\sqrt{J_2}} \right) \\ &= \lambda \left(aI_1 + \frac{2J_2}{2\sqrt{J_2}} \right) = \lambda (aI_1 + \sqrt{J_2}) = \lambda b = \frac{b}{\sqrt{3a^2 + 1/2}} \dot{e}\end{aligned}$$

Therefore,

$$\boldsymbol{\sigma} : \dot{\boldsymbol{\varepsilon}} = \frac{b}{\sqrt{3a^2 + 1/2}} \dot{e} \tag{2.98}$$

where

$$\boldsymbol{\sigma} : \mathbf{I} = \mathbf{I}^T \mathbf{I} = \begin{bmatrix} \sigma_{11} & \sigma_{12} & \sigma_{13} \\ \sigma_{21} & \sigma_{22} & \sigma_{23} \\ \sigma_{31} & \sigma_{32} & \sigma_{33} \end{bmatrix}^T \begin{bmatrix} 1 & 0 & 0 \\ 0 & 1 & 0 \\ 0 & 0 & 1 \end{bmatrix} = \sigma_{11} + \sigma_{22} + \sigma_{33} = tr\{\boldsymbol{\sigma}\} = I_1$$

We write the formal functional in terms of the Lagrange multiplier (k_1, μ_1) for the constraint conditions:

$$\begin{aligned}\Phi(\dot{\mathbf{u}}, k_1, \mu) = &\int_V \boldsymbol{\sigma} : \dot{\boldsymbol{\varepsilon}} dV - \int_V \mathbf{X} \cdot \dot{\mathbf{u}} dV \\ &+ \sum_{V_1 \in V} k_1 \int_{V_1} \left(\dot{\varepsilon}_V - \frac{3a}{\sqrt{3a^2 + 1/2}} \dot{e} \right) dV + \mu_1 \left(\int_{S_\sigma} \mathbf{T} \cdot \dot{\mathbf{u}} dS - 1 \right)\end{aligned} \tag{2.99}$$

in which k_1 and μ_1 are called the Lagrange multiplier.

Furthermore, from the stationary condition, the following simultaneous equations are obtained. $\int_V \boldsymbol{\sigma} : \delta\dot{\boldsymbol{\varepsilon}} dV - \int_V \mathbf{X} \cdot \delta\dot{\mathbf{u}} dV + \sum_{V_1 \in V} k_1 \int_{V_1} \left(\delta\dot{\varepsilon}_V - \frac{3a}{\sqrt{3a^2 + 1/2}} \delta\dot{e} \right) dV + \mu_1 \left(\int_{S_\sigma} \mathbf{T} \cdot \delta\dot{\mathbf{u}} dS \right) = 0$

$$\text{for} \forall \delta \dot{\mathbf{u}} \qquad (2.100)$$

$$\sum_{V_l \in V} \delta k_l \int_{V_l} \left(\dot{\varepsilon}_V - \frac{3a}{\sqrt{3a^2 + 1/2}} \dot{e} \right) dV = 0 \qquad \text{for} \forall \delta k_l \qquad (2.101)$$

$$\delta\mu_1 \left(\int_{S_\sigma} \mathbf{T} \cdot \dot{\mathbf{u}} dS - 1 \right) = 0 \qquad \text{for} \forall \delta\mu_1 \qquad (2.102)$$

The expression (2.100) and substituting internal dissipation rate equation (2.98), finally equation (2.103) is satisfied:

$$\int_V (\boldsymbol{\sigma} : \delta\dot{\boldsymbol{\varepsilon}}) dV - \int_V \mathbf{X} \cdot \delta\dot{\mathbf{u}} dV + \sum_{V_l \in V} k_l \int_{V_l} \left(\delta\dot{\varepsilon}_V - \frac{3a}{\sqrt{3a^2 + 1/2}} \delta\dot{e} \right) dV + \mu_1 \left(\int_{S_\sigma} \mathbf{T} \cdot \delta\dot{\mathbf{u}} dS \right) = 0$$

$$\Rightarrow \int_V \left(\frac{b}{\sqrt{3a^2 + 1/2}} \delta\dot{e} \right) dV - \int_V \mathbf{X} \cdot \delta\dot{\mathbf{u}} dV + \sum_{V_l \in V} k_l \int_{V_l} \left(\delta\dot{\varepsilon}_V - \frac{3a}{\sqrt{3a^2 + 1/2}} \delta\dot{e} \right) dV + \mu_1 \left(\int_{S_\sigma} \mathbf{T} \cdot \delta\dot{\mathbf{u}} dS \right) = 0$$

$$\Rightarrow \int_V \left(\frac{b}{\sqrt{3a^2 + 1/2}} \frac{\dot{\boldsymbol{\varepsilon}}}{\dot{e}} : \delta\dot{\boldsymbol{\varepsilon}} \right) dV - \int_V \mathbf{X} \cdot \delta\dot{\mathbf{u}} dV$$

$$+ \sum_{V_l \in V} k_l \int_{V_l} \left((\mathbf{I} : \delta\dot{\boldsymbol{\varepsilon}}) - \frac{3a}{\sqrt{3a^2 + 1/2}} \frac{\dot{\boldsymbol{\varepsilon}}}{\dot{e}} : \delta\dot{\boldsymbol{\varepsilon}} \right) dV + \mu_1 \left(\int_{S_\sigma} \mathbf{T} \cdot \delta\dot{\mathbf{u}} dS \right) = 0$$

$$\int_V \left(\frac{b - 3ak_l}{\sqrt{3a^2 + 1/2}} \frac{\dot{\boldsymbol{\varepsilon}}}{\dot{e}} + k_l \mathbf{I} \right) : \delta\dot{\boldsymbol{\varepsilon}} dV - \int_V \mathbf{X} \cdot \delta\dot{\mathbf{u}} dV + \mu_1 (\mathbf{T} dS) = 0 \qquad (2.103)$$

Here, we can see $\delta\dot{e} = \frac{\delta\dot{e}^2}{\delta\dot{e}} = \frac{\delta\dot{\boldsymbol{\varepsilon}}}{\delta\dot{e}} : \delta\dot{\boldsymbol{\varepsilon}} \approx \frac{\dot{\boldsymbol{\varepsilon}}}{\dot{e}} : \delta\dot{\boldsymbol{\varepsilon}}$

Therefore, Drucker-Prager yield function can be expressed as follows:

$$\boldsymbol{\sigma} = \frac{b - 3ak_l}{\sqrt{3a^2 + 1/2}} \frac{\dot{\boldsymbol{\varepsilon}}}{\dot{e}} + k_l \mathbf{I} \qquad (2.104)$$

The rigid plastic constitutive equation was expressed by Tamura (1991) as follow:

$$\boldsymbol{\sigma} = \boldsymbol{\sigma}^{(1)} + \boldsymbol{\sigma}^{(2)} = \gamma \frac{\partial f}{\partial \boldsymbol{\sigma}} + \beta \frac{\partial h}{\partial \dot{\varepsilon}} \tag{2.105}$$

The variable of γ is determined by inserting J_2 into the plastic potential of equation (2.87). On the other hand, the indeterminate stress parameter β still remains unknown until the boundary value problem with the kinematical constraint conditions of equation (2.97) is solved.

$$\dot{\boldsymbol{\varepsilon}} = \lambda \frac{\partial f(\boldsymbol{\sigma})}{\partial \boldsymbol{\sigma}} \Rightarrow \frac{\partial f(\boldsymbol{\sigma})}{\partial \boldsymbol{\sigma}} = \frac{\dot{\boldsymbol{\varepsilon}}}{\lambda} = \frac{\dot{\boldsymbol{\varepsilon}}}{\left(\frac{\dot{e}}{\sqrt{3a^2 + \frac{1}{2}}} \right)} = \sqrt{3a^2 + \frac{1}{2}} \frac{\dot{\boldsymbol{\varepsilon}}}{\dot{e}} \tag{2.106}$$

$$I_1^{(1)} = \mathrm{tr}\{\boldsymbol{\sigma}^{(1)}\} = \mathrm{tr}\left(\gamma \frac{\partial f(\boldsymbol{\sigma})}{\partial \boldsymbol{\sigma}} \right) = \gamma \left(a\mathbf{I} + \frac{\mathbf{s}}{2\sqrt{J_2}} \right) = 3a\gamma \tag{2.107}$$

$$\begin{aligned} \mathbf{s}^{(1)} &= \boldsymbol{\sigma}^{(1)} - P\mathbf{I} = \gamma \left(a\mathbf{I} + \frac{\mathbf{s}}{2\sqrt{J_2}} \right) - \left(\frac{1}{3} I_1^{(1)} \right) \mathbf{I} = \gamma \left(a\mathbf{I} + \frac{\mathbf{s}}{2\sqrt{J_2}} \right) - \left(\frac{1}{3} 3a\gamma \right) \mathbf{I} \\ &= \left(a\gamma \mathbf{I} + \frac{\mathbf{s}}{2\sqrt{J_2}} \gamma \right) - a\gamma \mathbf{I} = \frac{\mathbf{s}}{2\sqrt{J_2}} \gamma \end{aligned} \tag{2.108}$$

$$\sqrt{J_2^{(1)}} = \sqrt{\frac{1}{2} \left(\mathbf{s}^{(1)} : \mathbf{s}^{(1)} \right)} = \sqrt{\frac{1}{2} \left(\frac{\mathbf{s}}{2\sqrt{J_2}} \gamma : \frac{\mathbf{s}}{2\sqrt{J_2}} \gamma \right)} = \gamma \sqrt{\frac{1}{2} \left(\frac{\mathbf{s} : \mathbf{s}}{4J_2} \right)} = \frac{1}{2} \gamma \tag{2.109}$$

$$f(\boldsymbol{\sigma}) = a I_1^{(1)} + \sqrt{J_2^{(1)}} - b = 0$$

$$\Rightarrow a(3a\gamma) + \frac{1}{2}\gamma - b = 0$$

$$\Rightarrow \left(3a^2 + \frac{1}{2} \right) \gamma - b = 0$$

$$\Rightarrow \gamma = \frac{b}{\left(3a^2 + \frac{1}{2} \right)} \tag{2.110}$$

Therefore

$$\sigma^{(1)} = \gamma \frac{\partial f(\boldsymbol{\sigma})}{\partial \boldsymbol{\sigma}} = \frac{b}{\left(3a^2 + \frac{1}{2} \right)} \frac{\dot{\boldsymbol{\varepsilon}}}{\dot{e}} \tag{2.111}$$

Any strain rate which is compatible with Drucker-Prager's yield criterion must satisfy equation

(2.111). $\hat{\eta}$ is a coefficient determined from equation (2.111) on the dilation characteristics.

$$\frac{\partial h(\dot{\boldsymbol{\varepsilon}})}{\partial \dot{\boldsymbol{\varepsilon}}} = \frac{\partial}{\partial \dot{\boldsymbol{\varepsilon}}}\left(\dot{\varepsilon}_v - \frac{3a}{\sqrt{3a^2 + 1/2}}\dot{e}\right) = \frac{\partial(\dot{\varepsilon}_v)}{\partial \dot{\boldsymbol{\varepsilon}}} - \frac{3a}{\sqrt{3a^2 + 1/2}}\frac{\partial(\dot{e})}{\partial \dot{\boldsymbol{\varepsilon}}} = \frac{\partial \mathrm{tr}(\dot{\boldsymbol{\varepsilon}})}{\partial \dot{\boldsymbol{\varepsilon}}} - \frac{3a}{\sqrt{3a^2 + 1/2}}\frac{\partial(\dot{\boldsymbol{\varepsilon}}:\dot{\boldsymbol{\varepsilon}})^{1/2}}{\partial \dot{\boldsymbol{\varepsilon}}} \tag{2.112}$$

$$= \mathbf{I} - \frac{3a}{\sqrt{3a^2 + 1/2}}\frac{\dot{\boldsymbol{\varepsilon}}}{\dot{e}}$$

where

$$\frac{\partial(\dot{\boldsymbol{\varepsilon}}:\dot{\boldsymbol{\varepsilon}})^{1/2}}{\partial \dot{\boldsymbol{\varepsilon}}} = \frac{1}{2\sqrt{\dot{\boldsymbol{\varepsilon}}:\dot{\boldsymbol{\varepsilon}}}}\frac{\partial(\dot{\boldsymbol{\varepsilon}}:\dot{\boldsymbol{\varepsilon}})}{\partial \dot{\boldsymbol{\varepsilon}}} = \frac{1}{2\sqrt{\dot{\boldsymbol{\varepsilon}}:\dot{\boldsymbol{\varepsilon}}}}\left(\frac{\partial(\dot{\boldsymbol{\varepsilon}})}{\partial \dot{\boldsymbol{\varepsilon}}}:\dot{\boldsymbol{\varepsilon}} + \dot{\boldsymbol{\varepsilon}}\frac{\partial(\dot{\boldsymbol{\varepsilon}})}{\partial \dot{\boldsymbol{\varepsilon}}}\right) = \frac{1}{\sqrt{\dot{\boldsymbol{\varepsilon}}:\dot{\boldsymbol{\varepsilon}}}}\left(\frac{\partial(\dot{\boldsymbol{\varepsilon}})}{\partial \dot{\boldsymbol{\varepsilon}}}:\dot{\boldsymbol{\varepsilon}}\right) = \frac{1}{\dot{e}}\dot{\boldsymbol{\varepsilon}} = \frac{\dot{\boldsymbol{\varepsilon}}}{\dot{e}} \tag{2.113}$$

$$\boldsymbol{\sigma}^{(2)} = \hat{\beta}\frac{\partial h}{\partial \dot{\varepsilon}} = \hat{\beta}\left(\mathbf{I} - \frac{3a}{\sqrt{3a^2 + 1/2}}\frac{\dot{\boldsymbol{\varepsilon}}}{\dot{e}}\right) \tag{2.114}$$

The rigid plastic constitutive equation is expressed by Lagrange method after Tamura (1991) as follows:

$$\boldsymbol{\sigma} = \frac{b}{\sqrt{3a^2 + \frac{1}{2}}}\frac{\dot{\boldsymbol{\varepsilon}}}{\dot{e}} + \beta\left(\mathbf{I} - \frac{3a}{\sqrt{3a^2 + \frac{1}{2}}}\frac{\dot{\boldsymbol{\varepsilon}}}{\dot{e}}\right) = \frac{b - 3\beta a}{\sqrt{3a^2 + \frac{1}{2}}}\frac{\dot{\boldsymbol{\varepsilon}}}{\dot{e}} + \beta\mathbf{I} \tag{2.115}$$

The first term expresses the stress component uniquely determined for the yield function and the second term, the indeterminate stress component along the yield function.

Tamura.et.al derived rigid plastic constitutive stresses on the yield surface, obtained by decomposing on the basis of the flow rule; the result from rigid plastic constitutive equation (2.115) is quite consistent with the equation (2.104) by the upper bound theorem.

References

[1] AIJ (1988, 2001), Architectural Institute of Japan. Recommendations for design of building foundations, 430p.

[2] Aysen, A., 2002. Soil Mechanics – Basic Concepts and Engineering Applications. Balkema AA Publisher, 413–419.

[3] Button, S.J., 1953. The Bearing Capacity of Footing on Two-Layer Cohesive Subsoil, In: Proceedings of the 3rd Int. Conference on Soil Mechanics and Foundation Engineering, **1**, 332-335.

[4] Brown, J.D. and Meyerhof, G.G., 1969. Experimental Study of Bearing Capacity in Layered Clays, In: Proceedings of the 7th International Conference on Soil Mechanics and Foundation Engineering, Mexico, **2**, 45-51.

[5] Charnes, A., Lemke, C.E. and Zienkiewicz, O.C., 1959. Virtual work, linear programming and plastic limit analysis, In: Proc. Roy. Soc, A251, 110-116.

[6] Das, B. M., 1988. Principles of Foundation Engineering". Fourth Edition, Taylor and Francis Group.

[7] Das, B. M., 2009. Shallow foundation, bearing capacity and settlement, second Edition, Taylor and Francis Group, 344 p.

[8] De Beer, E. E., 1965. Bearing capacity and settlement of shallow foundations on sand, in "Bearing capacity and settlement of foundations", Proceedings of a symposium held at Duke University, 15p.

[9] De Beer, E. E., 1970. Experimental determination of the shape factors of sand, Geotechnique, **20**(4), 387-411.

[10] Drucker, D. C., and W. Prager, 1952. Soil mechanics and plastic analysis of limit design, Q. Appl. Math. 10, 157p..

[11] Edgar G. D., 2013. Assessment of the range of variation of N_γ from 60 estimation methods for footings on sand, Can. Geotech. J., **50**(7), 793-800.

[12] Georgiadis M., Butterfield, 1988. Displacements of footings on sand under eccentric and inclined loads, Can. Geotech. J., **25**(2), 199-212.

[13] Hanna A. M., Meyerhof G. G., 1981. Experimental evaluation of bearing capacity of footings subjected to inclined loads, Can. Geotech. J., **18**(4), 599-603.

[14] Hjiaj M., Lyamin A.V., Sloan S.W., 2005. Numerical limit analysis solutions for the bearing capacity factor N_γ, Int. J. of Solids Struct., 42, 1681-1704.

[15] Houlsby G. T., Cassidy M. J., 2002. A plasticity model for the behavior of footings on sand under combined loading, Géotechnique, **52**(2), 117-129.

[16] Koiter, W.T., 1960. General theorems for elastic-plastic solids, In: Progress in Solid Mechanics, **1**, 167-221.

[17] Martin, J. B., 1975. Plasticity, MIT Press, 931p.

[18] Merifield, R.S., Sloan, S.W. and Yu, H.S., 1999. Rigorous Plasticity Solutions for the Bearing Capacity of Two-Layered Clays, Geotechnique, **49**(4), 471-490.

[19] Meyerhof, G. G., 1951. Ultimate bearing capacity of foundations, Geotechnique, **2**(4), 301-332

[20] Meyerhof, G. G., 1963. Some recent research on the ultimate bearing capacity of foundations, Can. Geotech. J., **1**(1), 243-256.

[21] Meyerhof, G.G., 1974. Ultimate Bearing Capacity of Footings on Sand Layer Overlying Clay, Can. Geotech. J., **11**(2), 223-229.

[22] Meyerhof, G.G. and Hanna, A.M., 1978. Ultimate Bearing Capacity of Foundations on Layered Soils under Inclined Load, Can. Geotech. J., **15**(4), 565-572.

[23] Michalowski, R.L. and Shi, L., 1995. Bearing capacity of Footings over Two-Layer Foundation Soils, J. Geotech. Eng., **121**(5), 421-427.

[24] Michalowski, R. L., 1997. An estimate of the influence of soil weight on bearing capacity using limit analysis, Soils Found., **37**(4), 57-64

[25] Mohammed Hjiaj, Andrei V. Lyamin, Scott W. Sloan, 2004. Bearing capacity of a cohesive-frictional soil under non-eccentric inclined loading, Computers and Geotechnics, **31**(6), 491-516.

[26] Prandtl, L., 1921. Über die Eindringungsfestigkeit (Härte) Plastischer Baustoffe und die Festigkeit von Schneiden, Z. Angew. Math. Mech., 1, 15–20 (In Germany).

[27] Reissner, H., 1924. Zumerddruckproblem, In: Proc., 1st Int. Congress of Applied Mechanics, Delft, The Netherlands, 295–311 (In Germany).

[28] Loukidis D., Chakraborty T., Salgado R. 2008. Bearing capacity of strip footings on purely frictional soil under eccentric and inclined loads", Can. Geotech. J., **45**(6), 768-787.

[29] Pfeifle, T.W. and Das, B.M., 1979. Model Tests for Bearing Capacity in Sand, J. Geotech. Eng., ASCE, **105**(GT9), 1112-1116.

[30] Takeshi Hoshina, Satoru Ohtsuka and Koichi Isobe, 2011. Ultimate bearing capacity of ground by Rigid plastic finite element method taking account of stress dependent non-linear strength property, J. Appl. Mech. **6**, 191–200 (in Japanese).

[31] Tamura, T., 1990. Rigid-plastic finite element method in geotechnical engineering. Soc. Mater. Sci., Jpn. 7, 135–164.

[32] Tamura, T., Kobayashi, S. and Sumi, T., 1987. Limit analysis of soil structure by rigid plastic finite element method, Soils Found., **24**(1), 34-42.

[33] Terzaghi, K., 1943. Theoretical soil mechanics, New York, John Wiley, 528p.

[34] Wai-Fah C., 1975. Limit analysis and soil plasticity, Developments in Geotechnical Engineering 7, Elsevier, 638p.

[35] Yamamoto K., Lyamin A.V., Abbo A., Sloan S.W. and Hira M., 2009. Bearing capacity and failure mechanism of different types of foundations on sand, An estimate of the influence of soil weight on bearing capacity using limit analysis, Soils Found., **49**(2), 305-314.

[36] Zhu, M. and Michalowski, R. L., 2005. Shape Factors for limit Loads on Square and Rectangular Footings. J. Geotech. Geoenviron. Eng., **131**(2), 223-231.

[37] Zhu, M. and Michalowski, R. L., 2010. Bearing Capacity of Rectangular Footings on Two Layer Clay, American Society of Civil Engineers, **191**(15), 933-947.

CHAPTER 3
NUMERICAL FORMULATION ON RIGID PLASTIC FINITE ELEMENT METHOD

3.1 Introduction

In recent years, the finite element method (FEM) is widely accepted as one of the well-established and convenient technique for solving complex problems in various fields of engineering and mathematical physics. The latest four decades have observed a growing use of finite element method in geotechnical engineering. FEM has been applied to estimate the bearing capacity of strip footing on cohesionless soils such as Sloan and Randolph, 1982; Griffiths, 1982; Frydman and Burd, 1997. Rigid plastic finite element method is basically developed based on the upper bound theorem in the limit analysis. It is widely employed for the stability assessment of soil structures in geotechnical engineering. Tamura et al. derived the rigid plastic constitutive equation and proved FEM with the rigid plastic constitutive equation to match RPFEM developed by the upper bound theorem. The advantage of rigid plastic constitutive equation exists in the extensibility to more complicate material property such as the non-associated flow rule. In this chapter, the rigid plastic constitutive equation for the Drucker-Prager yield function is exhibited. Ohtsuka et al. (2011) derived the rigid plastic constitutive equation by introducing the dilatancy condition explicitly-modelled with the use of penalty method.

3.2 Rigid Plastic constitutive equation for Drucker –Prager yield function

The rigid plastic constitutive equation is expressed by Lagragian method after Tamura (1991) as equation (2.115):

$$\boldsymbol{\sigma} = \frac{b}{\sqrt{3a^2 + \frac{1}{2}}}\frac{\dot{\boldsymbol{\varepsilon}}}{\dot{e}} + \beta\left(\mathbf{I} - \frac{3a}{\sqrt{3a^2 + \frac{1}{2}}}\frac{\dot{\boldsymbol{\varepsilon}}}{\dot{e}}\right)$$

The first term expresses the stress component uniquely determined for the yield function and the second term, the indeterminate stress component along the yield function. The indeterminate stress parameter $\hat{\beta}$ still remains unknown until the boundary value problem with the kinematical

constraint conditions of equation (3.1) is solved.

Constraint condition : $h(\dot{\varepsilon}) = \dot{\varepsilon}_v - \frac{3\alpha}{\sqrt{3\alpha^2 + 1/2}}\dot{e} = \dot{\varepsilon}_v - \eta\dot{e} = 0$

To achieve internal dissipation rate and external force work rate, the formulation of the governing equations in the ultimate bearing capacity analysis based on constraints condition with volume change to solve an undefined stress β.

In this study, the constrain condition on strain rate is introduced into the constitutive equation directly with the use of penalty method (Ohtsuka et al., 2011). Penalty method is way to incorporate constraint condition directly to constitutive equation by using penalty constant.

Moreover, the rigid plastic constitutive equation requires convergence calculation because it is a non-linear constitutive equation of the displacement speed, to improve the efficiency of calculation is very important. Therefore, the purpose of speeding up the calculations, to achieve applied formulates Penalty method of incorporating constraints into the governing equation. First, we do derivation of the governing equations in the ultimate bearing capacity analysis. The functional based on the Penalty Law; Penalty multiplier (μ, κ) is created as follows:

$$\Phi(\dot{\mathbf{u}}) = \int_V \boldsymbol{\sigma} : \delta\dot{\varepsilon} dV - \int_V \mathbf{X}\cdot\dot{\mathbf{u}} dV + \int_V \kappa(\dot{\varepsilon}_V - \hat{\eta}\dot{e}) dV + \mu\left(\int_{S_\sigma} \mathbf{T}\cdot\delta\dot{\mathbf{u}} dS\right) \tag{3.1}$$

From stationary condition of the function $\Phi(\dot{\mathbf{u}}) = 0$, the following equation is obtained:

$$\begin{aligned}\Phi(\dot{\mathbf{u}}) = \int_V \frac{b}{\sqrt{3a^2 + 1/2}} \delta\dot{e} dV - \int_V \mathbf{X}\cdot\dot{\mathbf{u}} dV + \int_V \kappa(\dot{\varepsilon}_V - \hat{\eta}\dot{e})(\delta\dot{\varepsilon}_V - \eta\delta\dot{e}) dV \\ + \mu\left(\int_{S_\sigma} \mathbf{T}\cdot\dot{\mathbf{u}} dS - 1\right)\left(\int_{S_\sigma} \mathbf{T}\cdot\delta\dot{\mathbf{u}} dS\right) = 0\end{aligned} \tag{3.2}$$

$$\sum_{V_I \in V} \delta\kappa(\dot{\varepsilon}_V - \hat{\eta}\dot{e})^2 dV = 0 \qquad \text{for } \forall\delta\kappa \tag{3.3}$$

$$\delta\mu\left(\int_{S_\sigma} \mathbf{T}\cdot\dot{\mathbf{u}} dS - 1\right) = 0 \qquad \text{for } \forall\delta\mu \tag{3.4}$$

$$\begin{aligned}\Rightarrow \int_V \frac{b}{\sqrt{3a^2 + 1/2}} \frac{\dot{\boldsymbol{\varepsilon}}}{\dot{e}} : \delta\dot{\varepsilon} dV - \int_V \mathbf{X}\cdot\delta\dot{\mathbf{u}} dV + \kappa(\dot{\varepsilon}_V - \hat{\eta}\dot{e}) \int_V \left((\mathbf{I} : \delta\dot{\varepsilon}) - \left(\eta\frac{\dot{\boldsymbol{\varepsilon}}}{\dot{e}} : \delta\dot{\varepsilon}\right)\right) dV \\ + \mu\left(\int_{S_\sigma} \mathbf{T}\cdot\dot{\mathbf{u}} dS - 1\right)\int_{S_\sigma} \mathbf{T}\cdot\delta\dot{\mathbf{u}} dS = 0\end{aligned}$$

$$\Rightarrow \int_V \frac{b}{\sqrt{3a^2+1/2}} \frac{\dot{\boldsymbol{\varepsilon}}}{\dot{e}} : \delta\dot{\boldsymbol{\varepsilon}} dV - \int_V \mathbf{X}\cdot\delta\dot{\mathbf{u}} dV + \kappa(\dot{\varepsilon}_V - \hat{\eta}\dot{e})\int_V \left(\left(\mathbf{I} - \eta\frac{\dot{\boldsymbol{\varepsilon}}}{\dot{e}}\right) : \delta\dot{\boldsymbol{\varepsilon}}\right) dV$$
$$+ \mu\left(\int_{S_\sigma} \mathbf{T}\cdot\dot{\mathbf{u}} dS - 1\right)\int_{S_\sigma} \mathbf{T}\cdot\delta\dot{\mathbf{u}} dS = 0$$

$$\Rightarrow \int_V \frac{b}{\sqrt{3a^2+1/2}} \frac{\dot{\boldsymbol{\varepsilon}}}{\dot{e}} : \delta\dot{\boldsymbol{\varepsilon}} dV + \kappa(\dot{\varepsilon}_V - \eta\dot{e})\int_V \left(\left(\mathbf{I} - \hat{\eta}\frac{\dot{\boldsymbol{\varepsilon}}}{\dot{e}}\right) : \delta\dot{\boldsymbol{\varepsilon}}\right) dV$$
$$= -\mu\left(\int_{S_\sigma} \mathbf{T}\cdot\dot{\mathbf{u}} dS - 1\right)\int_{S_\sigma} \mathbf{T}\cdot\delta\dot{\mathbf{u}} dS + \int_V \mathbf{X}\cdot\delta\dot{\mathbf{u}} dV$$

$$\Rightarrow \int_V \frac{b}{\sqrt{3a^2+1/2}} \frac{\dot{\boldsymbol{\varepsilon}}}{\dot{e}} : \delta\dot{\boldsymbol{\varepsilon}} dV + \kappa(\dot{\varepsilon}_V - \hat{\eta}\dot{e})\int_V \left(\left(\mathbf{I} - \frac{3a}{\sqrt{3a^2+1/2}}\frac{\dot{\boldsymbol{\varepsilon}}}{\dot{e}}\right) : \delta\dot{\boldsymbol{\varepsilon}}\right) dV \tag{3.5}$$
$$= -\mu\left(\int_{S_\sigma} \mathbf{T}\cdot\dot{\mathbf{u}} dS - 1\right)\int_{S_\sigma} \mathbf{T}\cdot\delta\dot{\mathbf{u}} dS + \int_V \mathbf{X}\cdot\delta\dot{\mathbf{u}} dV$$

Here

$$\rho = -\mu\left(\int_{S_\sigma} \mathbf{T}\cdot\dot{\mathbf{u}} dS - 1\right) \tag{3.6}$$

$$\hat{\beta} = \kappa(\dot{\varepsilon}_V - \hat{\eta}\dot{e}) \tag{3.7}$$

Therefore, the constrain condition on strain rate is introduced into the constitutive equation directly with the use of penalty method

$$\boldsymbol{\sigma} = \frac{b}{\sqrt{3a^2+\frac{1}{2}}} \frac{\dot{\boldsymbol{\varepsilon}}}{\dot{e}} + \kappa(\dot{\varepsilon}_v - \hat{\eta}\dot{e})\left(\mathbf{I} - \frac{3a}{\sqrt{3a^2+\frac{1}{2}}}\frac{\dot{\boldsymbol{\varepsilon}}}{\dot{e}}\right) \tag{3.8}$$

where, κ is a penalty constant. This technique makes the computation more stable and faster. FEM with this constitutive equation provides the same formulation of the upper bound theorem in plasticity so that this method is called as RPFEM in this study.

From equation (3.2), (3.3) and (3.4) for all area, we can divide in the small areas as the spatial discretization as bellows:

$$\int_V \left(\frac{b}{\sqrt{3a^2+1/2}} \frac{\dot{\boldsymbol{\varepsilon}}}{\dot{e}} + \kappa(\dot{\varepsilon}_V - \hat{\eta}\dot{e})\left(\mathbf{I} - \frac{3a}{\sqrt{3a^2+1/2}}\frac{\dot{\boldsymbol{\varepsilon}}}{\dot{e}}\right)\right) : \delta\dot{\boldsymbol{\varepsilon}} dV = -\mu\left(\int_{S_\sigma} \mathbf{T}\cdot\dot{\mathbf{u}} dS - 1\right)\int_{S_\sigma} \mathbf{T}\cdot\delta\dot{\mathbf{u}} dS + \int_V \mathbf{X}\cdot\delta\dot{\mathbf{u}} dV$$

where

$$\int_V \left(\frac{b}{\sqrt{3a^2 + 1/2}} \frac{\dot{\boldsymbol{\varepsilon}}}{\dot{e}} + \kappa(\dot{\varepsilon}_V - \hat{\eta}\dot{e}) \left(\mathbf{I} - \frac{3a}{\sqrt{3a^2 + 1/2}} \frac{\dot{\boldsymbol{\varepsilon}}}{\dot{e}} \right) \right) : \delta\dot{\boldsymbol{\varepsilon}} dV = \int_V \left(\gamma \frac{\dot{\boldsymbol{\varepsilon}}}{\dot{e}} + \kappa \left(\mathbf{I} : \dot{\boldsymbol{\varepsilon}} - \eta \frac{\dot{\boldsymbol{\varepsilon}} : \dot{\boldsymbol{\varepsilon}}}{\dot{e}} \right) \left(\mathbf{I} - \eta \frac{\dot{\boldsymbol{\varepsilon}}}{\dot{e}} \right) \right) : \delta\dot{\boldsymbol{\varepsilon}} dV$$

$$= \int_V \left(\gamma \frac{(\mathbf{QB}\dot{\mathbf{U}})}{\dot{e}} + \kappa \left(\mathbf{m} : \mathbf{B}\dot{\mathbf{U}} - \hat{\eta} \frac{(\mathbf{QB}\dot{\mathbf{U}}) : \mathbf{B}\dot{\mathbf{U}}}{\dot{e}} \right) \left(\mathbf{m} - \hat{\eta} \frac{(\mathbf{QB}\dot{\mathbf{U}})}{\dot{e}} \right) \right) : (\mathbf{B}\delta\dot{\mathbf{U}}) dV$$

$$= (\mathbf{B}\delta\dot{\mathbf{U}})^T \int_V \left(\gamma \frac{(\mathbf{QB}\dot{\mathbf{U}})}{\dot{e}} + \kappa \left(\mathbf{m}^T \mathbf{B}\dot{\mathbf{U}} - \hat{\eta} \frac{(\mathbf{QB}\dot{\mathbf{U}})^T \mathbf{B}\dot{\mathbf{U}}}{\dot{e}} \right) \left(\mathbf{m} - \hat{\eta} \frac{(\mathbf{QB}\dot{\mathbf{U}})}{\dot{e}} \right) \right) dV$$

$$= \delta\dot{\mathbf{U}}^T \mathbf{B}^T \int_V \left(\gamma \frac{(\mathbf{QB}\dot{\mathbf{U}})}{\dot{e}} + \kappa \left(\mathbf{m} - \hat{\eta} \frac{(\mathbf{QB}\dot{\mathbf{U}})}{\dot{e}} \right) \left(\mathbf{m}^T \mathbf{B}\dot{\mathbf{U}} - \hat{\eta} \frac{(\mathbf{QB}\dot{\mathbf{U}})^T \mathbf{B}\dot{\mathbf{U}}}{\dot{e}} \right) \right) dV$$

$$= \delta\dot{\mathbf{U}}^T \int_V \mathbf{B}^T \left(\gamma \frac{(\mathbf{Q})}{\dot{e}} + \kappa \left(\mathbf{m} - \hat{\eta} \frac{(\mathbf{QB}\dot{\mathbf{U}})}{\dot{e}} \right) \left(\mathbf{m}^T - \hat{\eta} \frac{(\dot{\mathbf{U}}^T \mathbf{B}^T \mathbf{Q}^T)}{\dot{e}} \right) \right) \mathbf{B}\dot{\mathbf{U}} dV$$

$$= \delta\dot{\mathbf{U}}^T \int_V \mathbf{B}^T \mathrm{D}\mathbf{B}\dot{\mathbf{U}} dV$$

where $\mathbf{D} = \gamma \frac{(\mathbf{Q})}{\dot{e}} + \kappa \left(\mathbf{m} - \hat{\eta} \frac{(\mathbf{QB}\dot{\mathbf{U}})}{\dot{e}} \right) \left(\mathbf{m}^T - \hat{\eta} \frac{(\dot{\mathbf{U}}^T \mathbf{B}^T \mathbf{Q}^T)}{\dot{e}} \right)$

$$\Rightarrow \delta\dot{\mathbf{U}}^T \int_V \mathbf{B}^T \mathbf{D}\mathbf{B}\dot{\mathbf{U}} dV = -\mu \left(\int_{S_\sigma} \mathbf{T} \cdot \dot{\mathbf{u}} dS - 1 \right) \int_{S_\sigma} \mathbf{T} \cdot \delta\dot{\mathbf{u}} dS + \int_V \mathbf{X} \cdot \delta\dot{\mathbf{u}} dV$$

$$= -\mu \left(\int_{S_\sigma} (\mathbf{Nt}) \cdot (\mathbf{N}\dot{\mathbf{U}}) dS - 1 \right) \int_{S_\sigma} (\mathbf{Nt}) \cdot (\mathbf{N}\delta\dot{\mathbf{U}}) dS + \int_V (\mathbf{NX}) \cdot (\mathbf{N}\delta\dot{\mathbf{U}}) dV$$

$$\Rightarrow \delta\dot{\mathbf{U}}^T \int_V \mathbf{B}^T \mathbf{D}\mathbf{B}\dot{\mathbf{U}} dV = -\mu \left(\int_{S_\sigma} (\mathbf{Nt})^T (\mathbf{N}\dot{\mathbf{U}}) dS - 1 \right) \int_{S_\sigma} (\mathbf{N}\delta\dot{\mathbf{U}})^T (\mathbf{Nt}) dS + \int_V (\mathbf{N}\delta\dot{\mathbf{U}})^T (\mathbf{NX}) dV$$

$$\Rightarrow \delta\dot{\mathbf{U}}^T \int_V (\mathbf{B}^T \mathbf{DB}) dV\dot{\mathbf{U}} = -\mu \left(\int_{S_\sigma} (\mathbf{t}^T \mathbf{N}^T)(\mathbf{N}\dot{\mathbf{U}}) dS - 1 \right) \int_{S_\sigma} (\delta\dot{\mathbf{U}}^T \mathbf{N}^T)(\mathbf{Nt}) dS + \int_V (\delta\dot{\mathbf{U}}^T \mathbf{N}^T)(\mathbf{NX}) dV$$

$$\Rightarrow \delta\dot{\mathbf{U}}^T \left\{ \int_V (\mathbf{B}^T \mathbf{DB}) dV\dot{\mathbf{U}} + \left(\mu \left(\int_{S_\sigma} (\mathbf{t}^T \mathbf{N}^T \mathbf{N}\dot{\mathbf{U}}) dS - 1 \right) \int_{S_\sigma} (\mathbf{N}^T \mathbf{Nt}) dS - \int_V (\mathbf{N}^T \mathbf{NX}) dV \right) \right\} = 0$$

$$\Rightarrow \int_V (\mathbf{B}^T \mathbf{DB}) dV\dot{\mathbf{U}} + \left(\mu \left(\int_{S_\sigma} (\mathbf{t}^T \mathbf{N}^T \mathbf{N}\dot{\mathbf{U}}) dS - 1 \right) \int_{S_\sigma} (\mathbf{N}^T \mathbf{Nt}) dS - \int_V (\mathbf{N}^T \mathbf{NX}) dV \right) = 0$$

$$\Rightarrow \int_V (\mathbf{B}^T \mathbf{DB}) dV\dot{\mathbf{U}} = -\mu \left(\int_{S_\sigma} (\mathbf{t}^T \mathbf{N}^T \mathbf{N}\dot{\mathbf{U}}) dS - 1 \right) \int_{S_\sigma} (\mathbf{N}^T \mathbf{Nt}) dS + \int_V (\mathbf{N}^T \mathbf{NX}) dV$$

Here, replace as below to the above part of governing equation.

$$\int_V (\mathbf{B}^T \mathbf{DB}) dV\dot{\mathbf{U}} = K\dot{\mathbf{U}}$$

$$\int_{S_\sigma} \left(\mathbf{N}^{\mathrm{T}}\mathbf{N}t\right)dS = F$$

$$\int_{V} \left(\mathbf{N}^{\mathrm{T}}\mathbf{N}X\right)dV = X$$

$\dot{\mathrm{U}}$ is decided by convergence calculate.

Therefore,

$$\int_{\mathrm{V}} \left(\mathbf{B}^{\mathrm{T}}\mathbf{D}\mathbf{B}\right)\mathrm{dV}\dot{\mathrm{U}} = -\mu\left(\int_{\mathrm{S}_\sigma} \left(\mathrm{t}^{\mathrm{T}}\mathbf{N}^{\mathrm{T}}\mathbf{N}\dot{\mathrm{U}}\right)\mathrm{dS} - 1\right)\int_{\mathrm{S}_\sigma} \left(\mathbf{N}^{\mathrm{T}}\mathbf{N}\mathrm{t}\right)\mathrm{dS} + \int_{\mathrm{V}} \left(\mathbf{N}^{\mathrm{T}}\mathbf{N}\mathrm{X}\right)\mathrm{dV}$$

$$\Rightarrow \mathrm{K}\dot{\mathbf{U}} = -\mu\left(\mathrm{F}^{\mathrm{T}}\dot{\mathbf{U}} - 1\right)\mathrm{F} + \mathrm{X}$$
$$\Rightarrow \mathrm{K}\dot{\mathbf{U}} + \mu\mathrm{F}\left(\mathrm{F}^{\mathrm{T}}\dot{\mathbf{U}} - 1\right) = \mathrm{X}$$
$$\Rightarrow \mathrm{K}\dot{\mathbf{U}} + \left(\mu\mathrm{F}\mathrm{F}^{\mathrm{T}}\dot{\mathbf{U}} - \mu\mathrm{F}\right) = \mathrm{X}$$
$$\Rightarrow \mathrm{K}\dot{\mathbf{U}} + \mu\mathrm{F}\mathrm{F}^{\mathrm{T}}\dot{\mathbf{U}} = \mu\mathrm{F} + \mathrm{X}$$
$$\Rightarrow \left(\mathrm{K} + \mu\mathrm{F}\mathrm{F}^{\mathrm{T}}\right)\dot{\mathbf{U}} = \mu\mathrm{F} + \mathrm{X}$$
$$\Rightarrow \overline{\mathrm{K}}\dot{\mathbf{U}} = \mu\mathrm{F} + \mathrm{X}$$

where $\overline{K}$ is all stiffness matrix.

3.3 Rigid plastic constitutive equation of sandy soils

3.3.1 Strength tests of Toyoura sand by Tatsuoka et al.

As mentioned above, the effect of confining pressure on shear strength is clearly presented in Fig. 3.1 through experiments by Tatsuoka et al. on Toyoura sand. This figure shows that the internal friction angle decreases with the increase in confining pressure for constant void ratio. In this study, in order to estimate the influence of pressure level on ϕ in triaxial compression, the relationship between internal friction angle and first stress invariant is arranged in the normalization form. The general property in internal friction angle is surveyed against confining pressure. Fig. 3.1 indicates that the internal friction angle ϕ can be inferred by confining pressure for various void ratios. Fig. 3.2 demonstrates the relationship between internal friction angle ϕ and first stress invariant I_1 at failure. In reality, the friction angle decreases with an increase in the first stress variant in a logarithmic function. The range of the first stress variant is chosen according to test results. The secant friction angle corresponding to the peak of each first stress variant was larger than the approximated value obtained from the Mohr-Coulomb approach. Although the relationship is different depending on the void ratio, the figure shows the internal friction angle decreased with an increase in first stress invariant, irrespective of void ratio.

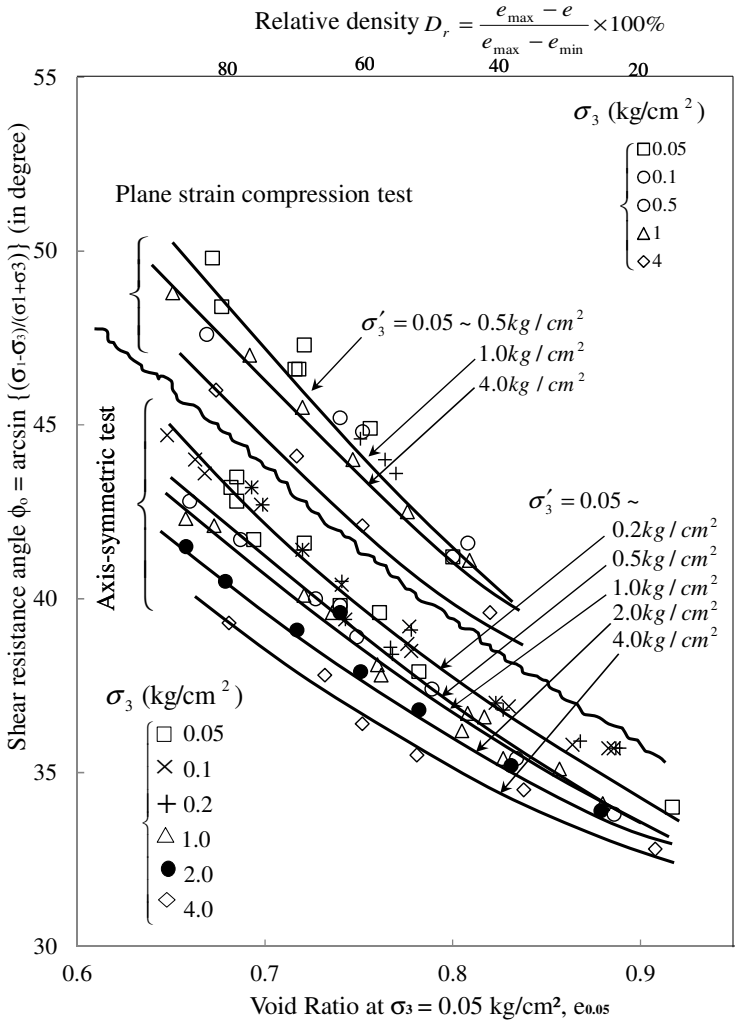

Figure 3.1. Experimental result of Toyoura sand (Tatsuoka et al., 1986)

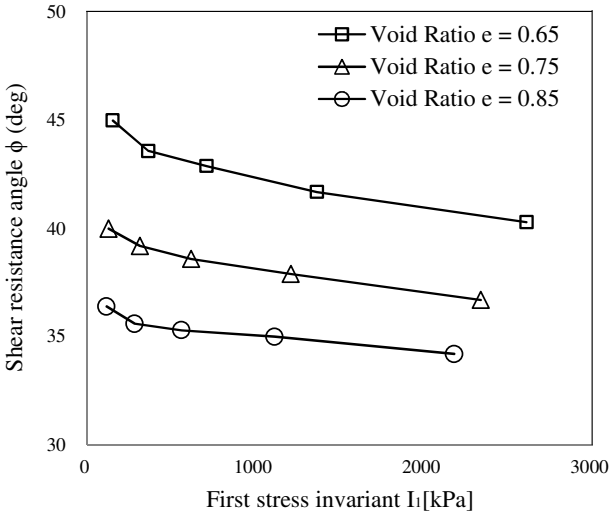

Figure 3.2. Relationship between internal friction angle and first stress invariant for Toyoura sand

The relationship between the internal friction angle and the first stress invariant is different from void ratio. This figure also shows the internal friction angle decreased with the increase in the first stress invariant. However, Fig. 3.3 indicates the relationship between normalized internal friction angle and normalized first stress invariant. ϕ_0 and I_{10} are the reference values of internal friction angle and first stress invariant. The figure shows that the normalized internal friction angles display a similar trend irrespective of void ratio, which means that the obtained relationship exhibits the common property of Toyoura sand.

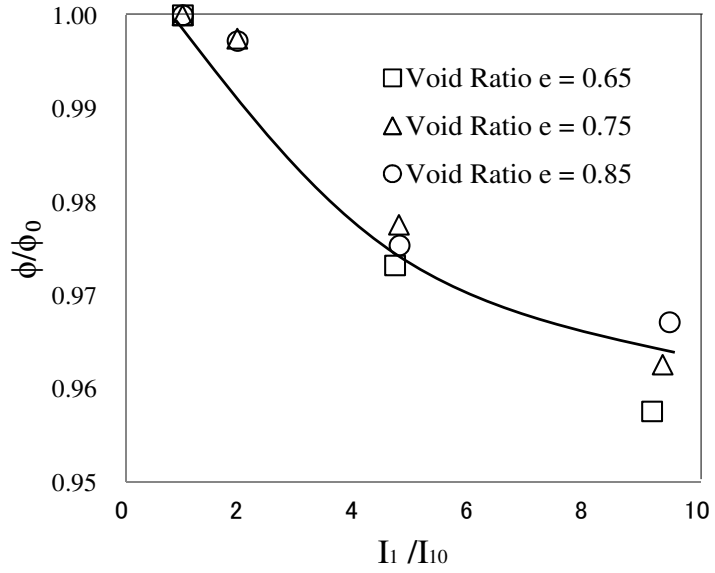

Figure 3.3. Relationship between normalized internal friction angle ϕ/ϕ_0 and normalized first stress invariable I_1/I_{10} for Toyoura sand

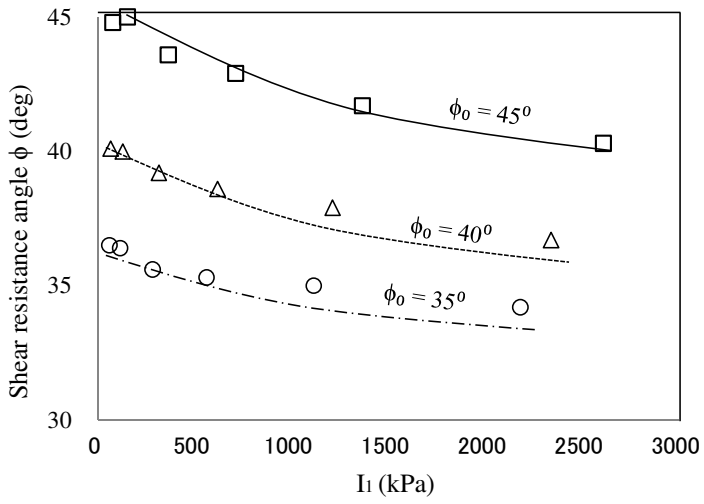

a) Relationship between internal friction angle and first stress invariant

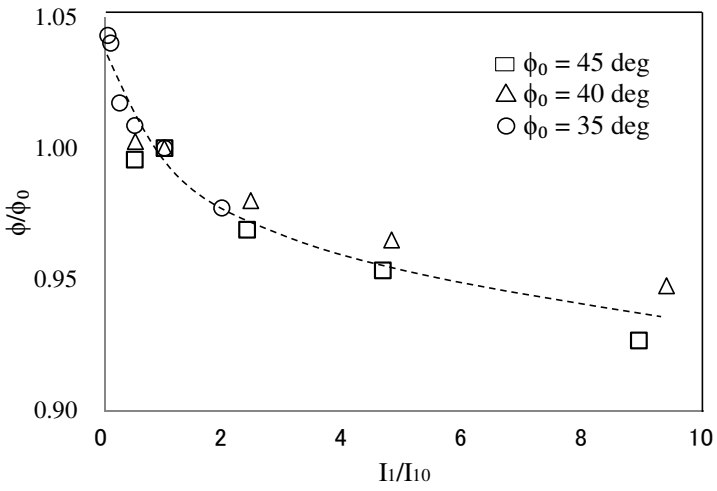

b) Relationship between normalized internal friction angle and normalized first stress invariant

Figure 3.4. Relationship between internal friction angle and first stress invariant of Toyoura sand

Fig. 3.4a expresses the internal friction angle of Toyoura sand for different void ratios and Fig. 3.4b shows the normalized curves for Fig. 3.4a. Although the different values of ϕ_0 and $I_{10}$are employed for normalization, the curves show the identical relationship between the normalized internal friction angle and the normalized first stress invariant in the figure. The obtained relationship, therefore, express the general property in the internal friction angle which is applicable to Toyoura sand.

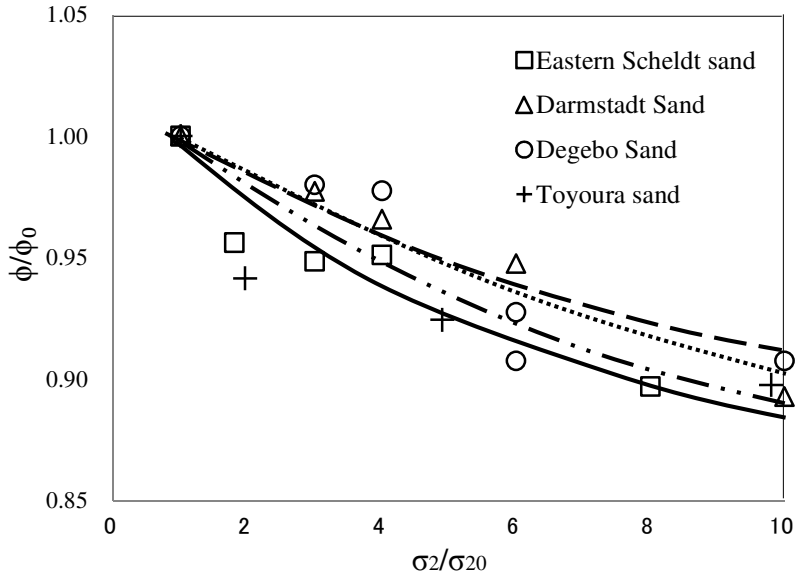

Figure 3.5. Relationship between ϕ/ϕ_0 and σ/σ_{20} for various kinds of sand

Hettler and Gudehus (1988) used three different types of sands which are Degebo sand, Eastern Scheldt sand and Darmstadt sand. The results from experiments show that the internal friction angle depends on the lateral stress in triaxial test. The normalized internal friction angle ϕ/ϕ_0 and the normalized lateral stress σ/σ_{20} for all types of soils show the same trends as shown in Fig. 3.5. It persuaded that the obtained relationship in the figure can be applied not only to Toyoura sand but also to various kinds of sands. Hettler and Gudehus (1988) have conducted triaxial test for some other sands and proposedthe formula showing the relationship between internal friction angle ϕ and ϕ_0 as below:

$$\phi = \arcsin \frac{\sin \phi^*}{\left(\frac{\sigma_2}{\sigma_{20}}\right)^{\zeta} + \sin \phi_0 \left[1 - \left(\frac{\sigma_2}{\sigma_{20}}\right)^{\zeta}\right]} \tag{3.9}$$

where, σ_2 : lateral stress, ζ estimated from triaxial tests.

ϕ^* : internal friction angle for the specific lateral stress σ_{20}.

Hettler and Gudehus (1988) also indicated that ζ is close to 0.1 and kept unchanged for various sands and densities as Table 1. Tatsuoka et al. (1986) and Ueno et al. (1998) indicated that the effect of confining pressure is considerable. Therefore, this study improves the rigid plastic finite element method by introducing the non-linear shear strength property against the confining pressure.

Table 1. Data for different sands

Sand	ϕ_0 (°)	σ_{20} (kPa)	ζ
Toyoura	41	10	0.1
Degebo	40	50	0.1
Eastern Scheldt	38	50	0.08
Darmstadt	43.8	50	0.1

Regarding Fig. 3.5, the references I_{10} and ϕ_0 are chosen depended on the examiner in the laboratory.

However, the property of the normalization between internal friction angle and first stress invariant always holds irrespective of the reference value of the confining pressure in the standardization of internal friction angle. Tatsuoka et al. (1986) and Ueno et al. (1998) [42] indicated that the effect of confining pressure is considerable. Therefore, this study improves the rigid plastic finite element method by introducing the non-linear shear strength property against the confining pressure.

3.3.2 Proposal of rigid plastic constitutive equation for non-linear strength property

In this study, the higher order hyperbolic function is introduced into the yield function of sandy soils as follows:

$$f(\boldsymbol{\sigma}) = aI_1 + (J_2)^n - b = 0 \tag{3.10}$$

where a and b are the soil constants. The index n expresses the degree in non-linearity in shear strength against the first stress invariant. Eq. (3.10) is identical with Drucker-Prager yield function in case of n=1/2. The non-linear parameters *a*, *b* and *n* are identified by the testing data. In the figure, the results by triaxial compression test are plotted for various confining stresses. Based on the associated flow rule, the strain rate is obtained as follows for the yield function of Eq. (3.10)

$$\dot{\boldsymbol{\varepsilon}} = \lambda \frac{\partial f(\boldsymbol{\sigma})}{\partial \boldsymbol{\sigma}} = \lambda \frac{\partial}{\partial \boldsymbol{\sigma}} \left(aI_1 + (J_2)^n - b \right) = \lambda \left(a\mathbf{I} + nJ_2^{n-1}\mathbf{s} \right) \tag{3.11}$$

where $\dfrac{\partial J_2^n}{\partial \boldsymbol{\sigma}} = nJ_2^{n-1} \dfrac{\partial J_2}{\partial \boldsymbol{\sigma}} = nJ_2^{n-1}\mathbf{s}$ (3.12)

Equivalence strain velocity

$$\begin{aligned} \dot{\mathbf{e}} = \sqrt{\dot{\boldsymbol{\varepsilon}} : \dot{\boldsymbol{\varepsilon}}} &= \sqrt{\left(\lambda \left(a\mathbf{I} + nJ_2^{n-1}\mathbf{s} \right) : \lambda \left(a\mathbf{I} + nJ_2^{n-1}\mathbf{s} \right) \right)} \\ &= \lambda \sqrt{a^2 (\mathbf{I} : \mathbf{I}) + anJ_2^{n-1}\mathbf{I} : \mathbf{s} + \left(nJ_2^{n-1} \right)^2 \mathbf{s} : \mathbf{s}} \\ &= \lambda \sqrt{3a^2 + \left(n^2 J_2^{2n-2} \right) \left(2J_2^1 \right)} = \lambda \sqrt{3a^2 + \left(2n^2 J_2^{2n-1} \right)} \end{aligned} \tag{3.13}$$

$$\Rightarrow \lambda = \frac{1}{\sqrt{3a^2 + \left(2n^2 J_2^{2n-1} \right)}} \dot{\mathbf{e}} \tag{3.14}$$

In the above equation, λ is the plastic multiplier. The volumetric strainrate is expressed as follows:

$$\dot{\varepsilon}_v = \mathrm{tr}\dot{\boldsymbol{\varepsilon}} = \mathrm{tr}\left(\lambda\left(a\mathbf{I} + nJ_2^{n-1}\mathbf{s}\right)\right) = 3a\lambda = \frac{3a}{\sqrt{3a^2 + 2n^2(b - aI_1)^{2-1/n}}}\dot{e} \tag{3.15}$$

The first invariant I_1 is identified from Eq. (3.10) to Eq. (3.15) as the following equation:

$$I_1 = \frac{b}{a} - \frac{1}{a}\left\{\frac{1}{2n^2}\left[\left(3a\frac{\dot{e}}{\dot{\varepsilon}_v}\right)^2 - 3a^2\right]\right\}^{\frac{n}{2n-1}} \tag{3.16}$$

Deviatoric stress

$$\dot{\boldsymbol{\varepsilon}} = \lambda\left(a\mathbf{I} + nJ_2^{n-1}\mathbf{s}\right) \tag{3.17}$$

$$\mathbf{s} = \frac{1}{n}\left(3a\frac{\dot{\boldsymbol{\varepsilon}}}{\dot{\varepsilon}_v} - a\mathbf{I}\right)\left\{\left\{\frac{1}{2n^2}\left[\left(3a\frac{\dot{e}}{\dot{\varepsilon}_v}\right)^2 - 3a^2\right]\right\}^{\frac{n}{2n-1}}\right\} \tag{3.18}$$

$$\boldsymbol{\sigma} = \mathbf{s} + \frac{1}{3}I_1\mathbf{I}$$

$$= \frac{1}{n}\left(3a\frac{\dot{e}}{\dot{\varepsilon}_v} - a\mathbf{I}\right)\left\{\frac{1}{2n^2}\left[\left(3a\frac{\dot{e}}{\dot{\varepsilon}_v}\right)^2 - 3a^2\right]\right\}^{\frac{1-n}{2n-1}} + \frac{1}{3}\left(\frac{b}{a} - \frac{1}{a}\left\{\frac{1}{2n^2}\left[\left(3a\frac{\dot{e}}{\dot{\varepsilon}_v}\right)^2 - 3a^2\right]\right\}^{\frac{n}{2n-1}}\right)\mathbf{I}$$

$$\boldsymbol{\sigma} = \frac{3a}{n}\left\{\frac{1}{2n^2}\left[\left(3a\frac{\dot{e}}{\dot{\varepsilon}_v}\right)^2 - 3a^2\right]\right\}^{\frac{1-n}{2n-1}}\frac{\dot{\boldsymbol{\varepsilon}}}{\dot{\varepsilon}_v}$$

$$+\left(\frac{b}{3a} - \frac{1}{3a}\left[\frac{1}{2n^2}\left(3a\frac{\dot{e}}{\dot{\varepsilon}_v}\right)^2 - 3a^2\right]^{\frac{n}{2n-1}} - \frac{a}{n}\left[\frac{1}{2n^2}\left(3a\frac{\dot{e}}{\dot{\varepsilon}_v}\right)^2 - 3a^2\right]^{\frac{1-n}{2n-1}}\right)\mathbf{I}$$

In this study, the non-linear rigid plastic constitutive equation for confining pressure is finally obtained as follows:

$$\boldsymbol{\sigma} = \frac{3a}{n}\left\{\frac{1}{2n^2}\left[\left(3a\frac{\dot{e}}{\dot{\varepsilon}_v}\right)^2 - 3a^2\right]\right\}^{\frac{1-n}{2n-1}}\frac{\dot{\boldsymbol{\varepsilon}}}{\dot{\varepsilon}_v}$$

$$+\left(\frac{b}{3a} - \frac{1}{3a}\left[\frac{1}{2n^2}\left(3a\frac{\dot{e}}{\dot{\varepsilon}_v}\right)^2 - 3a^2\right]^{\frac{n}{2n-1}} - \frac{a}{n}\left[\frac{1}{2n^2}\left(3a\frac{\dot{e}}{\dot{\varepsilon}_v}\right)^2 - 3a^2\right]^{\frac{1-n}{2n-1}}\right)\mathbf{I} \tag{3.19}$$

In this equation, stress is uniquely determined for plastic strain rate and it is different from Eq. (2.115) for Drucker-Prager yield function.

References

[1] Du N. L., Ohtsuka S., Hoshina T., Isobe K., 2016. Discussion on size effect of footing in ultimate bearing capacity of sandy soil using rigid plastic finite element method", Soils and Found., 56(1).

[2] Houlsby G. T., Cassidy M. J., 2002. A plasticity model for the behavior of footings on sand under combined loading", Géotechnique, **52**(2), 117-129.

[3] Meyerhof, G. G., 1951. Ultimate bearing capacity of foundations, Géotechnique, **2**(4), 301-332.

[4] Meyerhof, G. G., 1963. Some recent research on the ultimate bearing capacity of foundations", Can. Geotech. J., **1**(1), 243-256

[5] Takeshi Hoshina, Satoru Ohtsuka and Koichi Isobe, 2011. Ultimate bearing capacity of ground by Rigid plastic finite element method taking account of stress dependent non-linear strength property, J. Appl. Mech. **6**, 191–200 (in Japanese).

[6] Tamura, T., 1990. Rigid-plastic finite element method in geotechnical engineering. Soc. Mater. Sci., Jpn. 7, 135–164.

[7] Tatsuoka, F., Sakamoto, M., Kawamura, T. and Fukushima, S., 1986. Strength and deformation characteristics of sand in plane strain compression at extremely low pressures, Soils Found., **26**(1), 65– 84.

[8] Tastuoka, F., Goto, S. and Sakamoto, M., 1986c. Effects of some factors on strength and deformation characteristics of sand at low pressures, Soils Found., **26**(4), 79-97.

[9] Ueno, K., Miura, K. and Maeda, Y., 1998. Prediction of ultimate bearing capacity of surface footings with regard to size effects, Soils Found., **38**(3), 165-178.

CHAPTER 4

NUMERICAL SIMULATION ON RIGID PLASTIC FINITE ELEMENT METHOD

4.1 Ultimate bearing capacity of footing under plane strain condition using rigid Plastic constitutive equation for Drucker –Prager yield function

In this study, the input parameters for ultimate bearing capacity analysis under plane strain condition are derived from triaxial compression tests in the same way with the conventional methods. If the computed results show the good agreement between the RPFEM and the conventional formulas, it indicates RPFEM can provide a good estimation for ultimate bearing capacity since the conventional formulas are developed semi-empirically. In this study, ultimate bearing capacity of strip footing subjected to uniform vertical load is investigated by RPFEM. The load is applied at the center of footing with the width *B*. This footing is modeled by a solid element, the strength of which is set large to be rigid. The typical finite element mesh and the boundary condition employed for RPFEM are shown in Fig. 4.1.

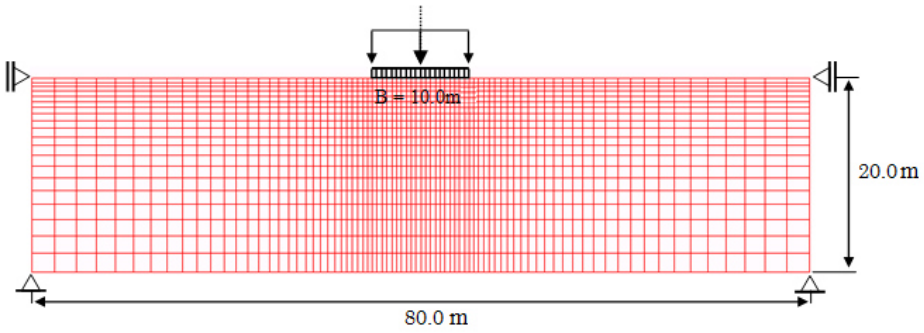

Figure 4.1 Typical finite element mesh and boundary condition in case of B=10m

In the case of vertical load, the typical finite element mesh and the boundary condition employed for RPFEM are shown in Fig. 4.1. This study computed the ultimate bearing capacity for internal friction angle ϕ=20deg, ϕ=30deg and ϕ=40deg, the obtained results are presented in Figs.4.2a, 4.2b and 4.2c. The bigger the footing width is, the higher the ultimate bearing capacity is. The values obtained from RPFEM with Drucker-Prager (DP) yield function are coincident with the results from the formulas of Meyerhof and Euro-code 7 when the footing

width is less than 30m. Since the Euro-code formula employs the different concepts regarding the bearing capacity factor, it leads to the ultimate bearing capacity values different from the other formula. Thus, the discrepancies among them become larger at the footing width of 100m. This width seems too large in practice, but it is considered clearly to discuss the size effect of footing on ultimate bearing capacity.

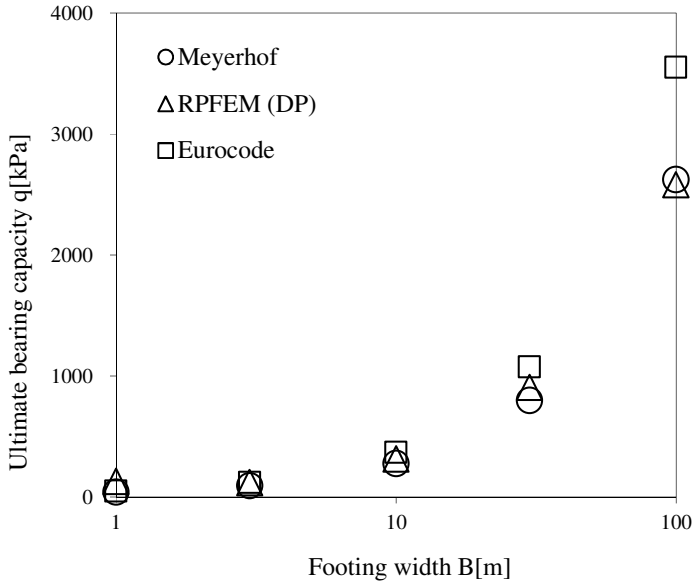

(a) ϕ = 20deg.

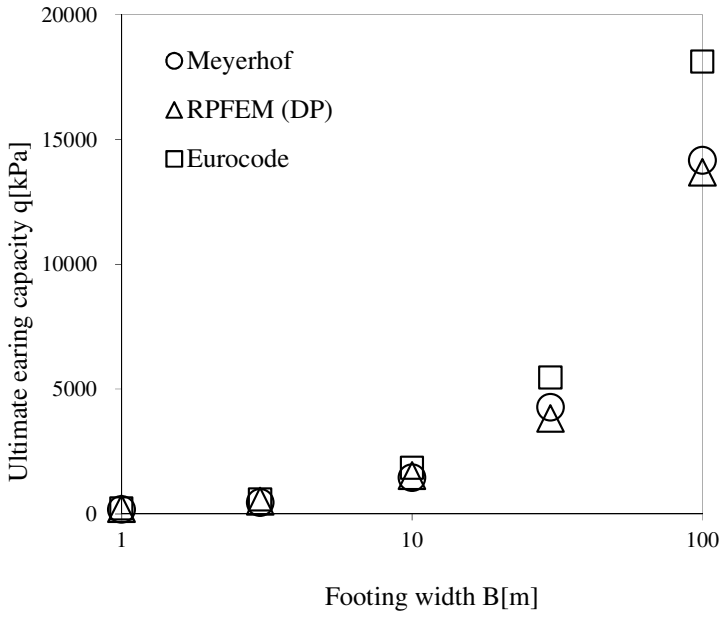

(b) ϕ = 30deg.

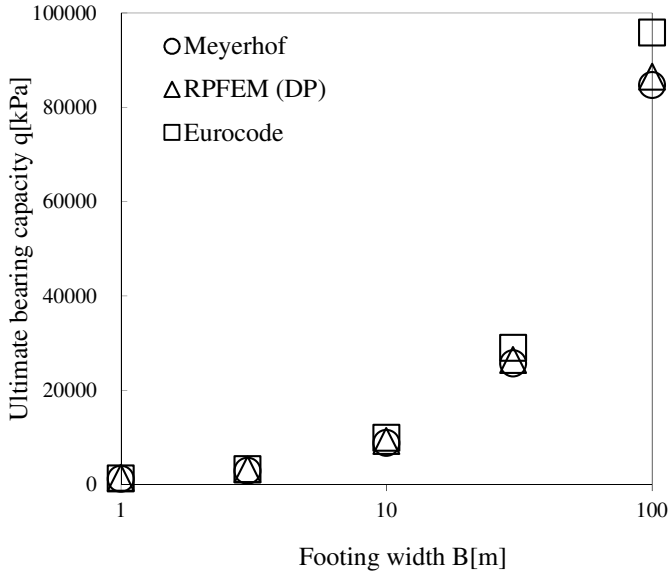

(c) ϕ = 40deg

Figure 4.2. Ultimate bearing capacity for vertical load application in case (a) ϕ = 20deg, (b) ϕ = 30deg and (b) ϕ = 40deg.

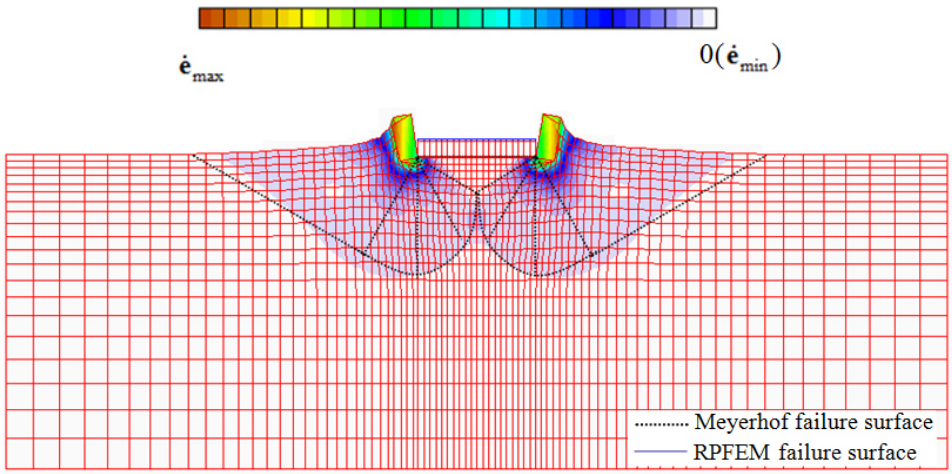

Figure 4.3. Deformation diagrams of the Drucker-Prager yield function with B=10m

Ultimate bearing capacity is computed for B=10m and ϕ=30deg. The obtained velocity field is shown in Fig. 4.3 which indicates the typical failure mode of ground. The norm of strain rate, $\dot{e}$ is presented by contour lines. It is illustrated by the range between $\dot{e}_{max}$ and $0(\dot{e}_{min})$ since it is basically indeterminate and the relative magnitude in $\dot{e}$ affects the magnitude of ultimate

bearing capacity. The slip-line assumed in the conventional bearing capacity formula is also plotted in the figure. The failure mode that is inferred by computation result is similar with the slip-line assumed in the conventional formula. It is difficult to determine the slip-line by RPFEM since FEM is based on the continuum theory. However, it can be seen to provide the similar slip-line although it is slightly smaller than that of the conventional formula. In case of rigid footing, stress concentration is widely known to generate at edge of footing. It causes a problem of singularity in stress distribution of ground. Since finite element analysis is based on continuous function for shape function, it can't analyze the singularity problem directly. Thus, it analyzes the problem approximately. In sandy soil, the shear strength at edge of footing is affected by free stress condition of ground surface outside the footing. The degree of singularity in stress distribution is, therefore, comparatively moderate in case of sandy soil since the shear strength depends on confining stress. In this study, no special numerical technique to analyze the ultimate bearing capacity is employed as the past references (Ukritchon et al., (2003) and Lyamin et al., (2002)). As shown in Fig. 4.3, the velocity field of ground at edge of footing is obtained greatly from the viewpoint of total balance in velocity field. It seems to reflect the above-mentioned problem, but it is due to the limitation of regular finite element method. This problem is partly resolved by using finer finite elements. The applicability of rigid plastic finite element method is examined through the comparison with the past bearing capacity formulas and finite element analysis. In preliminary analysis, the effect of mesh size on ultimate bearing capacity was investigated by comparing bearing capacities computed for 1640 and 3423 element meshes which produces ultimate bearing capacity of 201.9 kPa, 504.9 kPa, 1530.7 kPa, 3822.1 kPa and 13691.2 kPa. The finite element meshes in this study produce ultimate bearing capacity of 201.8 kPa, 503.8 kPa, 1528.8 kPa, 3821.7 kPa and 13685.4 kPa with footing widths: 1m, 3m, 10m, 30m and 100m, respectively. The obtained results are almost coincident for all cases where the footing width is varied from 1m to 100m. Thus, the employed finite element meshes provide good estimation for various cases in this study.

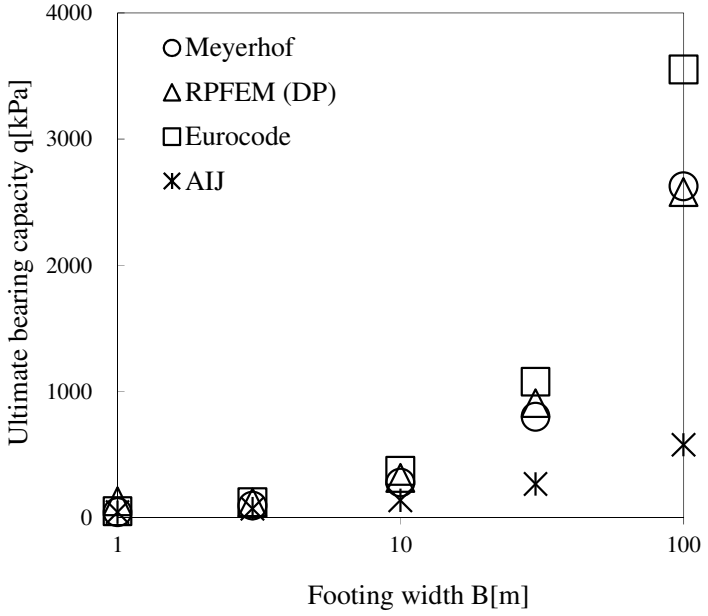

(a) ϕ = 20deg

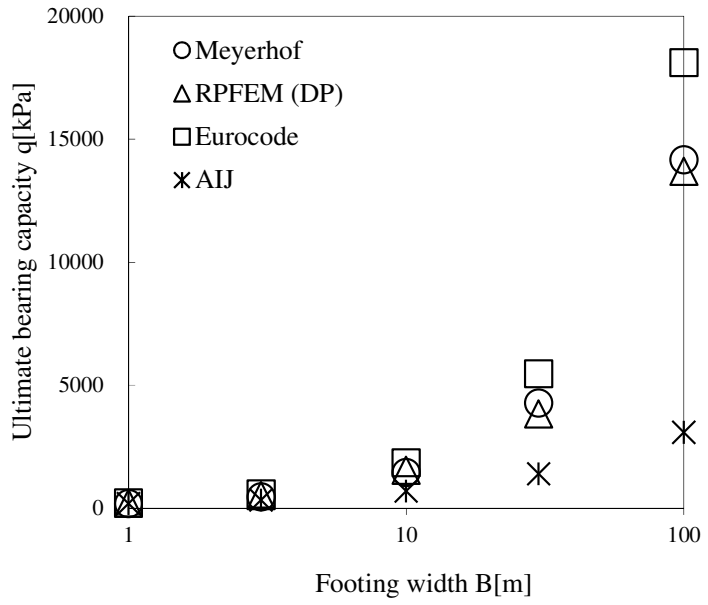

(b) ϕ = 30deg

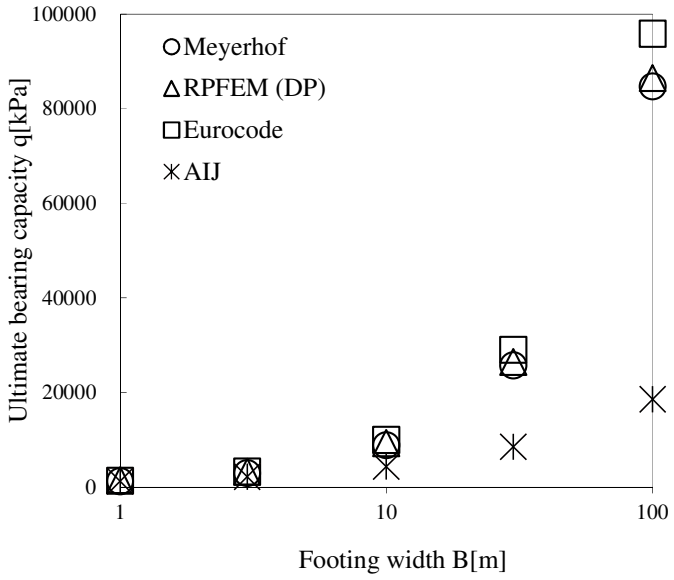

(c) ϕ = 40deg

Figure 4.4. Effect of footing width on ultimate bearing capacity for vertical load application

AIJ formula takes into account the size effect of footing on ultimate bearing capacity. Fig. 4.4 indicates the comparison in ultimate bearing capacity among AIJ formula and others. The results from AIJ formula are smaller than those from others that don't consider the size effect of footing. A great discrepancy can be seen in ultimate bearing capacity at footing width of 100m. Since AIJ formula is developed by semi-experimentally, it implies RPFEM needs to take into account the size effect of footing in ultimate bearing capacity assessment.

4.2 Ultimate bearing capacity of footing under plane strain condition using rigid Plastic constitutive equation for non-linear shear strength property

In bearing capacity problem, the larger the footing width is, the higher the confining stress is. This leads the internal friction angle to be decreased as discussed above. It is, therefore, necessary to apply the non-linear shear strength property against the confining stress to take into account the size effect of footing on ultimate bearing capacity. On the other hand, the internal friction angle is set constant in RPFEM in case of the Drucker-Prager yield function. Therefore, the ultimate bearing capacity calculated by using the non-linear rigid-plastic constitutive equation becomes smaller than that obtained from the Drucker-Prager yield function. It means

that the size effect of footing is properly taken into account in computation. Non-linear yield function (Eq.2.21) is defined by the parameters a, b, and n which are derived from the experiment. In this study, a series of numerical simulation are conducted for Toyoura sand based on the experiment of Tatsuoka (1986). Through the case studies, the non-linear shear strength parameters of Toyoura sand are set as a=0.24, b=2.4 (kPa) and n=0.56 for case internal friction angle 30deg and a=0.28, b=2.8 (kPa) and n=0.57 for case internal friction angle 40deg, respectively.

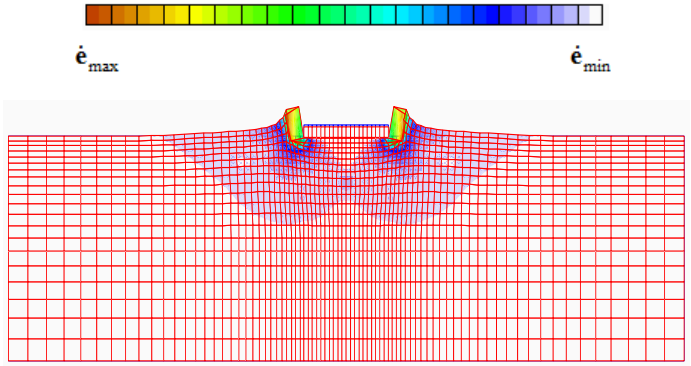

Figure 4.5. Deformation diagram of the non-linear shear strength with B=10m

Fig.4.5 shows the deformation of ground at the limit state computed by multiplying arbitrary time increment to the velocity field obtained by RPFEM for B=10m.The obtained failure mode of ground is similar to that in Fig. 4.3 for the linear shear strength of Drucker-Prager yield function. However, the deformation area in the case of linear shear strength is obtained larger than that in the case of non-linear shear strength, especially around the edge of footing.

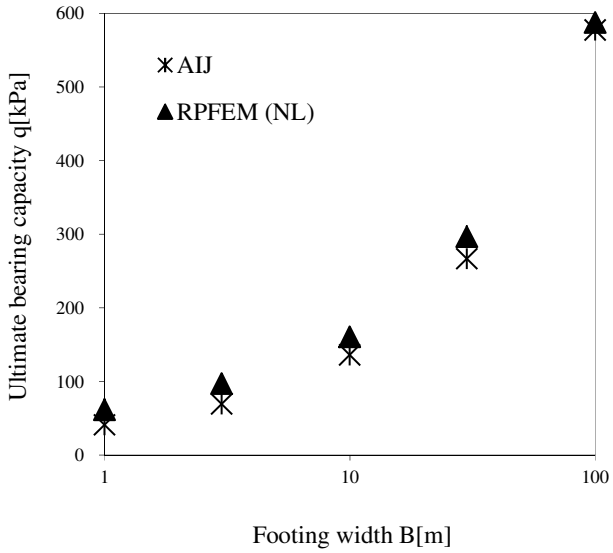

(a) ϕ_0 = 20deg

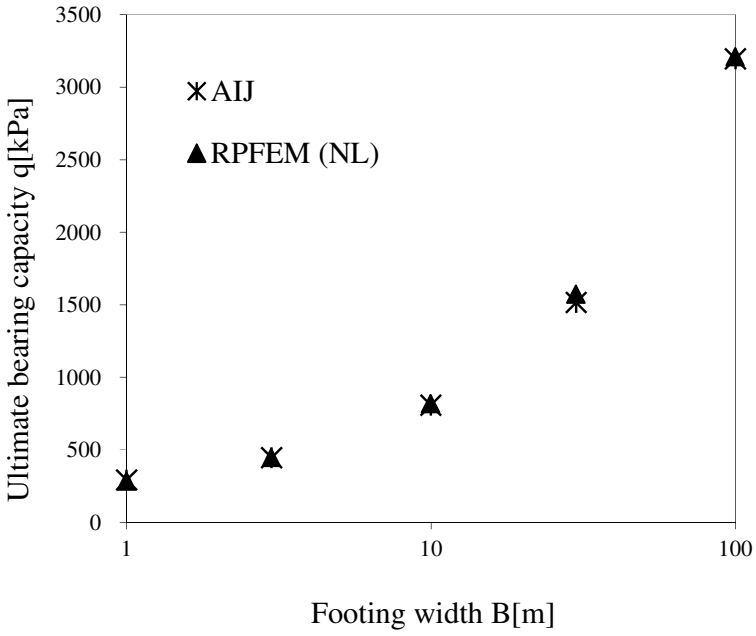

(b) ϕ_0 = 30deg

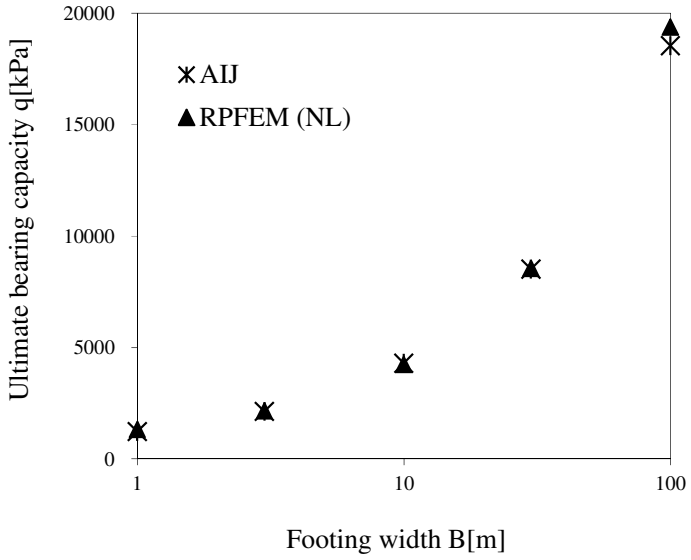

(c) ϕ_0 = 40deg.

Figure 4.6. Ultimate bearing capacity with non-linear shear strength in case (a) ϕ_0 = 20deg, (b) ϕ_0 = 30deg. and (c) ϕ_0 = 40deg.

Fig. 4.6 shows the results of RPFEM with non-linear shear strength in the case the internal friction angle of 30 and 40 deg. In the figure, these results are clearly identical with those of AIJ. It means that the results obtained by employing non-linear shear strength property is rational

and it shows that the size effect of footing in ultimate bearing capacity can be well expressed by considering the non-linear shear strength against the confining pressure.

References

[1] AIJ (1988, 2001), Architectural Institute of Japan. Recommendations for design of building foundations, 430p.

[2] Du L. Nguyen, Ohtsuka S., Hoshina T., Isobe K., 2016. Discussion on size effect of footing in ultimate bearing capacity of sandy soil using rigid plastic finite element method, Soils Found., **56**(1).

[3] Georgiadis M., Butterfield, 1988. Displacements of footings on sand under eccentric and inclined loads", Can. Geotech. J., **25**(2), 199-212.

[4] Hanna A. M., Meyerhof G. G., 1981. Experimental evaluation of bearing capacity of footings subjected to inclined loads", Can. Geotech. J., **18**(4), 599-603.

[5] Houlsby G. T., Cassidy M. J., 2002. A plasticity model for the behavior of footings on sand under combined loading, Géotechnique, **52**(2), 117-129.

[6] Meyerhof, G. G., 1951. Ultimate bearing capacity of foundations, Géotechnique, **2**(4), 301-332.

[7] Meyerhof, G. G., 1963. Some recent research on the ultimate bearing capacity of foundations", Can. Geotech. J., **1**(1), 243-256

[8] Mohammed Hjiaj, Andrei V. Lyamin, Scott W. Sloan, 2004. Bearing capacity of a cohesive-frictional soil under non-eccentric inclined loading", Computers and Geotechnics, **31**(6), 491-516.

[9] Loukidis D., Chakraborty T., Salgado R., 2008. Bearing capacity of strip footings on purely frictional soil under eccentric and inclined loads", Can. Geotech. J., **45**(6), 768-787.

[10] Takeshi Hoshina, Satoru Ohtsuka and Koichi Isobe, 2011. Ultimate bearing capacity of ground by Rigid plastic finite element method taking account of stress dependent non-linear strength property, J. Appl. Mech. **6**, 191–200 (in Japanese).

[11] Tamura, T., 1990. Rigid-plastic finite element method in geotechnical engineering. Soc. Mater. Sci., Jpn. 7, 135–164.

CHAPTER 5

DISCUSSION ON SIZE EFFECT OF FOOTING ON ULTIMATE BEARING CAPACITY

The conventional RPFEM with Drucker-Prager function does not take into account the size effect on ultimate bearing capacity, which is considered in the AIJ formula, because RPFEM is based on the same framework with the other conventional ultimate bearing capacity formulae. This study improves RPFEM by using the non-linear shear strength property of soils and introduces the rigid plastic constitutive equation of parabolic yield function regarding the confining pressure. This study has shown that internal friction angle is not constant and decreases with the increase in confining pressure in sandy soils. It implies the confining pressure dependency in soil shear strength may be one of the most important factors affecting the size effect of footing.

5.1 Effect of non-linear shear strength property of sandy soils

The computed results are utilized to determine the bearing capacity factor N_γ for the various internal friction angle from 0 deg to 40 deg. The obtained bearing capacity factor N_γ is compared with these factors defined based on the empirical method by Meyerhof (1963 - Semi-empirical), Muhs and Weiss (1969-Euro-code7, Semi-empirical). Although the cohesion of soils (c = 1 kN/m^2) is introduced into the analysis to make the computation process stable, it does not affect the ultimate bearing capacity too much. Therefore, Eqs. 5.1 and 5.2 are applied to approximately define N_γ. The bearing capacity factor N_γ of RPFEM for Drucker –Prager is calculated by the following equation:

$$N_\gamma^{DP} = \frac{2q^{DP}}{\gamma_1 B} \tag{5.1}$$

On the other hand, the bearing capacity factors N_γ for non-linear shear strength is determined by the equation:

$$N_\gamma^{NL} = \frac{2q^{NL}}{\gamma_1 B} \tag{5.2}$$

The bearing capacity factor N_γ was compared among the bearing capacity formulas of AIJ,

Euro-code 7 and Meyerhof with RPFEM. Fig. 5.1 shows the comparison in bearing capacity factor by changing internal friction angle from 0 to 40 deg. As shown in the figure, the bearing capacity factor by RPFEM employing non-linear shear strength against the confining pressure match those by AIJ formula in the wide range of internal friction angle. It is obtained smaller than that by the formulas of Euro-code 7 and Meyerhof. When the internal friction angle less than 30deg, there is not so much difference in bearing capacity factor among them. But, the difference becomes greater at the internal friction angle of 40 deg.

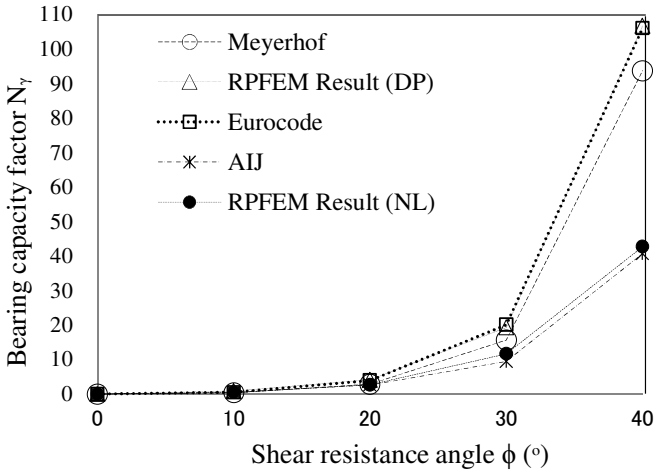

Figure 5.1. Relationship between bearing capacity factor N_γ and internal friction angle ϕ

5.2 Effect of multi-layered ground system

In ultimate bearing capacity assessment for multi-layered ground, the current ultimate bearing capacity formula cannot provide an estimation for complicate ground conditions. On the other hand, RPFEM can estimate various ultimate bearing capacity problems of footing which are difficult to solve by the conventional method due to the complicate conditions of material property and geometry of footing. Thus, this study discusses the size effect of footing on ultimate bearing capacity for multi-layered ground where sand layer overlays clay layer. FEM is a powerful tool to analyze the complicated boundary value problems. It is applicable to non-uniform materials such as the multi-layered ground and provides a good estimation for problems. Fig. 5.2a shows that thin sand layer overlays thick clay bed. In the conventional method, a sand mass of approximately truncated pyramidal shape is assumed to be pushed into the clay bed so that, the friction angle of sand layer and the cohesion of clay bed are mobilized in the combined failure zone. The ultimate bearing capacity is computed by the equilibrium

equation of sand block. Although the selected value of the side angles of the block α can have a main influence on the calculated bearing capacity, it is often not clear how its value should be nominated. In practice, the side angles of the block α proposed by various researchers are different from each other; for example, a value of α of $\tan^{-1}0.5$ is often adopted (Houlsby et al. 1989), 30 (deg) for Yamaguchi and Terashi (1971), $\tan^{-1}0.5$ for Kraft and helfrich (1983) and ϕ for Baglioni et al. (1982). On the other hand, in the case of thick sand layer, the multi-layered ground can be modeled into uniform ground in the assessment of ultimate bearing capacity of footing. Thus, the size effect of footing on ultimate bearing capacity is exerted. However, these failure modes depend on the relationship between the footing width and the thickness of sand layer. The ultimate bearing capacity of footing is investigated for the footing width from 1 to 100m under the condition of sand layer as 10m in thickness. It is performed by three methods of conventional method based on Meyerhof, RPFEM for uniform sandy soil and RPFEM for multi-layered ground.

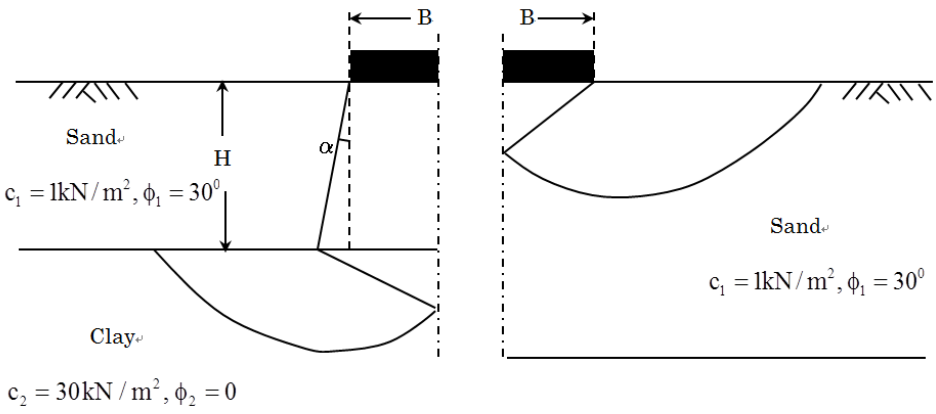

a) Thin layer b) Thick layer

Figure 5.2 Failure modes of soils in multi-layered ground

In conventional methods, Hanna and Meyerhof (1980) are perhaps the most widely used in practice. Their methods are also known as punching shear models, as they assume the sand layer to be in a state of passive failure along vertical planes beneath the footing edges. For a strip footing of width *B* on the upper sand layer, Meyerhof and Hana (1980) proposed the ultimate bearing capacity given by

$$q = c_2 N_c + \frac{1}{B}\gamma_1 H^2 K_s \tan\phi_1 \tag{5.3}$$

where c_2 : representative strength of underlying clay $(\mathrm{kN/m^2})$

B: footing width (m)

γ_1: unit weight of sand $(\mathrm{kN/m^3})$

H: thickness of the sand below the footing (m)

K_s: punching shear coefficient

ϕ_1 : internal friction angle of sand (deg)

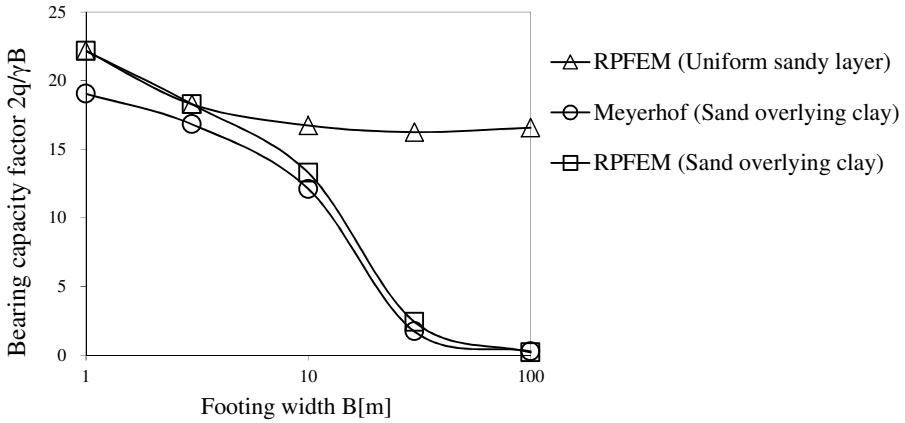

Figure 5.3. Effect of footing width on bearing capacity factor $2q/\gamma B$ in case of multi-layered ground

Fig. 5.3 shows the size effect of footing width on bearing capacity factor $2q/\gamma B$ in the case of multi-layered ground. From the results by RPFEM, the ultimate bearing capacity of footing the width of which is within 3m is obtained to match that of uniform sandy soils. In the conventional method, by assuming diffusion of stress from the footing to the clay bed through the sand layer, the ultimate bearing capacity of footing is assessed by the failure of clay layer. It is widely employed to assess the ultimate bearing capacity, but the assumption of stress diffusion has not been clarified and the contribution of sand layer to the ultimate bearing capacity is not taken into account. Therefore, the results of ultimate bearing capacity of footing from RPFEM are different with the results from Meyerhof's formula at the footing size from 10m to 30m. At bigger footing width, the multi-layered ground can be modeled into uniform clay ground in the assessment of ultimate bearing capacity of footing. This leads the ultimate

bearing capacity results from RPFEM is similar to the results from Meyerhof's formula at footing size 100m as shown in Fig. 5.3.

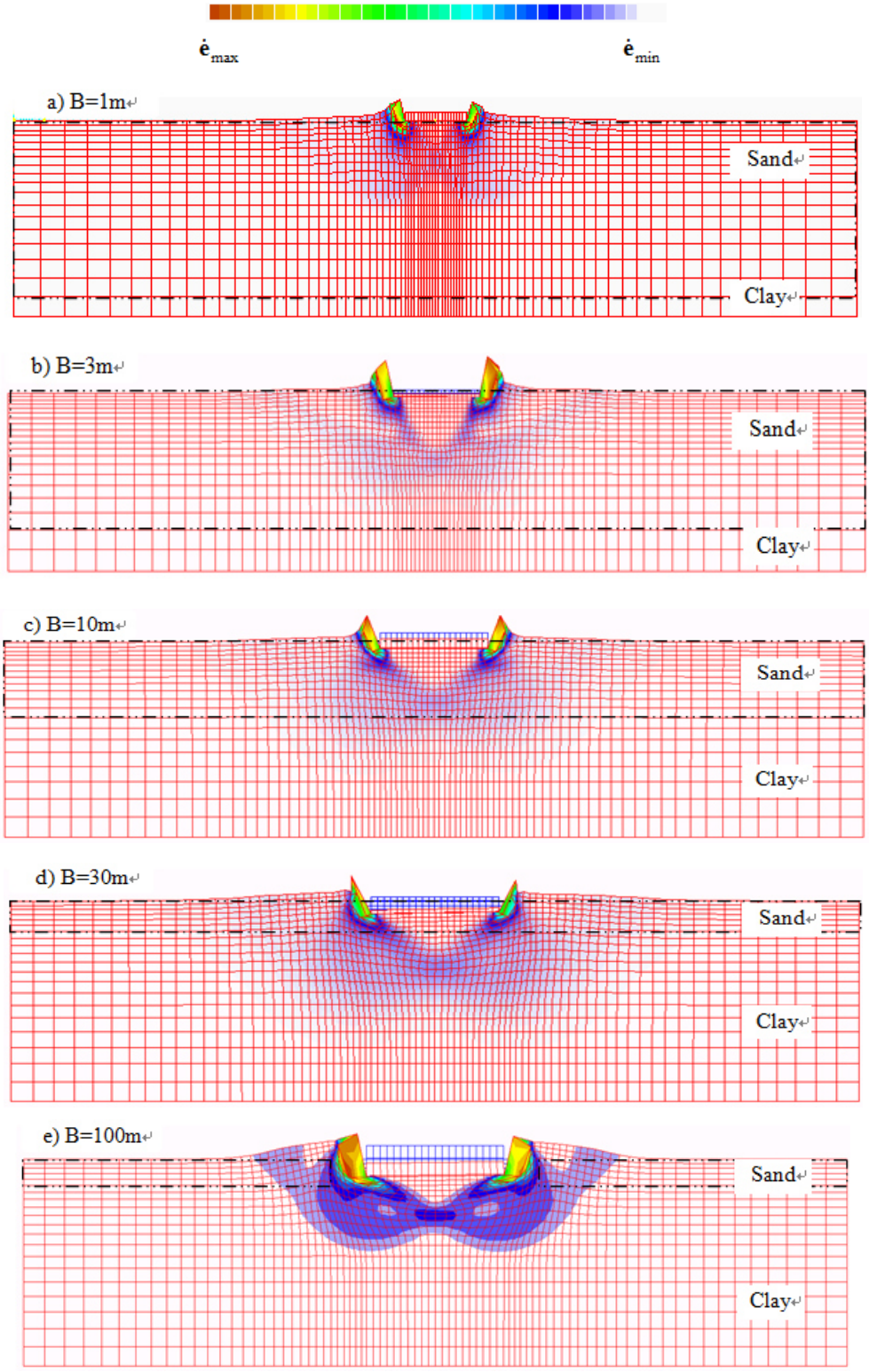

Figure 5.4. Failure mechanism and strain rate distribution in the ground at various widths of footing (a) *B*=1m, (b) *B*=3m, (c) *B*=10m, (d) *B*=30m, (e) *B*=100m

Fig. 5.4 illustrates the deformation of ground according to strain rate distribution for the footing width from 1 to 100m. By comparing Fig. 5.4a to Fig. 5.4e, it can be seen that the area in ground failure becomes wider as the footing width is larger. It is inside the sand layer when the footing width is small. But it expands to the clay layer with the increase in footing width. Size effect of footing in ultimate bearing capacity can be observed for not only uniform grounds, but also multi-layered grounds. Since the ultimate bearing capacity formula is developed for uniform grounds, the applicability of the method is severely limited in design practice. The results in both ultimate bearing capacity and failure mode are shown appropriately obtained for the prescribed footing width. Through the examination on the computed results, the developed rigid plastic FEM is proved to afford a rational assessment for the problems in which the ultimate bearing capacity is difficult to be assessed by using the current bearing capacity formulas.

5.3 Discussion

(1) Bearing capacity factor N_γ was compared among the bearing capacity formulas of AIJ, Euro-code 7 and Meyerhof with RPFEM by changing internal friction angle from 0 to 40 deg. The bearing capacity factor by RPFEM employing non-linear shear strength against the confining pressure matched those by AIJ formula in the wide range of internal friction angle. It was obtained smaller than that by the formulas of Euro-code 7 and Meyerhof. The difference in bearing capacity factor was shown greater at the internal friction angle of 40 deg.

(2) Size effect of footing in the case of multi-layered ground was investigated for the ground where sand layer overlaid clay layer. By simulation results, the size effect of footing was clearly shown to be generated by the change in failure mode of ground due to footing width.

(3) Wide applicability of developed RPFEM to the assessment of ultimate bearing capacity was shown through the case studies.

References

[1] AIJ (1988, 2001), Architectural Institute of Japan. Recommendations for design of building foundations, 430p.

[2] Du L. Nguyen, Ohtsuka S., Hoshina T., Isobe K., 2016. Discussion on size effect of footing in ultimate bearing capacity of sandy soil using rigid plastic finite element method", Soils and Found., 56(1).

[3] Edgar G. D., 2013. Assessment of the range of variation of N_γ from 60 estimation methods for footings on sand, Can. Geotech. J., **50**(7), 793-800.

[4] Frydman, S., and Burd, H. J., 1997. Numerical studies of ultimate bearing capacity factor, N_γ", J. Geotech. Geoenviron. Eng., **123**(1), 20-29.

[5] Georgiadis M., Butterfield, 1988. Displacements of footings on sand under eccentric and inclined loads", Can. Geotech. J., **25**(2), 199-212.

[6] Hanna, A., M., and Meyerhof, G. G., 1980. Design charts for ultimate bearing capacity of foundations on sand overlying soft clay, Can. Geotech. J., **17**(2), 300-303.

[7] Hettler, A. and Gudehus, G., 1988. Influence of the foundation width on the ultimate bearing capacity factor", Soils Found., **28**(4), 81-92.

[8] Hjiaj, M., Lyamin, A. V., Sloan, S. W., 2005. Numerical limit analysis solutions for the ultimate bearing capacity factor N_γ, Int. J. Sol. Struct., **42**, 1681 – 1704.

[9] Houlsby G. T., Cassidy M. J., 2002. A plasticity model for the behavior of footings on sand under combined loading", Géotechnique, **52**(2), 117-129.

[10] Meyerhof, G. G., 1951. Ultimate bearing capacity of foundations, Geotechnique, **2**(4), 301-332

[11] Meyerhof, G. G., 1963. Some recent research on the ultimate bearing capacity of foundations", Can. Geotech. J., **1**(1), 243-256

[12] Meyerhof, G. G., 1974. Ultimate bearing capacity of footings on sand layer overlying clay", Can. Geotech. J., **11**(2), 223-229

[13] Okamura M, Takemura J, Kimura T, 1997. Centrifuge model tests on ultimate bearing capacity and deformation of sand layer overlying clay, Soils Found., **38**(1), 181–194.

[14] Okamura M, Takemura J, Kimura T, 1997. Ultimate bearing capacity predictions of sand overlying clay based on limit equilibrium methods, Soils Found., **37**(1), 73–87.

[15] Mohammed Hjiaj, Andrei V. Lyamin, Scott W. Sloan, 2004. Bearing capacity of a cohesive-frictional soil under non-eccentric inclined loading, Computers and Geotechnics, **31**(6), 491-516.

[16] Loukidis D., Chakraborty T., Salgado R. 2008. Bearing capacity of strip footings on purely frictional soil under eccentric and inclined loads", Can. Geotech. J., **45**(6), 768-787.

[17] Shiraishi, S., 1990. Variation in ultimate bearing capacity factors of dense sand assessed by mode loading tests, Soils Found., **30**(1), 17-26.

[18] Siddiquee, M. S. A., Tatsuoka, F., Tanaka, T., Tani, K., Yoshida, K. and Morimoto, T., 2001. Model tests and FEM simulation of some factors affecting the ultimate bearing capacity of a footing on sand, Soils Found., **41**(2), 53 – 76.

[19] Takeshi Hoshina, Satoru Ohtsuka and Koichi Isobe, 2011. Ultimate bearing capacity of ground by Rigid plastic finite element method taking account of stress dependent non-linear strength property, J. Appl. Mech. **6**, 191–200 (in Japanese).

[20] Tamura, T., 1990. Rigid-plastic finite element method in geotechnical engineering. Soc. Mater. Sci., Jpn. 7, 135–164.

[21] Yamamoto, K., Otani, J., 2002. Ultimate bearing capacity and failure mechanism of reinforced foundations based on rigid-plastic finite element formulation", Geotextiles and Geomembrances, 367-393.

[22] Yamamoto, N., Randolph, M. F. and Einav, I., 2009. Numerical study of the effect of foundation size for a wide range of sands, J. Geotech. Geoenviron. Eng., ASCE, **135**(1), 37-45.

CHAPTER 6
ULTIMATE BEARING CAPACITY OF FOOTING ON SANDY SOIL AGAINST COMBINED LOADING

The ultimate bearing capacity of footing related to inclined loads is an important aspect in geotechnical engineering. Because the number of superstructure buildings has increased and great earthquakes occur regularly, estimating the ultimate bearing capacity of footing with considering the effect of footing width is necessary. The strip footings are often subjected to the inclined loads and the combined loads. The ultimate bearing capacity for combined vertical and horizontal loads (with no moments) is resolved by Green (1954). The general case of vertical, horizontal and moment loads has received less attention. Several authors (notably Meyerhof 1953, Hansen 1970 and Vesic 1975) provide procedures for a general case; however they only conduct empirical generalizations of the simpler cases without examining in detail.

Under such circumstances the ultimate bearing capacity theories presented in Chapter 2 need some modification, and this is the subject of discussion in this chapter. The chapter is divided into two major parts. The first part discusses the ultimate bearing capacities of footing subjected to centric inclined loads, and the second part is devoted to the ultimate bearing capacity of footing under vertical, horizontal and moment combination.

In previous geotechnical research, the combined vertical and horizontal load is referred as the inclined loads. Their results showed that the vertical bearing capacity significantly decreased when the inclined angle $\theta = \text{atan}(H/V)$ increased. Many researchers provide procedures for a general case; however they only conduct empirical generalizations of the simpler cases without examining in detail.

There are few analyses related to inclined load for sandy soils except Loukidis et al. (2008). However, the effect of footing width on ultimate bearing capacity is not considered directly. As shown in Eqs. 2.5 and 2.6, the size effect of footing is large in case of sandy soil. It can be seen in the combined load space of vertical, horizontal and moment loads. This is a major topic of this study.

There are few analyses related to inclined load for sandy soils except Loukidis et al. (2008). However, the effect of footing width on ultimate bearing capacity is not considered directly. The

inclination coefficient proposed by Loukidis et al. (2008) is also shown. They proposed the inclination factor i_γ based on the FE analysis as follows:

$$i_\gamma = \frac{V}{V_0} = \left(1 - \frac{(H/V)}{\tan\phi}\right)^{(1.5\tan\phi+0.4)^2} \tag{6.1}$$

This research investigated the ultimate bearing capacity of footing on sandy soils against the combined load of vertical, horizontal and moment loads. This research applied rigid plastic finite element method which employs the rigid plastic constitutive equation in which non-linear shear strength properties against confining pressure in case the internal friction angle of 30 and 40 deg. The vertical load *V*, horizontal load *H* and moment *M*, which were applied at the center of the footing, were subjects in this study. The analytical method provides the reliable computational results. The relation in normalization form of H/V_0 vs V/V_0 and V/V_0 vs M/BV_0 were acquired and then were compared with the relationship by Meyerhof (1956), Architectural Institute of Japan (1988, 2001) and Loukidis et al. (2008).

6.1 Ultimate bearing capacity for combined vertical and horizontal loads

The rigid plastic finite element method was used to assess the ultimate bearing capacity of strip footings of which the width varied from 1m to 100m, subjected to the inclined load at an inclination angle θ with respect to the vertical. The boundary conditions and typical mesh for analysis are shown in figure 6.1.

Because of the absence of loading symmetry, the entire soil domain of dimensions will be considered in this section and in the next section. The numerical simulation procedure used for the computation of the (*H*, *V*) failure envelope (where *H* and *V* are the horizontal and vertical ultimate footing loads respectively).

For inclined load, the application of RPFEM is limited to the case where the contact pressure between footing and ground is positive. In other words, the ratio *H*/*V* is set comparatively in small range. Further detailed discussion will not conducted in this study.

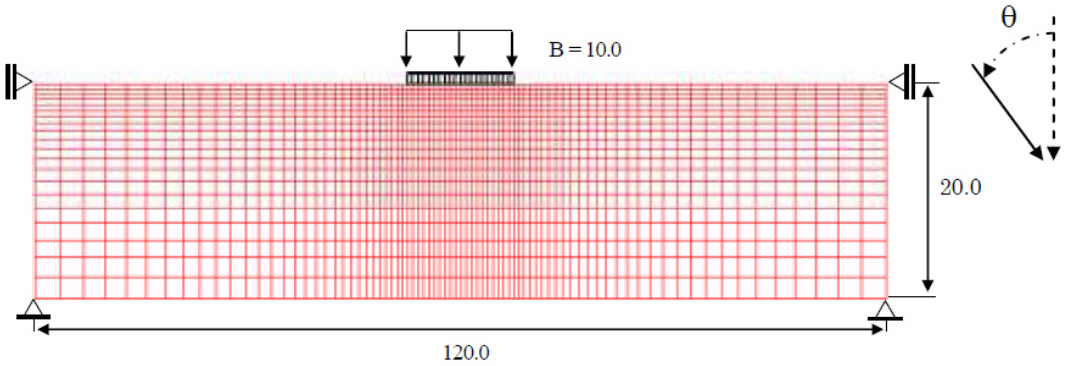

a) Typical mesh for analysis

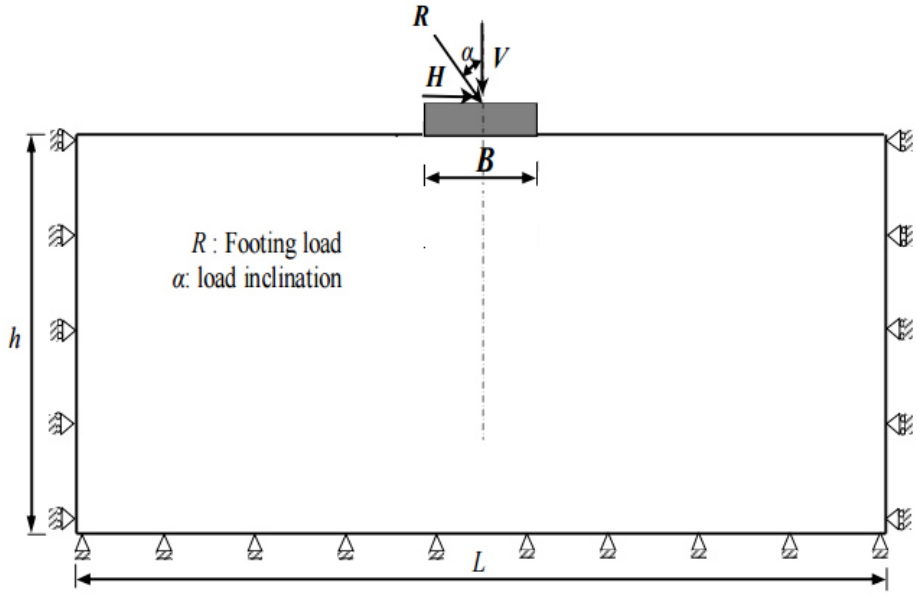

b) Problem geometry and boundary conditions

Figure 6.1 Formulation of finite element method

Figure 6.2 and figure 6.6 provide the RPFEM result on the relationship between normalized horizontal and vertical loads on *H-V* space in case ϕ_o = 30deg and 40deg. Two cases considered include (i) linear shear strength property and (ii) non-linear shear strength property. The results by AIJ and Meyerhof formulae are also shown. Since AIJ formula employs the same coefficient with Meyerhof method, the results in normalization form from AIJ and Meyerhof show unique and coincident line.

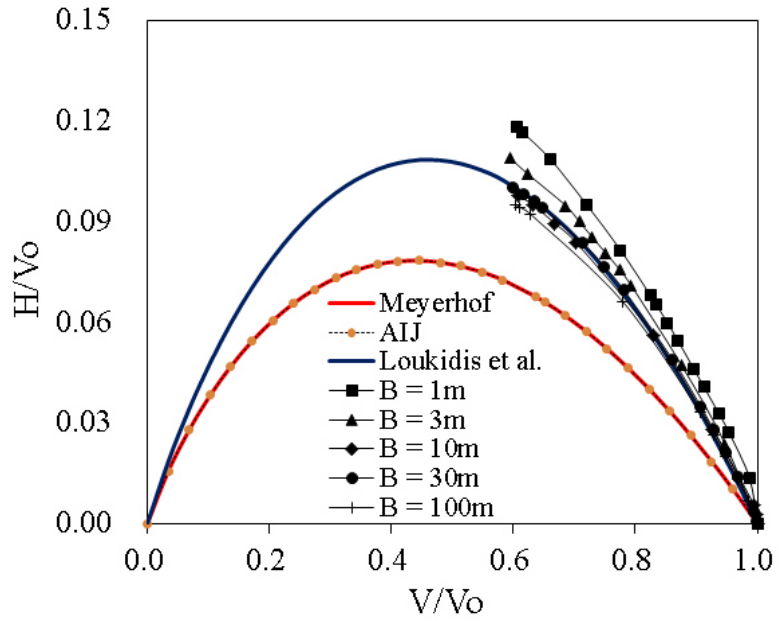

a) RPFEM with linear shear strength properties

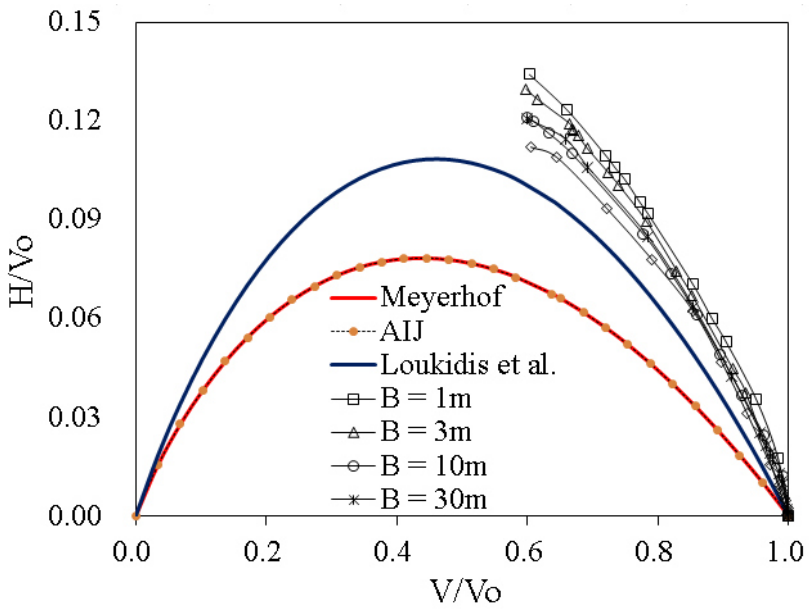

b) RPFEM with non-linear shear strength properties

Figure 6.2 The relation between normalized horizontal and vertical loads in case ϕ_o = 30deg

Figs. 6.2a and 6.6a. In the figure, the normalized horizontal load is indicated greater than those of Meyerhof and AIJ. The obtained results by RPFEM are plotted for various footing widths. It is apparent that the results match with the model of Eq. 6.1 by Loukidis et al. though they are

varied for footing width.

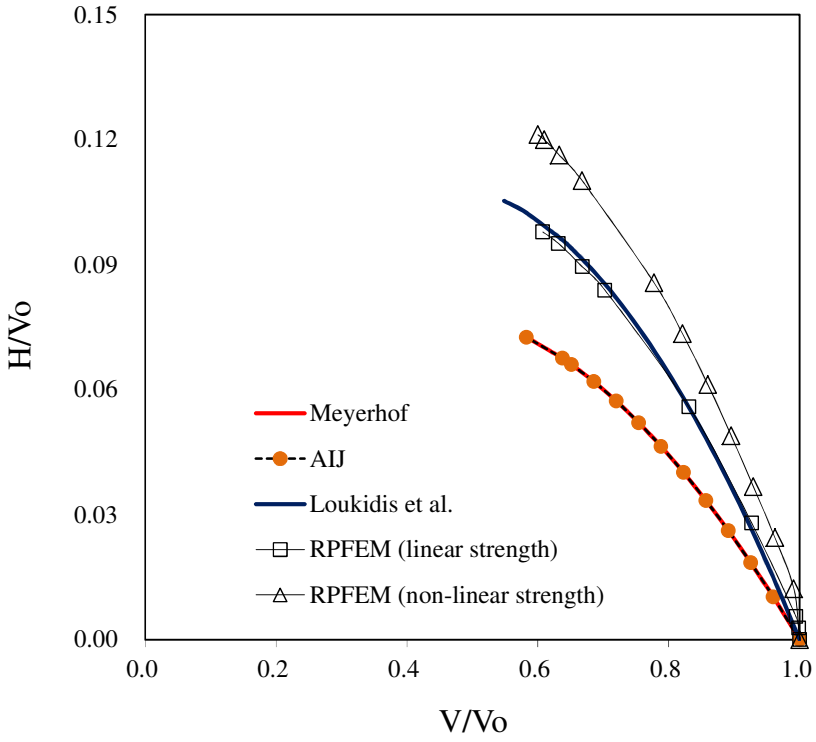

Figure 6.3 Comparison inclination coefficients among the various methods at footing width B = 10m in case ϕ = 30 deg

Fig. 6.3 and 6.7 indicate the ultimate load in H/V_0 and V/V_0 space to compare the inclination coefficient among the various methods at B=10m in case ϕ_o = 30deg and 40 deg. It is readily seen that RPFEM affords the identical results by Loukidis et al. in case of linear shear strength, but the greater results than that by Loukidis et al. in case of non-linear shear strength. Although ϕ is constant in case of linear shear strength, ϕ decreases by confining pressure in case of non-linear shear strength. Since the decrease in ϕ mostly depends on the magnitude of vertical load, the decrease in ultimate bearing capacity is largest for vertical loading. For the inclined load, the decrease in ϕ becomes moderate with the increase in inclination angle of inclined load. It derives the normalized horizontal load in case of non-linear shear strength greater than that of linear shear strength.

Figure 6.4 and figure 6.5 shows failure mechanism from analyses with resistance angle ϕ = 30deg.

a) B = 1m (H = 30kN)

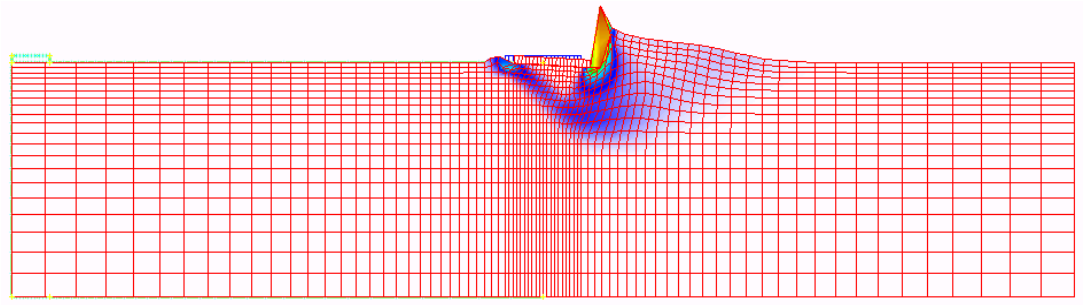

b) B = 10m (H = 500kN)

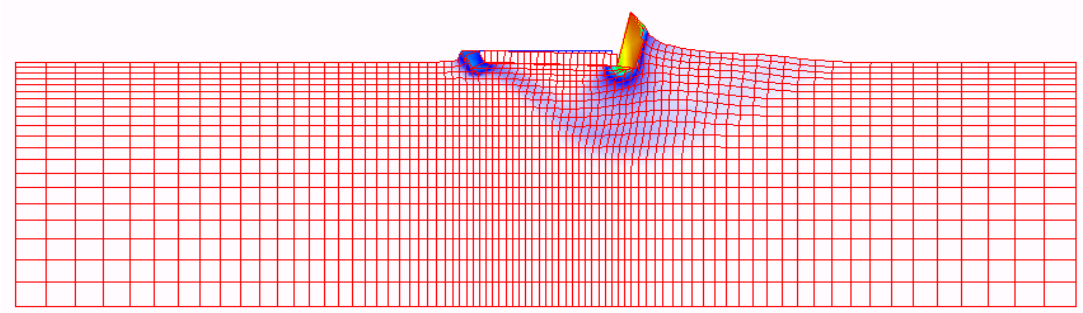

c) B = 100m (H = 30000kN)

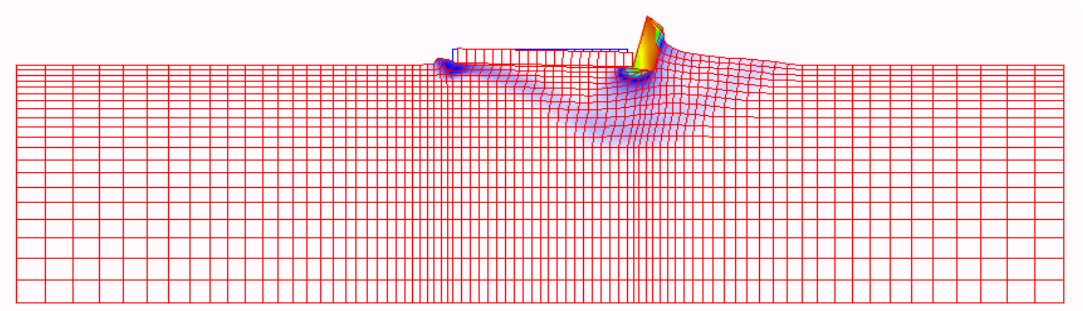

Figure 6.4.Deformatin mechanism from analysis in case internal friction angle ϕ = 30deg with non-linear shear strength properties

a) B = 1m (H = 30kN)

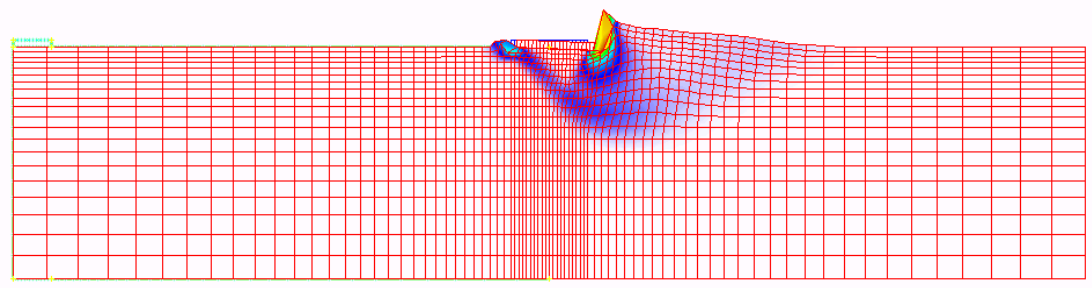

b) B = 10m (H = 500kN)

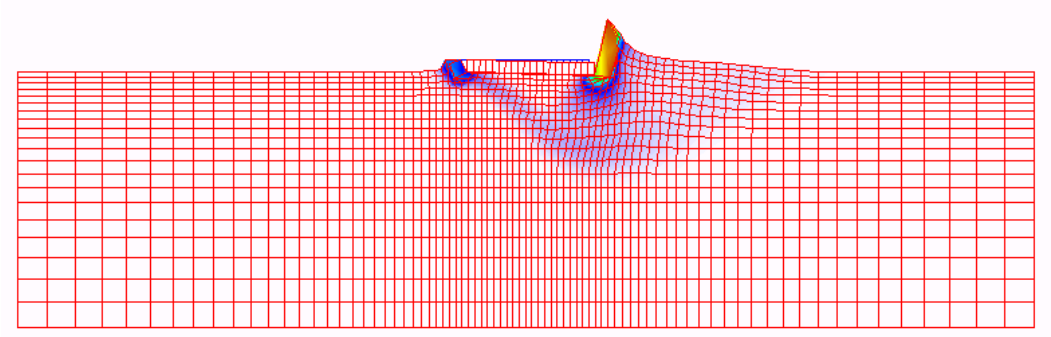

c) B = 100m (H = 30000kN)

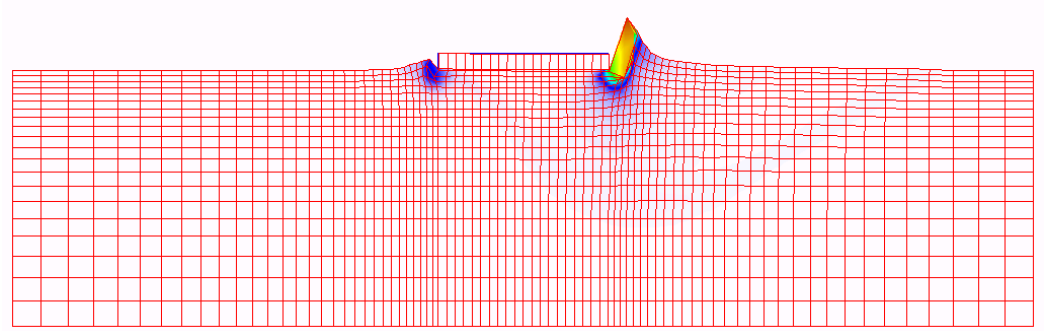

Figure 6.5.Deformatin mechanism from analysis in case internal friction angle ϕ = 30deg with linear shear strength properties

Figs. 6.2b and 6.6b indicate the inclination coefficient in case of non-linear shear strength. AIJ formula is developed by taking account of the size effect of footing. However, since the inclination coefficient of Meyerhof is introduced into the formula, the applicability of AIJ formula for inclined load has not been examined. The results by RPFEM taking account of non-linear shear strength are plotted in the figure.

In case phi = 40deg, the relationship between normalized H/Vo and V/Vo of non-linear shear strength and linear shear strength decrease and oscillate around AIJ at footing width 1m and 30m, corresponding.

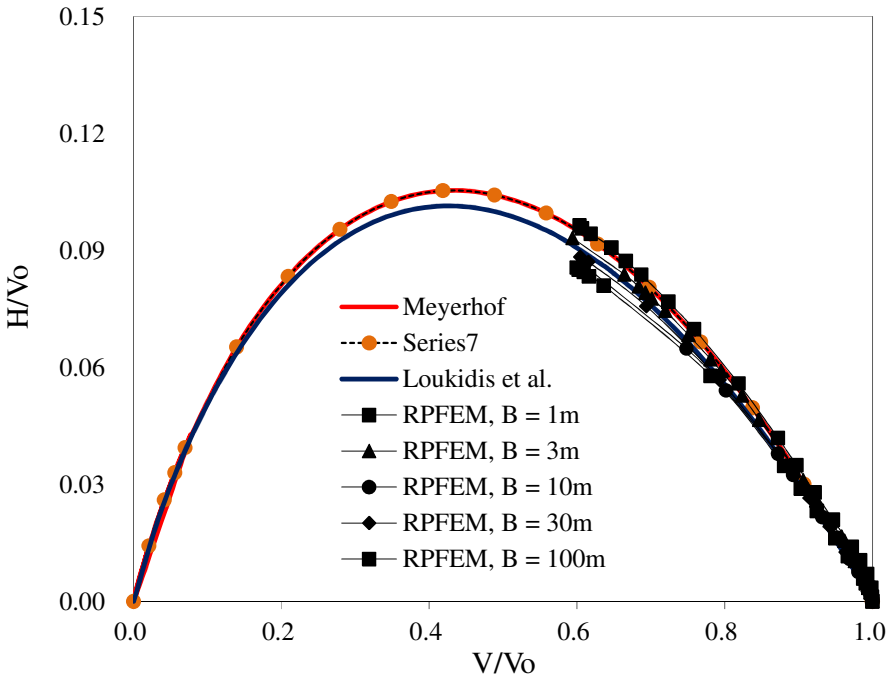

a) RPFEM with linear shear strength properties

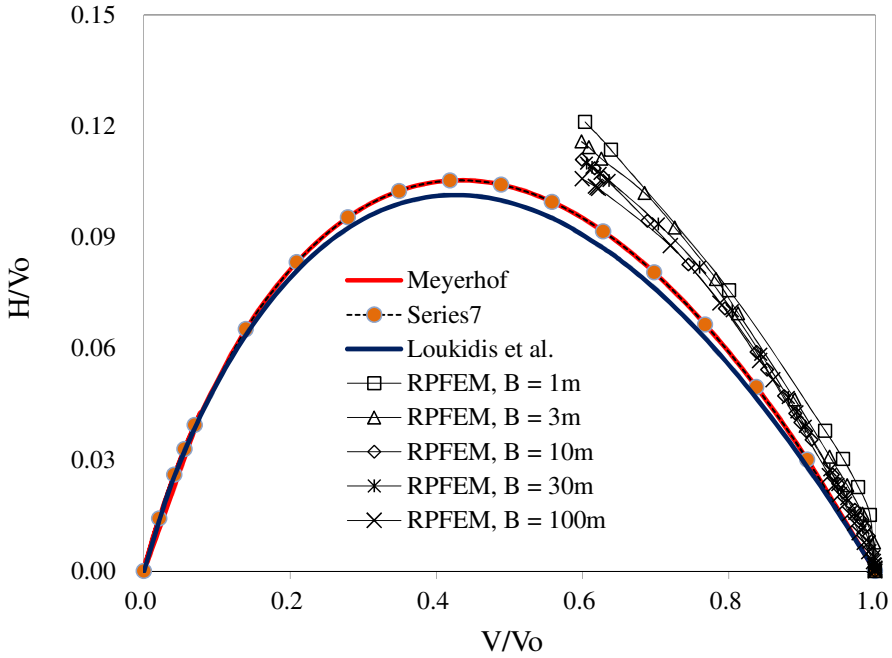

b) RPFEM with non-linear shear strength properties

Figure 6.6 Relationship between normalized horizontal load and vertical load in case resistance angle ϕ = 40deg

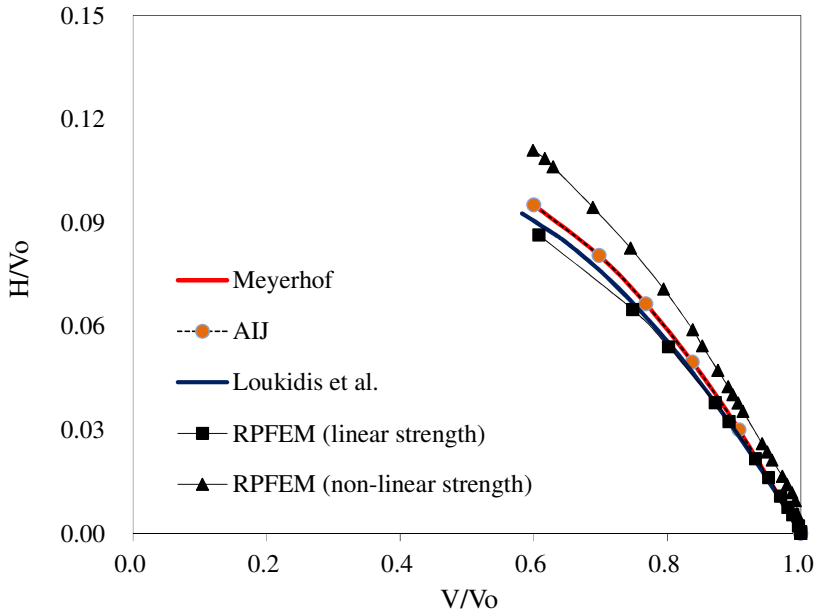

Figure 6.7 Comparison inclination coefficients among the various methods at footing width B = 10m in case ϕ = 40deg

Figure 6.8 and figure 6.9 shows failure mechanism from analyses with resistance angle ϕ = 40deg.

a) B = 1m (H = 30kN)

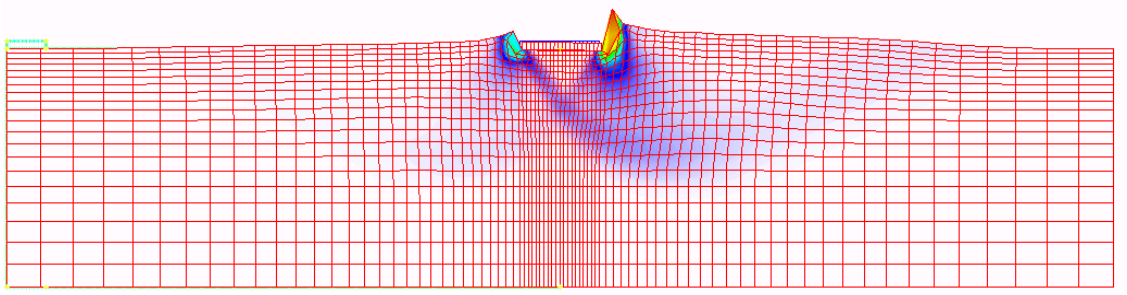

b) B = 10m (H = 500kN)

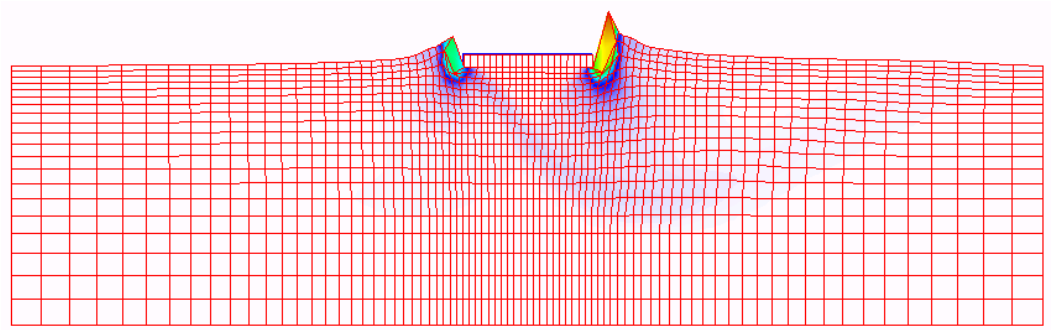

c) B = 100m (H = 30000kN)

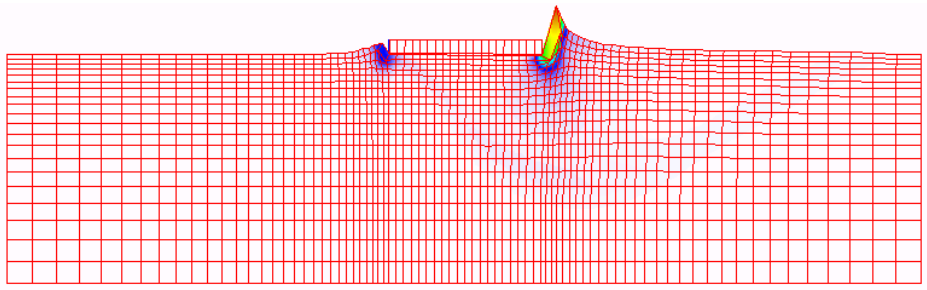

Figure 6.8 Deformatin mechanism from analysis in case resistance angle ϕ = 40deg with non-linear shear strength properties

a) B = 1m (H = 30kN)

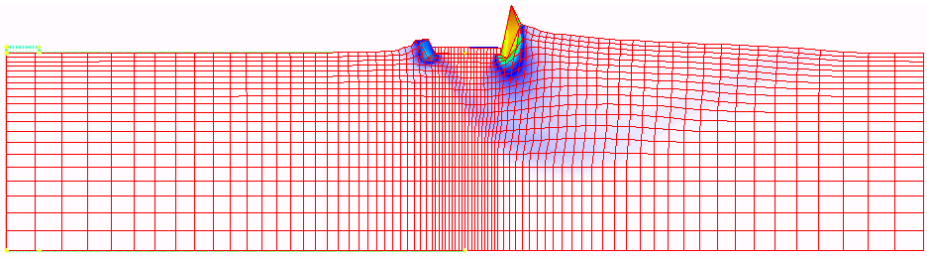

b) B = 10m (H = 500kN)

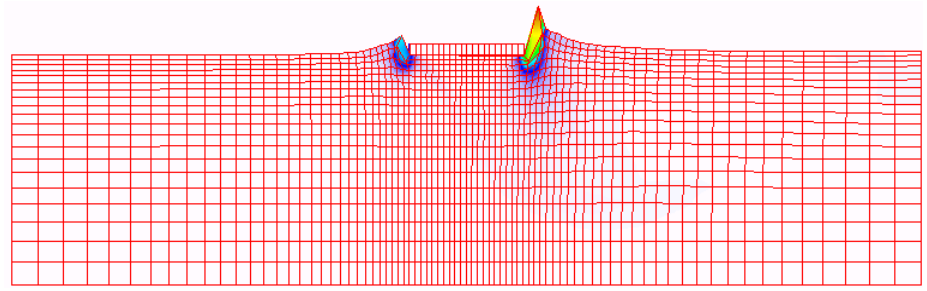

c) B = 100m (H = 30000kN)

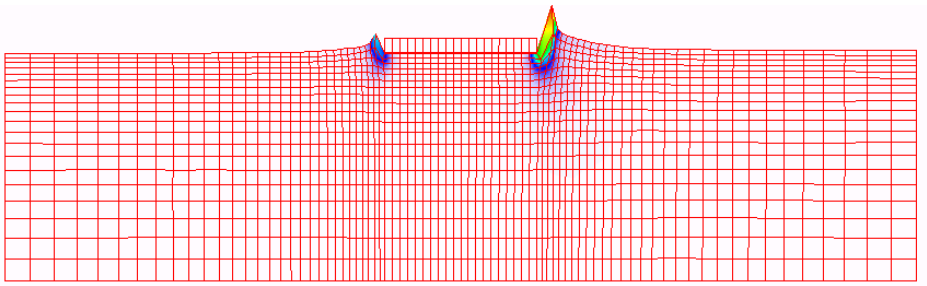

Figure 6.9 Deformatin mechanism from analysis in case resistance angle ϕ = 40deg with linear shear strength properties

The results from analysis computation show that the failure mechanism is asymmetrical and confined to one side of the footing for all values of the inclination angle when ϕ = 30deg (Fig.

6.4, Fig. 6.5) and ϕ = 40deg (Fig. 6.8, Fig. 6.9). Furthermore,the failure modes of ground for non-linear and linear shear strength. They are similar, but the deformation area in the case of linear shear strength is larger than that in case of the non-linear shear strength. The mechanism is found composed of three different zones and similar to the mechanism assumed by Meyerhof and Hansen.

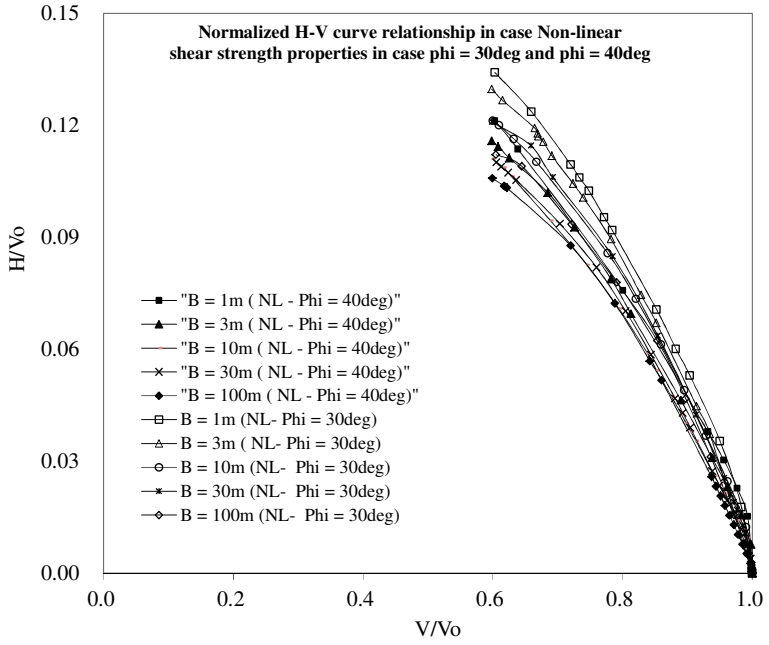

a) Non-linear shear strength properties

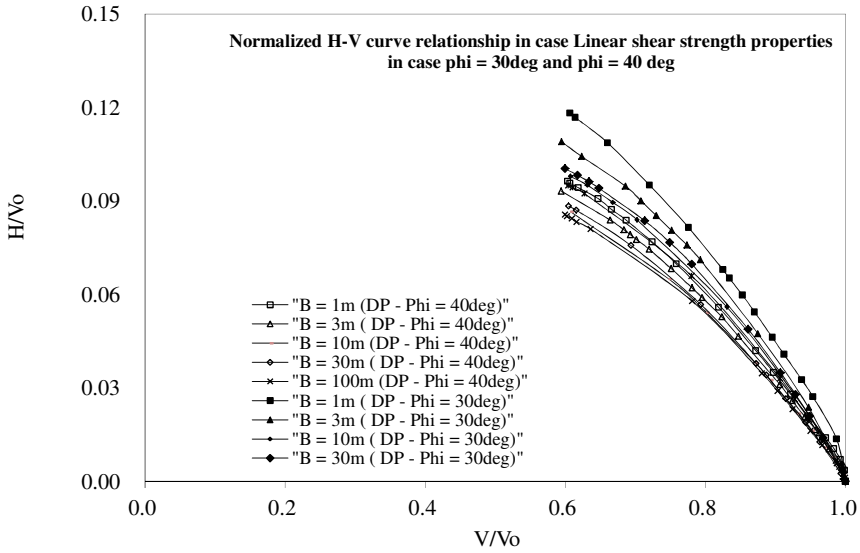

b) Linear shear strength properties

Figure 6.10 Relationship between Normalized Horizontal load and vertical load for LINEAR and NON-LINEAR shear strength properties for difference value of internal friction angle

From Fig. 6.10a and 6.10b, the results showed that the relationship between H/Vo and V/Vo of small internal friction angle (30deg) is higher than those of larger internal friction angle (40deg) at the same footing width.

Moreover, the results from RPFEM have the same trend for various magnitude of footing width.

6.2 Ultimate bearing capacity for vertical, horizontal and moment loads

The type of loads, which is often known as combined loads, is important to the stability of superstructure where footings are subjected to vertical, horizontal and moment loads combination. Typically, the vertical force is stemmed from the weight of superstructure $q_{v_0} = \gamma_{st} \times h$, while the horizontal load comes from the seismic coefficient k_h = 0; 0.1; 0.2; 0.3; 0.4.

The overturning moment load is caused by the horizontal load:

$$M_0 = q_{h_0} \times B \times \frac{1}{2} h \tag{6.2}$$

A series of finite element analysis were conducted for sandy soil with Using sandy soil with unit weight γ_{soil} = 18 kN/m^3, Density of building γ_{st}= 18 kN/m^3, cohesion c = 5 kN/m^2, internal friction angle $\phi = 30^0$ and $\phi = 40^0$, the footing width 1m, 10m and 30m were computed. Initial loads are considered as Fig. 6.11.

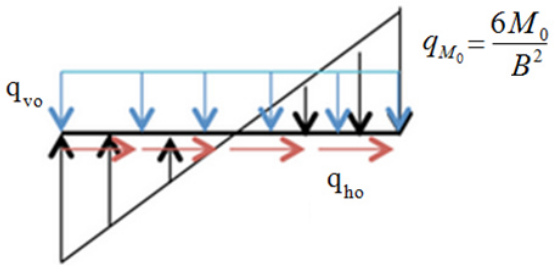

Figure 6.11 Initial loads applied to computation

The moment load is given to the footing by the external force where the summations in vertical and horizontal loads are zero and the resultant moment at the center of footing is same with the prescribed moment load. The results demonstrated the interaction between the vertical, horizontal and moment loads. Fig. 6.12 shows the representative finite element meshes of

analysis.

At each height of superstructure value, the ultimate bearing capacity of footings subjected to combined loading was computed under the condition of seismic load applied to superstructure. By changing superstructure height and the seismic coefficient k_h, the forces q_h, q_v and the moment load was computed.

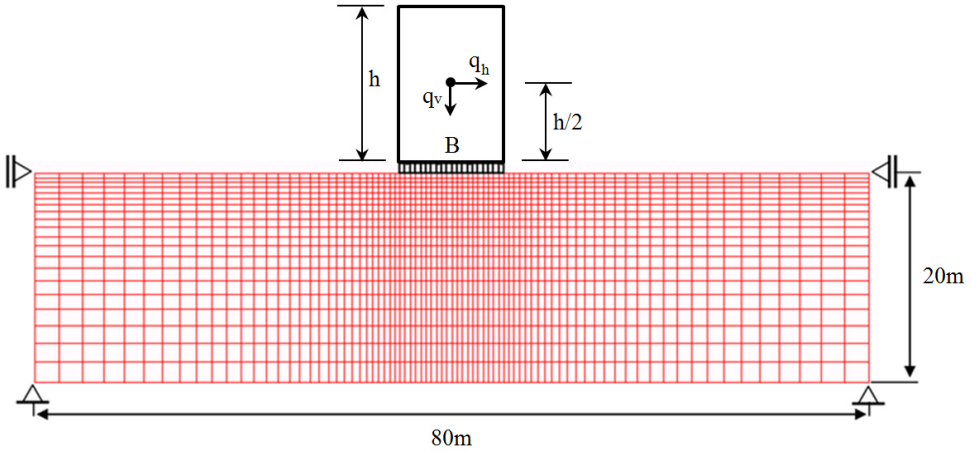

Figure 6.12 Representative finite element meshes under superstructure on the strip footings condition

Ultimate bearing of footing related to inclined loads or combined loads (vertical, horizontal and moment loads combination) is an important aspect in geotechnical engineering. Meyerhof and others (e.g. Hansen, 1970, Vesic, 1975) conducted empirical generalizations of the simpler cases without examining in detail. Moreover, the size effect of footing does not consider in the previous research. In this chapter, the ultimate bearing capacity of footing that is subjected to the combined loads of strip footing has been investigated.

Fig. 6.13 shows ultimate bearing capacity of footing in the normalized V-M form by changing footing width (1m, 10m and 30m) at the internal friction angle of 30 deg and 40deg. The results from Fig. 6.13a showed that the normalized load V/V_0 decreases with an increase in M/BV_0. In the case of linear strength, the values that represent the relationship between the normalized V/V_0 and M/BV_0 obtained greater than that by RPFEM employing non-linear shear strength. When the internal friction angle is 40 deg (Fig. 6.13b) , there is no much difference in the normalized V/V_0 and M/BV_0 among footing width 1m, 10m and 30m in case linear strength. But the difference becomes greater in case non-linear strength. It is explained that this case

influences the internal friction angle responding to the confining stress. It means that the effect of moment load in non-linear case is clearer than that in linear shear strength property.

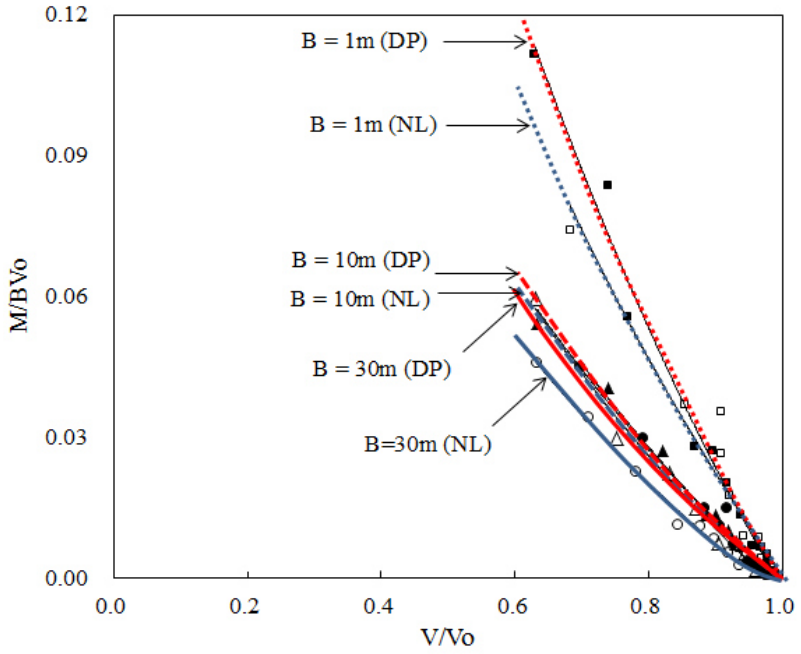

a) ϕ_o = 30deg

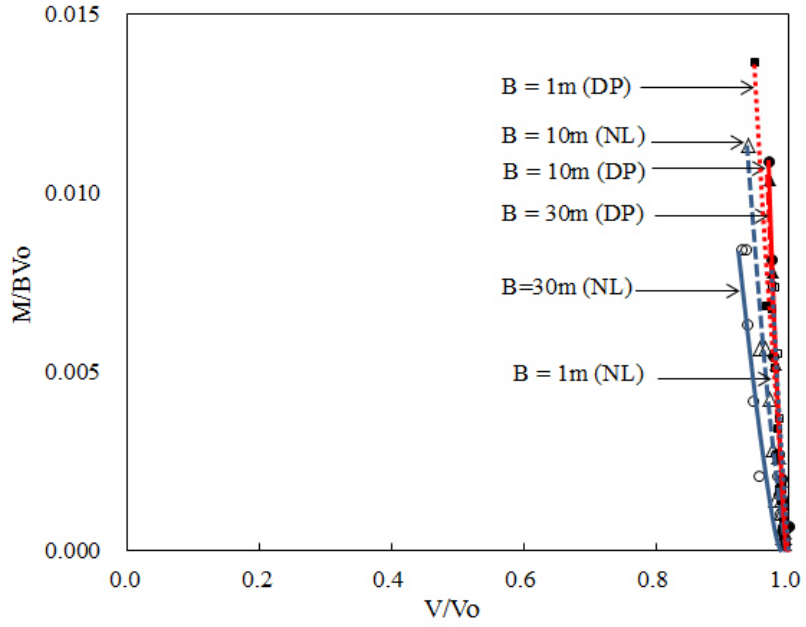

b) ϕ_o = 40deg

Figure 6.13 The relation between normalized vertical and moment load*s*

Figs. 6.14 and 6.15 show the distribution of equivalent strain rate and Figs. 6.16 and 6.17 show

the contour plot of pressure in the ground in case ϕ = 30deg. The results indicated clearer the effect of moment load in non-linear case than that in linear shear strength property.

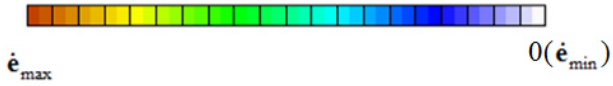

k_h = 0.1 k_h = 0.4

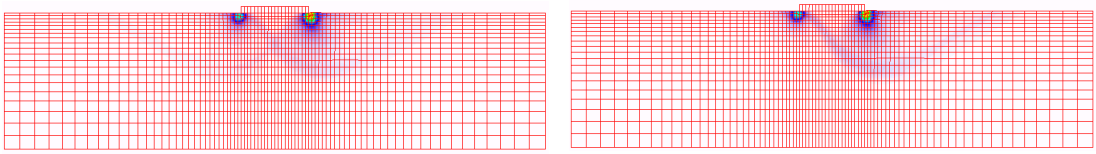

a) Linear shear strength property

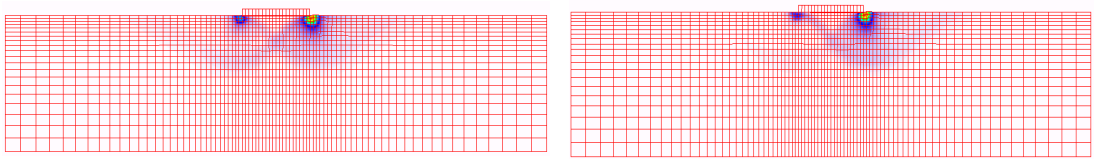

b) Non-linear shear strength property

Figure 6.14 Deformation mechanism analysis subjected to combined loads in case ϕ_o = 30deg with B/h = 1

k_h = 0.1 k_h = 0.4

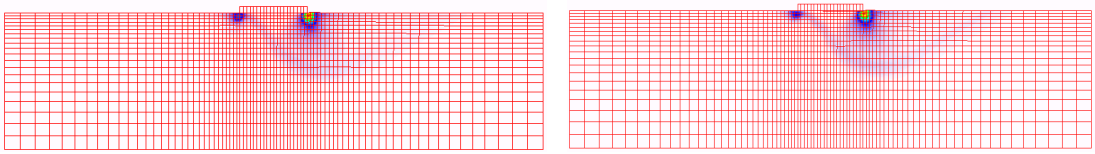

a) Linear shear strength property

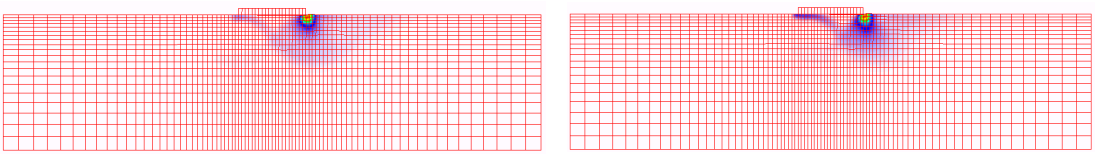

b) Non-linear shear strength property

Figure 6.15 Deformation mechanism analysis subjected to combined loads in case ϕ_o = 30deg with B/h = 0.25

k_h = 0.1 k_h = 0.4

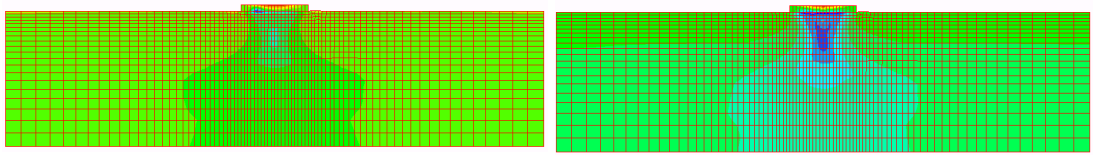

a) Linear shear strength property

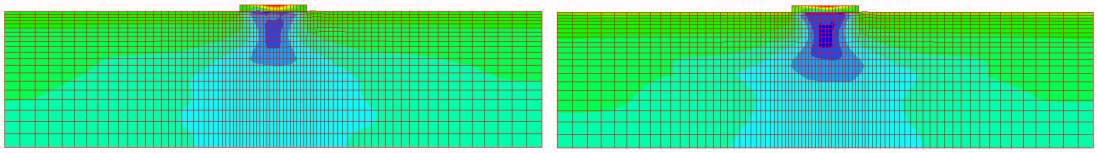

b) Non-linear shear strength property

Figure 6.16 Contour plot of mean stress subjected to combined loads in case ϕ_o = 30deg with B/h = 1

k_h = 0.1 k_h = 0.4

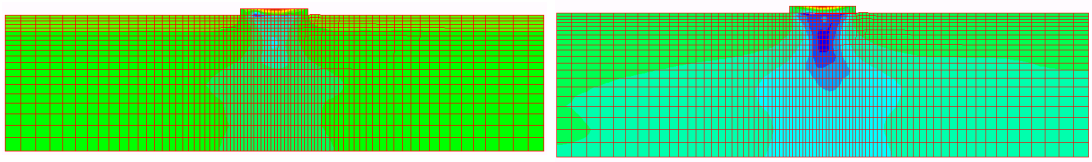

a) Linear shear strength property

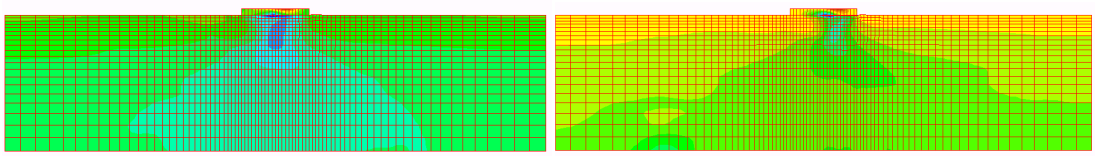

b) Non-linear shear strength property

Figure 6.17 Contour plot of mean stress subjected to combined loads in case ϕ_o = 30deg with B/h = 0.25

References

[1] AIJ (1988, 2001), Architectural Institute of Japan. Recommendations for design of building foundations, 430p.

[2] Du, L. Nguyen, Ohtsuka, S., Hoshina, T., Isobe, K., Kaneda, K., 2013. Ultimate bearing capacity analysis of ground against inclined load by taking account of non-linear properties of shear strength. Int. J. GEOMATE **5**(2), 678–684.

[3] Du, N. L., Ohtsuka, S., Hoshina, T., Isobe, K. and Kaneda, K., 2016. Ultimate bearing capacity of footing on sandy soil against combined load of vertical, horizontal and moment loads", Int. J. GEOMATE **10**(1), 1649-1655

[4] Farah C. A., 2004. Ultimate bearing capacity of shallow foundations on layered soils, Master thesis, Concordia university, Canada, 68p.

[5] Georgiadis M., Butterfield, 1988. Displacements of footings on sand under eccentric and inclined loads", Can. Geotech. J., **25**(2), 199-212.

[6] Hanna A. M., Meyerhof G. G., 1981. Experimental evaluation of bearing capacity of footings subjected to inclined loads, Can. Geotech. J., **18**(4), 599-603.

[7] Hansen, B., 1970. A revised and extended formula for bearing capacity for bearing capacity", Bulletin of Danish Geotechnical Institute, Copenhagen, Denmark, **28**, 5-11.

[8] Houlsby G. T., Cassidy M. J., 2002. A plasticity model for the behavior of footings on sand under combined loading", Géotechnique, **52**(2), 117-129.

[9] Houlsby G. T., Puzrin A. M., 1999. The bearing capacity of a strip footing on clay under combined loading", Proc. R. Soc. Lond. A, **455**, 893-916.

[10] Krabbenhoft, S., Damkilde, L., and Krabbenhoft K., 2012. Lower-bound calculations of the bearing capacity of eccentrically loaded footings in cohesionless soil, Can. Geotech. J., **49**(3), 298-310

[11] Loukidis D., Chakraborty T., Salgado R., 2008. Bearing capacity of strip footings on purely frictional soil under eccentric and inclined loads, Can. Geotech. J., **45**(6), 768-787.

[12] Martin A. M., 1994. Physical and numerical modelling of offshore foundations under combined loads", Doctoral thesis, The university of Oxford, 306p.

[13] Meyerhof, G. G., 1951. Ultimate bearing capacity of foundations, Geotechnique, **2**(4),

301-332.

[14] Meyerhof, G. G., 1956. Rupture surfaces in sand under oblique loads (discussion)", Journal of soil mechanics and foundations division, ASCE, **82**(SM3).

[15] Meyerhof, G. G., 1963. Some recent research on the ultimate bearing capacity of foundations", Can. Geotech. J., **1**(1), 243-256.

[16] Mohammed Hjiaj, Andrei V. Lyamin, Scott W. Sloan, 2004. Bearing capacity of a cohesive-frictional soil under non-eccentric inclined loading, Computers and Geotechnics, **31**(6), 491-516.

[17] Ngo-Tran C. L, 1996. The analysis of offshore foundations subjected to combined loading", Doctoral thesis, The university of Oxford, 236p.

[18] Takeshi Hoshina, Satoru Ohtsuka and Koichi Isobe, 2011. Ultimate bearing capacity of ground by Rigid plastic finite element method taking account of stress dependent non-linear strength property, J. Appl. Mech. **6**, 191–200 (in Japanese).

[19] Tamura, T., 1990. Rigid-plastic finite element method in geotechnical engineering. Soc. Mater. Sci., Jpn. 7, 135–164.

[20] Ukritchon, B., Whittle, A. W., and Klangvijit, C., 2003. Calculation of bearing capacity factor N_γ using numerical limit analysis, J. Geotech. Geoenviron. Eng., ASCE, **129**(6), 468-474.

[21] Vesic, A. S., 1975. Bearing capacity of shallow foundations, In "Foundation Engineering Handbook", ed. H. F. Winterkorn & H. Y. Fang, Van Nostrand, New York, 121-147

CHAPTER 7

CONCLUDING REMARKS

7.1 Main fidings

Terzaghi (1943) and others (e.g. Meyerhof, 1951, 1963) have proposed many formulas to evaluate ultimate bearing capacity. However, the application of formulas is limited due to their disadvantages. Rigid plastic finite element method is effective to solve the complex problems such as multi-layered soil and footing shape in the three dimensional condition. Moreover, limit state analysis is possible to be conducted without the assumption on potential failure modes. In this study, RPFEM is employed for the assessment of ultimate bearing capacity. The applicability of the method is presented through the comparison with those by the semi-experimental ultimate bearing capacity formulas.

Size effect of footing is observed in ultimate bearing capacity, but basically not accounted in the ultimate bearing capacity formulas. In this study two discussions on the size effect were conducted. One is the size effect in case of a uniform sandy ground and the other is in case of a multi-layered ground. On sandy soils, a rigid plastic constitutive equation is proposed by considering the experiments, where the secant internal friction angle reduces with the increase in confining pressure. This equation is expressed by the higher order parabolic function and easily applied to RPFEM. The obtained ultimate bearing capacity shows a good agreement with that of the ultimate bearing capacity formula by Architectural Institute of Japan (AIJ, 1998, 2001) which takes into account the size effect of footing. It is clear that RPFEM with the use of proposed constitutive equation provides a good estimation in ultimate bearing capacity assessment by considering the size effect of footing.

The size effect of footing in ultimate bearing capacity is also observed in case of multi-layered ground. In conventional methods, it is difficult to assess the ultimate bearing capacity for multi-layered ground due to the complexity in failure mode of ground. RPFEM is, however, applicable boundary value problems. Through the case studies for various footing widths, the change in both ultimate bearing capacity and failure mode due to footing width is shown properly simulated.

Moreover, ultimate bearing of footing related to inclined loads or combined loads (vertical, horizontal and moment loads combination) is an important aspect in geotechnical engineering. Meyerhof and others (e.g. Hansen, 1970, Vesic, 1975) conducted empirical generalizations of the simpler cases without examining in detail. Moreover, the size effect of footing does not consider in the previous research. In this study, the ultimate bearing capacity of footing that is subjected to the inclined loads and the combined loads of strip footing has been investigated. The obtained conclusions are summarized as follows:

(1) On sandy soils, the size effect of footing in ultimate bearing capacity was well simulated by RPFEM with the use of proposed constitutive equation. It was proved by the comparison in ultimate bearing capacity between the semi-experimental bearing capacity formula of AIJ and RPFEM.

(2) Rigid plastic constitutive equation was proposed for sandy soils based on the experiments by Tatsuoka and other researchers for various soils. The relationship between the secant internal friction angle and first stress invariant was uniquely expressed in normalized form although some scatters existed. The yield function was modeled into the higher order parabolic function regarding the first stress invariant.

(3) Bearing capacity factor N_γ was compared among the bearing capacity formulas of AIJ, Euro-code 7 and Meyerhof with RPFEM by changing internal friction angle from 0 to 40 deg. The bearing capacity factor by RPFEM employing non-linear shear strength against the confining pressure matched those by AIJ formula in the wide range of internal friction angle. It was obtained smaller than that by the formulas of Euro-code 7 and Meyerhof. The difference in bearing capacity factor was shown greater at the internal friction angle of 40 deg.

(4) Size effect of footing in the case of multi-layered ground was investigated for the ground where sand layer overlaid clay layer. By simulation results, the size effect of footing was clearly shown to be generated by the change in failure mode of ground due to footing width.

(5) Wide applicability of developed RPFEM to the assessment of ultimate bearing capacity was shown through the case studies.

(6) The results from analysis computation show that the failure mechanism is asymmetrical and confined to one side of the footing for all values of the inclination angle. Furthermore, the

mechanism seems to be composed of three different zones and similar to the one assumed by Meyerhof and Hansen

(7) Ultimate load space in normalized vertical and horizontal loads was shown to match with that by Loukidis et al. (2008), Meyerhof (1956) and AIJ (1988, 2001) in case internal friction angle 40deg and be greater than those by Meyerhof (1956) and AIJ (1988, 2001) in case internal friction angle 30deg of linear shear strength. Moreover, the internal friction angle decreases by confining pressure and the decrease is the most for the case of vertical loading. It makes the obtained result greater than that by Loukidis et al. in case of non-linear shear strength

(8) In the case of linear strength, the values that represent the relationship between the normalized V/V_0 and M/BV_0 obtained greater than that by RPFEM employing non-linear shear strength and normalized load V/V_0 decreases with an increase in M/BV_0. At the internal friction angle of 40 deg, there is no much difference in the normalized V/V_0 and M/BV_0 among footing width 1m, 10m and 30m in case linear strength.

(9) Effect of non-linear strength was investigated for combined loading case (horizontal and vertical loads vs horizontal, vertical and moment loads). From computation results, the non-linear strength was clearly shown by the change in failure mode of ground.

(10) The non-linear shear strength model for sandy soil is employed in RPFEM to evaluate the size effect of footing on ultimate bearing capacity. Through the case studies the applicability of the method was clearly exhibited.

7.2 Future research

7.2.1 Propose new model based on the modified stress tensor t_{ij}

A. Druker – Prager yield function

Propose new model based on the modified stress tensor t_{ij} to describe uniquely the deformation and strength of soils under three different principle stresses.

- Influence of intermediate principal stress on the deformation and strength of geomaterials.

- Dependence of the direction of plastic flow on the stress paths.

- Influence of density and/or confining pressure on the deformation and strength of geomaterials.

Table 7.1 Comparison between tensors and scalars related to stress and strain increments in the ordinary concept and the t_{ij} concept

	Ordinary Concept	*t_{ij} Concept*
Tensor normal to reference plane	δ_{ij} (unit tensor)	a_{ij} (tensor normal to SMP)
Stress tensor	σ_{ij}	t_{ij}
Mean stress	$p = \sigma_{ij}\,\delta_{ij}/3$	$t_N = t_{ij}a_{ij}$
Deviatoric stress tensor	$s_{ij} = \sigma_{ij} - p\delta_{ij}$	$t'_{ij} = t_{ij} - t_N a_{ij}$
Deviatoric stress	$q = \sqrt{(3/2)s_{ij}s_{ij}}$	$t_s = \sqrt{t_{ij}t_{ij}}$
Stress ratio tensor	$\eta_{ij} = s_{ij}/p$	$x_{ij} = t'_{ij}/t_N$
Stress ratio	$\eta = q/p$	$X = t_s/t_N$
Strain increment normal to reference plane	$d\varepsilon_v = d\varepsilon_{ij}\delta_{ij}$	$d\varepsilon^*_N = d\varepsilon_{ij}a_{ij}$
Deviatoric strain increment tensor	$de_{ij} = d\varepsilon_{ij} - d\varepsilon_v\delta_{ij}/3$	$d\varepsilon'_{ij} = d\varepsilon_{ij} - d\varepsilon^*_N a_{ij}$
Strain increment parallel to reference plane	$d\varepsilon_d = \sqrt{(2/3)de_{ij}de_{ij}}$	$d\varepsilon^*_s = \sqrt{d\varepsilon_{ij}d\varepsilon_{ij}}$

Drucker – Prager yield function

$$f(t) = a\mathbf{t}_N + \frac{t_s}{\sqrt{3}} - b = 0 \tag{7.1}$$

where

$$a = \frac{\tan\phi}{\sqrt{9+12\tan^2\phi}} \tag{7.2}$$

$$b = \frac{3c}{\sqrt{9+12\tan^2\phi}} \tag{7.3}$$

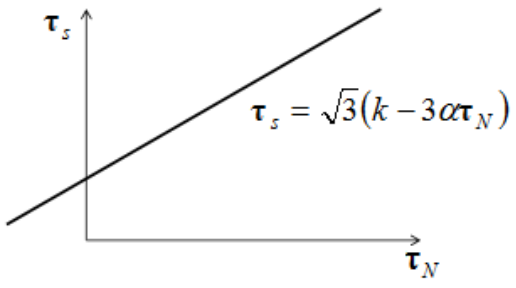

Figure 7.1 Drucker-Prager yield function in t_{ij} space

$$\dot{\varepsilon} = \Lambda\frac{\partial f(\mathbf{t})}{\partial \mathbf{t}} = \Lambda\left(\frac{\partial f(\mathbf{t})}{\partial \mathbf{t}_N}\frac{\partial \mathbf{t}_N}{\partial \mathbf{t}_{ij}} + \frac{\partial f(\mathbf{t})}{\partial \mathbf{t}_S}\frac{\partial \mathbf{t}_S}{\partial \mathbf{t}_{ij}}\right)$$

- $\frac{\partial f(\mathbf{t})}{\partial \mathbf{t}_N} = \alpha$
- $\frac{\partial \mathbf{t}_N}{\partial \mathbf{t}_{ij}} = \frac{\partial (\mathbf{t}_{kl} a_{kl})}{\partial \mathbf{t}_{ij}} = a_{ij}$
- $\frac{\partial f(\mathbf{t})}{\partial \mathbf{t}_S} = \frac{1}{\sqrt{3}}$
- $\frac{\partial \mathbf{t}_S}{\partial \mathbf{t}_{kl}} = \frac{\partial \mathbf{t}_S}{\partial \mathbf{t}'_{ij}} \cdot \frac{\partial \mathbf{t}'_{ij}}{\partial \mathbf{t}_{kl}}$

$$\frac{\partial \mathbf{t}_S}{\partial \mathbf{t}'_{kl}} = \frac{1}{2\sqrt{\mathbf{t}'_{kl}\mathbf{t}'_{kl}}} 2\mathbf{t}'_{ikl} = \frac{\mathbf{t}'_{kl}}{\sqrt{\mathbf{t}'_{ij}\mathbf{t}'_{ij}}} = \frac{\mathbf{t}_{kl} - t_N a_{kl}}{\mathbf{t}_S}$$

$$\frac{\partial \mathbf{t}'_{kl}}{\partial \mathbf{t}_{ij}} = \frac{\partial}{\partial \mathbf{t}_{ij}} (\mathbf{t}_{kl} - t_N a_{kl}) = \frac{\partial \mathbf{t}_{ikl}}{\partial \mathbf{t}_{ij}} - \frac{\partial (t_N a_{kl})}{\partial \mathbf{t}_{ij}} = \delta_{ik}\delta_{jl} - \frac{\partial t_N}{\partial \mathbf{t}_{ij}} a_{kl} = \delta_{ik}\delta_{jl} - a_{ij}a_{kl}$$

$$\dot{\bar{\varepsilon}} = \Lambda \frac{\partial f(\mathbf{t})}{\partial \mathbf{t}} = \Lambda \left(\alpha a_{ij} - \frac{1}{\sqrt{3}} \frac{\mathbf{t}_{kl} - t_N a_{kl}}{\mathbf{t}_S} (\delta_{ik}\delta_{jl} - a_{ij}a_{kl}) \right) = \Lambda \left(\alpha a_{ij} - \frac{1}{\mathbf{t}_S \sqrt{3}} (\mathbf{t}_{kl}\delta_{ik}\delta_{jl} - \mathbf{t}_{kl}a_{ij}a_{kl} - t_N a_{kl}\delta_{ik}\delta_{jl} + t_N a_{kl}a_{ij}a_{kl}) \right)$$

$$= \Lambda \left(\alpha a_{ij} - \frac{1}{\mathbf{t}_S \sqrt{3}} (\mathbf{t}_{ij} - \mathbf{t}_N a_{ij} - t_N a_{ij} + t_N a_{ij}a_{kl}a_{kl}) \right)$$

$$= \Lambda \left(\alpha a_{ij} - \frac{1}{\mathbf{t}_S \sqrt{3}} (\mathbf{t}_{ij} - t_N a_{ij}a_{kl}a_{kl}) \right)$$

We have:

$$a_{11} = \frac{a_1 + a_2}{2} + \frac{a_1 - a_2}{2} \cos 2\alpha$$

$$a_{22} = \frac{a_1 + a_2}{2} - \frac{a_1 - a_2}{2} \cos 2\alpha$$

$$a_{33} = a_3$$

$$a_{12} = a_{21} = \frac{a_1 - a_2}{2} \sin 2\alpha$$

$$a_{23} = a_{13} = 0$$

$$a_1^2 + a_2^2 + a_3^2 = 1$$

Therefore

$$\mathrm{a_{kl}a_{kl}} = \mathrm{a_{ll}a_{ll}} = \mathrm{a_{11}a_{11} + a_{21}a_{21} + a_{31}a_{31} + a_{12}a_{12} + a_{22}a_{22} + a_{32}a_{32} + a_{13}a_{13} + a_{23}a_{23} + a_{33}a_{33}}$$

$$= \mathrm{a_{11}a_{11} + a_{22}a_{22} + a_{33}a_{33} + 2a_{12}a_{12}}$$

$$a_{kl}a_{kl} = \left(\frac{a_1+a_2}{2}+\frac{a_1-a_2}{2}\cos 2\alpha\right)^2 + \left(\frac{a_1+a_2}{2}-\frac{a_1-a_2}{2}\cos 2\alpha\right)^2 + a_3^2 + 2\left(\frac{a_1-a_2}{2}\sin 2\alpha\right)^2$$
$$= a_1^2 + a_2^2 + a_3^2 = 1$$

$$\Rightarrow \dot{\bar{\varepsilon}} = \Lambda\frac{\partial f(\mathbf{t})}{\partial \mathbf{t}} = \Lambda\left(\alpha a_{ij} - \frac{1}{\mathbf{t}_S\sqrt{3}}\left(\mathbf{t}_{ij} - t_N a_{ij}\right)\right) = \Lambda\left(\alpha a_{ij} - \frac{\mathbf{t}'_{ij}}{\mathbf{t}_S\sqrt{3}}\right) \tag{7.4}$$

$$\dot{e}_{SMP} = \sqrt{\dot{\bar{\varepsilon}} : \dot{\bar{\varepsilon}}} = \sqrt{\Lambda\left(\alpha a_{ij} - \frac{\mathbf{t}'_{ij}}{\mathbf{t}_S\sqrt{3}}\right) : \Lambda\left(\alpha a_{ij} - \frac{\mathbf{t}'_{ij}}{\mathbf{t}_S\sqrt{3}}\right)} = \Lambda\sqrt{\left(\alpha a_{ij} - \frac{\mathbf{t}'_{ij}}{\mathbf{t}_S\sqrt{3}}\right) : \left(\alpha a_{ij} - \frac{\mathbf{t}'_{ij}}{\mathbf{t}_S\sqrt{3}}\right)}$$
$$= \Lambda\sqrt{\alpha^2 a_{ij}a_{ij} - 2\frac{\alpha}{\mathbf{t}_S\sqrt{3}}\left(\mathbf{t}'_{ij} : a_{ij}\right) + \frac{1}{3}\frac{\mathbf{t}'_{ij} : \mathbf{t}'_{ij}}{\mathbf{t}_s^2}} = \Lambda\sqrt{\alpha^2 - 2\frac{\alpha}{\mathbf{t}_S\sqrt{3}}\left(\mathbf{t}_{ij}a_{ij} - t_N a_{ij}a_{ij}\right) + \frac{1}{3}} \tag{7.5}$$
$$= \Lambda\sqrt{\alpha^2 + \frac{1}{3}}$$

$$\frac{\partial f(\mathbf{t})}{\partial \mathbf{t}_{ij}} = \frac{\dot{\bar{\varepsilon}}}{\Lambda} = \sqrt{\alpha^2 + \frac{1}{3}}\frac{\dot{\bar{\varepsilon}}}{\dot{e}_{SMP}}$$

$$\Rightarrow \Lambda = \frac{\dot{e}_{SMP}}{\sqrt{\alpha^2 + \frac{1}{3}}} \tag{7.6}$$

$$I_1^{(1)} = t_N{}^{(1)} = tr\left\{t_{ij}^{(1)}\right\} = tr\left\{\gamma\frac{\partial f(\mathbf{t})}{\partial \mathbf{t}}\right\} = tr\left\{\gamma\left(\alpha a_{ij} - \frac{\mathbf{t}'_{ij}}{\mathbf{t}_S\sqrt{3}}\right)\right\}$$
$$= \gamma\left\{\alpha a_{11} - \frac{t'_{11}}{\sqrt{3}\mathbf{t}_S}\right\} + \gamma\left\{\alpha a_{22} - \frac{t'_{22}}{\sqrt{3}\mathbf{t}_S}\right\} + \gamma\left\{\alpha a_{33} - \frac{t'_{33}}{\sqrt{3}\mathbf{t}_S}\right\} \tag{7.7}$$
$$= \gamma\alpha\left(a_{11} + a_{22} + a_{33}\right) - \frac{t'_{11} + t'_{22} + t'_{33}}{\sqrt{3}\mathbf{t}_S}$$
$$= \gamma\alpha a_{ii} = \gamma\alpha a_i \qquad (S_{ii} = 0 \Rightarrow t'_{ii} = 0)$$

$$t'^{(1)}_{ij} = t^{(1)}_{ij} - t_N{}^{(1)}a_{ij} = \gamma\left\{\alpha a_{ij} - \frac{\mathbf{t}'_{ij}}{\mathbf{t}_S\sqrt{3}}\right\} - \gamma\alpha a_i a_{ij}$$

$$t_s = \sqrt{t'^{(1)}_{ij} : t'^{(1)}_{ij}} = \sqrt{\left(\gamma\left\{\alpha a_{ij} - \frac{\mathbf{t}'_{ij}}{\mathbf{t}_S\sqrt{3}}\right\} - \gamma\alpha a_i a_{ij}\right) : \left(\gamma\left\{\alpha a_{ij} - \frac{\mathbf{t}'_{ij}}{\mathbf{t}_S\sqrt{3}}\right\} - \gamma\alpha a_i a_{ij}\right)}$$
$$= \gamma\sqrt{\left(\left\{\alpha a_{ij} - \frac{\mathbf{t}'_{ij}}{\mathbf{t}_S\sqrt{3}}\right\} - \alpha a_i a_{ij}\right) : \left(\left\{\alpha a_{ij} - \frac{\mathbf{t}'_{ij}}{\mathbf{t}_S\sqrt{3}}\right\} - \alpha a_i a_{ij}\right)}$$
$$= \gamma\sqrt{\left\{\alpha a_{ij} - \frac{\mathbf{t}'_{ij}}{\mathbf{t}_S\sqrt{3}}\right\} : \left\{\alpha a_{ij} - \frac{\mathbf{t}'_{ij}}{\mathbf{t}_S\sqrt{3}}\right\} - 2\left\{\alpha a_{ij} - \frac{\mathbf{t}'_{ij}}{\mathbf{t}_S\sqrt{3}}\right\} : \left\{\alpha a_i a_{ij}\right\} + \alpha^2\left\{a_i a_{ij} : a_i a_{ij}\right\}}$$

$$\mathrm{t_s} = \gamma\sqrt{\alpha^2 - 0 + \frac{1}{3} - 2\left(\alpha^2 - \frac{\mathbf{t}'_{ij}}{\mathbf{t}_S\sqrt{3}} : \{\alpha a_i a_{ij}\}\right) + \alpha^2\{a_i : a_i\}\{a_{ij} : a_{ij}\}} \tag{7.8}$$

$$= \frac{1}{\sqrt{3}}\gamma$$

$$f(\mathbf{t}) = \alpha(\gamma\alpha a_i) + \frac{1}{\sqrt{3}}\frac{1}{\sqrt{3}}\gamma - k = 0$$

$$\Rightarrow \gamma\left(\alpha^2 a_i - \frac{1}{3}\right) - k = 0$$

$$\Rightarrow \gamma = \frac{k}{\left(\alpha^2 a_i - \frac{1}{3}\right)} \tag{7.9}$$

$$t_{ij}^{(1)} = \gamma\frac{\partial f(\mathbf{t})}{\partial \mathbf{t}} = \frac{k}{\left(\alpha^2 a_i - \frac{1}{3}\right)}\sqrt{\alpha^2 + \frac{1}{3}}\frac{\dot{\bar{\varepsilon}}}{\dot{e}_{SMP}} \tag{7.10}$$

$$\begin{aligned}
\dot{\varepsilon}^{v}_{\mathrm{SMP}} = tr\{\dot{\bar{\varepsilon}}\} &= tr\left\{\Lambda\frac{\partial f(\mathbf{t})}{\partial \mathbf{t}}\right\} = tr\left\{\Lambda\left(\alpha a_{ij} - \frac{\mathbf{t}'_{ij}}{\mathbf{t}_S\sqrt{3}}\right)\right\} \\
&= \Lambda\left\{\alpha a_{11} - \frac{t'_{11}}{\sqrt{3}\mathbf{t}_S}\right\} + \Lambda\left\{\alpha a_{22} - \frac{t'_{22}}{\sqrt{3}\mathbf{t}_S}\right\} + \Lambda\left\{\alpha a_{33} - \frac{t'_{33}}{\sqrt{3}\mathbf{t}_S}\right\} \\
&= \Lambda\alpha(a_{11} + a_{22} + a_{33}) - \frac{t'_{11} + t'_{22} + t'_{33}}{\sqrt{3}\mathbf{t}_S} \\
&= \Lambda\alpha a_{ii} = \Lambda\alpha a_i \qquad (\mathrm{S_{ii}} = 0 \Rightarrow t'_{ii} = 0) \\
&= \frac{\alpha a_{ii}}{\sqrt{\alpha^2 + \frac{1}{3}}}\dot{e}_{SMP}
\end{aligned} \tag{7.11}$$

$$\mathrm{h}(\dot{\varepsilon}_{SMP}) = \dot{\varepsilon}^{v}_{\mathrm{SMP}} - \frac{\alpha a_{ii}}{\sqrt{\alpha^2 + \frac{1}{3}}}\dot{e}_{SMP} = 0 \tag{7.12}$$

$$\frac{\partial h(\dot{\varepsilon}_{vSMP})}{\partial \dot{\varepsilon}_{vSMP}} = \frac{\partial}{\partial \dot{\varepsilon}_{vSMP}}\left(\dot{\varepsilon}^{v}_{SMP} - \frac{\alpha a_{ii}}{\sqrt{\alpha^2 + \frac{1}{3}}}\dot{e}_{\mathrm{SMP}}\right)$$

$$= \frac{\partial \dot{\varepsilon}_{vSMP}}{\partial \dot{\varepsilon}_{vSMP}} - \frac{a_{ii}\alpha}{\sqrt{\alpha^2 + \frac{1}{3}}}\frac{\partial \dot{e}_{\mathrm{SMP}}}{\partial \dot{\varepsilon}_{vSMP}}$$

$$= \frac{\partial \mathrm{tr}\{\dot{\bar{\varepsilon}}\}}{\partial \dot{\boldsymbol{\varepsilon}}_{SMP}} - \frac{a_{ii}\alpha}{\sqrt{\alpha^2 + \frac{1}{3}}}\frac{\partial\left(\dot{\bar{\varepsilon}} : \dot{\bar{\varepsilon}}\right)^{1/2}}{\partial \dot{\boldsymbol{\varepsilon}}_{SMP}}$$

$$\frac{\partial h(\dot{\varepsilon}_{vSMP})}{\partial \dot{\varepsilon}_{vSMP}} = \mathbf{I} - \frac{a_{ii}\alpha}{\sqrt{\alpha^2 + \frac{1}{3}}} \frac{\partial (\dot{\bar{\varepsilon}} : \dot{\bar{\varepsilon}})^{1/2}}{\partial \dot{\boldsymbol{\varepsilon}}_{SMP}}$$

$$= \mathbf{I} - \frac{a_{ii}\alpha}{\sqrt{\alpha^2 + \frac{1}{3}}} \frac{\dot{\bar{\varepsilon}}}{\dot{e}_{SMP}}$$

$$\frac{\partial (\dot{\bar{\varepsilon}} : \dot{\bar{\varepsilon}})^{1/2}}{\partial \dot{\bar{\varepsilon}}} = \frac{1}{2\sqrt{\dot{\bar{\varepsilon}} : \dot{\bar{\varepsilon}}}} \frac{\partial (\dot{\bar{\varepsilon}} : \dot{\bar{\varepsilon}})}{\partial \dot{\bar{\varepsilon}}}$$

✧ $$= \frac{1}{2\sqrt{\dot{\bar{\varepsilon}} : \dot{\bar{\varepsilon}}}} \left(\frac{\partial (\dot{\bar{\varepsilon}})}{\partial \dot{\bar{\varepsilon}}} : \dot{\bar{\varepsilon}} + \dot{\bar{\varepsilon}} : \frac{\partial (\dot{\bar{\varepsilon}})}{\partial \dot{\bar{\varepsilon}}} \right) = \frac{1}{\sqrt{\dot{\bar{\varepsilon}} : \dot{\bar{\varepsilon}}}} \left(\frac{\partial (\dot{\bar{\varepsilon}})}{\partial \dot{\bar{\varepsilon}}} : \dot{\bar{\varepsilon}} \right)$$

$$= \frac{1}{\dot{e}_{SMP}} \dot{\bar{\varepsilon}}$$

$$t_{ij}^{(2)} = \beta \frac{\partial h(\dot{\bar{\varepsilon}})}{\partial \dot{\bar{\varepsilon}}} = \beta \left(\mathbf{I} - \frac{a_{ii}\alpha}{\sqrt{\alpha^2 + \frac{1}{3}}} \frac{\dot{\bar{\varepsilon}}}{\dot{e}_{SMP}} \right) \tag{7.13}$$

$$t_{ij} = t_{ij}^{(1)} + t_{ij}^{(2)} = \frac{k}{\left(\alpha^2 a_i - \frac{1}{3} \right)} \sqrt{\alpha^2 + \frac{1}{3}} \frac{\dot{\bar{\varepsilon}}}{\dot{e}_{SMP}} + \beta \left(\mathbf{I} - \frac{a_i \alpha}{\sqrt{\alpha^2 + \frac{1}{3}}} \frac{\dot{\bar{\varepsilon}}}{\dot{e}_{SMP}} \right)$$

$$t_{ij} = t_{ij}^{(1)} + t_{ij}^{(2)} = \frac{k}{\left(\alpha^2 a_i - \frac{1}{3} \right)} \sqrt{\alpha^2 + \frac{1}{3}} \frac{\dot{\bar{\varepsilon}}}{\dot{e}_{SMP}} + \beta \left(\mathbf{I} - \frac{a_i \alpha}{\sqrt{\alpha^2 + \frac{1}{3}}} \frac{\dot{\bar{\varepsilon}}}{\dot{e}_{SMP}} \right) \tag{7.14}$$

$$= \frac{k}{\left(\alpha^2 a_i - \frac{1}{3} \right)} \sqrt{\alpha^2 + \frac{1}{3}} \frac{\dot{\bar{\varepsilon}}}{\dot{e}_{SMP}} + \kappa \left(\dot{\boldsymbol{\varepsilon}}_{ij}^{v} - \eta \dot{e} \right) \left(\mathbf{I} - \frac{a_i \alpha}{\sqrt{\alpha^2 + \frac{1}{3}}} \frac{\dot{\bar{\varepsilon}}}{\dot{e}_{SMP}} \right)$$

$$= \gamma \frac{\dot{\bar{\varepsilon}}}{\dot{e}_{SMP}} + \kappa \left(\dot{\boldsymbol{\varepsilon}}_{SMP}^{v} - \eta \dot{e}_{SMP} \right) \left(\mathbf{I} - \eta \frac{\dot{\bar{\varepsilon}}}{\dot{e}_{SMP}} \right)$$

$$t_{ij} = t_{ij}^{(1)} + t_{ij}^{(2)} = \gamma \frac{\dot{\bar{\varepsilon}}}{\dot{e}_{SMP}} + \kappa \left(\dot{\boldsymbol{\varepsilon}}_{SMP}^{v} - \eta \dot{e} \right) \left(\mathbf{I} - \eta \frac{\dot{\bar{\varepsilon}}}{\dot{e}_{SMP}} \right)$$

$$= \gamma \frac{\mathbf{Q}}{\dot{e}_{SMP}} \dot{\bar{\varepsilon}} + \kappa \left(\mathbf{m} : \dot{\bar{\varepsilon}} - \eta \frac{\mathbf{Q}\dot{\bar{\varepsilon}} : \dot{\bar{\varepsilon}}}{\dot{e}_{SMP}} \right) \left(\mathbf{m} - \eta \frac{\mathbf{Q}\dot{\bar{\varepsilon}}}{\dot{e}_{SMP}} \right)$$

$$\begin{aligned} \mathrm{t}_{ij} = \mathrm{t}_{ij}^{(1)} + \mathrm{t}_{ij}^{(2)} \quad &= \gamma \frac{\mathbf{Q}}{\dot{\mathrm{e}}_{\mathrm{SMP}}} \dot{\bar{\varepsilon}} + \kappa \left(\mathbf{m}^{\mathbf{T}} \dot{\bar{\varepsilon}} - \eta \frac{\dot{\bar{\varepsilon}}^{\mathrm{T}} \mathbf{Q}^{\mathbf{T}} \dot{\bar{\varepsilon}}}{\dot{\mathrm{e}}_{\mathrm{SMP}}} \right) \left(\mathbf{m} - \eta \frac{\mathbf{Q} \dot{\bar{\varepsilon}}}{\dot{\mathrm{e}}_{\mathrm{SMP}}} \right) \\ &= \left[\gamma \frac{\mathbf{Q}}{\dot{\mathrm{e}}_{\mathrm{SMP}}} + \kappa \left(\mathbf{m} - \eta \frac{\mathbf{Q}}{\dot{\mathrm{e}}_{\mathrm{SMP}}} \right) \left(\mathbf{m}^{\mathbf{T}} - \eta \frac{\dot{\varepsilon}_{ij}^{\mathrm{T}} \mathbf{Q}^{\mathbf{T}}}{\dot{\mathrm{e}}_{\mathrm{SMP}}} \right) \right] \dot{\bar{\varepsilon}} \\ &= D^{p} \dot{\bar{\varepsilon}} \end{aligned} \tag{7.15}$$

On the other hand:

$$\begin{aligned} \sigma_{ij} = a_{ij}^{-1} t_{ij} = a_{ij}^{-1} &\left[\gamma \frac{\mathbf{Q}}{\dot{e}_{SMP}} + \kappa \left(\mathbf{m} - \eta \frac{\mathbf{Q}}{\dot{e}_{SMP}} \right) \left(\mathbf{m}^{\mathbf{T}} - \eta \frac{\dot{\varepsilon}_{ij}^{T} \mathbf{Q}^{\mathbf{T}}}{\dot{e}_{SMP}} \right) \right] \dot{\bar{\varepsilon}} \\ &= a_{ij}^{-1} \mathrm{D}^{\mathrm{p}} \dot{\bar{\varepsilon}} \end{aligned} \tag{7.16}$$

Relationship between $\dot{\bar{\varepsilon}}_{\mathrm{ij}} (in\, t_{ij} \text{ space}) \text{and} \, \dot{\varepsilon}_{ij}$ $(in\, \sigma_{ij}$ space)

$$\begin{aligned} & W = \sigma_{ij} \dot{\varepsilon}_{\mathrm{ij}} = t_{ij} \dot{\bar{\varepsilon}}_{\mathrm{ij}} = a_{ik} \sigma_{kj} \dot{\bar{\varepsilon}}_{\mathrm{ij}} = a_{ki} \sigma_{ij} \dot{\bar{\varepsilon}}_{\mathrm{kj}} = \sigma_{ij} a_{ki} \dot{\bar{\varepsilon}}_{\mathrm{kj}} \\ & \Rightarrow \dot{\varepsilon}_{\mathrm{ij}} = a_{ki} \dot{\bar{\varepsilon}}_{\mathrm{kj}} \\ & \Rightarrow \dot{\varepsilon} = a^{T} \dot{\bar{\varepsilon}}_{\mathrm{kj}} \\ & \Rightarrow \dot{\bar{\varepsilon}} = a^{-T} \dot{\varepsilon} \end{aligned} \tag{7.17}$$

We can check：

$$\begin{aligned} W = t_{ij} \dot{\bar{\varepsilon}}_{\mathrm{ij}} &= \left(a_{ik} \sigma_{kj} \right) \left(a^{-T} \dot{\varepsilon} \right) = tr\left(\sigma^{T} a^{T} a^{-T} \dot{\varepsilon} \right) \\ &= tr\left(\sigma^{T} \dot{\varepsilon} \right) \\ &= \sigma : \dot{\varepsilon} \end{aligned}$$

$$\Rightarrow \dot{\bar{\varepsilon}} = a^{-T} \dot{\varepsilon} \tag{7.18}$$

Equilibrium equation:

$$\int_{V} \boldsymbol{\sigma} : \delta \boldsymbol{\varepsilon} dV = \rho \int_{S_\sigma} \mathbf{T} \cdot \delta \mathbf{u} dS + \int_{V} \mathbf{X} \cdot \delta \mathbf{u} dV \tag{7.19}$$

Constraint condition： $\int_{S_\sigma} \mathbf{T} \cdot \dot{\mathbf{u}} dS = 1$

The load factor ρ instead incorporate to constraint condition by using penalty method:

$$\rho = -\mu \left(\int_{S_\sigma} \mathbf{T} \cdot \dot{\mathbf{u}} dS - 1 \right) \tag{7.20}$$

So we have:

$$\int_{V} \boldsymbol{\sigma} : \delta \boldsymbol{\varepsilon} dV = -\mu \left(\int_{S_\sigma} \mathbf{T} \cdot \dot{\mathbf{u}} dS - 1 \right) \int_{S_\sigma} \mathbf{T} \cdot \delta \mathbf{u} dS + \int_{V} \mathbf{X} \cdot \delta \mathbf{u} dV \tag{7.21}$$

$\int \sigma : \delta \bar{\varepsilon} dv = \int \left(a_{ij}^{-1} \mathbf{D} \dot{\bar{\varepsilon}} dv \right) : \left(\mathbf{B} \delta \dot{\mathbf{U}} \right) dv = \left(\mathbf{B} \delta \dot{\mathbf{U}} \right)^{T} \int a_{ij}^{-1} \mathbf{D} \dot{\bar{\varepsilon}} dv = \delta \dot{\mathbf{U}}^{T} \int \mathbf{B}^{T} a_{ij}^{-1} \mathbf{D} \dot{\bar{\varepsilon}} dv = \delta \dot{\mathbf{U}}^{T} \int \mathbf{B}^{T} a_{ij}^{-1} \mathbf{D} \dot{\bar{\varepsilon}} dv$

$$-\mu\left(\int_{S_\sigma}\mathbf{T}\cdot\dot{\mathbf{u}}dS-1\right)\int_{S_\sigma}\mathbf{T}\cdot\delta\dot{\mathbf{u}}dS+\int_V\mathbf{X}\cdot\delta\dot{\mathbf{u}}dV=-\mu\left(\int_{S_\sigma}(\mathbf{NT})\cdot(\mathbf{N}\dot{\mathbf{U}})dS-1\right)\int_{S_\sigma}(\mathbf{NT})\cdot(\mathbf{N}\delta\dot{\mathbf{U}})dS$$
$$+\int_V(\mathbf{NX})\cdot(\mathbf{N}\delta\dot{\mathbf{U}})dV$$
$$=-\mu\left(\int_{S_\sigma}(\mathbf{NT})^{\mathrm{T}}(\mathbf{N}\dot{\mathbf{U}})dS-1\right)\int_{S_\sigma}(\mathbf{N}\delta\dot{\mathbf{U}})^{\mathrm{T}}(\mathbf{NT})dS+\int_V(\mathbf{N}\delta\dot{\mathbf{U}})^{\mathrm{T}}(\mathbf{NX})dV$$
$$=-\mu\left(\int_{S_\sigma}(\mathbf{T}^{\mathrm{T}}\mathbf{N}^{\mathrm{T}})(\mathbf{N}\dot{\mathbf{U}})dS-1\right)\int_{S_\sigma}(\delta\dot{\mathbf{U}}^{\mathrm{T}}\mathbf{N}^{\mathrm{T}})(\mathbf{N}t)dS+\int_V(\delta\dot{\mathbf{U}}^{\mathrm{T}}\mathbf{N}^{\mathrm{T}})(\mathbf{NX})dV$$
$$=-\delta\dot{\mathbf{U}}^{\mathrm{T}}\mu\left(\int_{S_\sigma}(\mathbf{T}^{\mathrm{T}}\mathbf{N}^{\mathrm{T}}\mathbf{N}\dot{\mathbf{U}})dS-1\right)\int_{S_\sigma}(\mathbf{N}^{\mathrm{T}}\mathbf{NT})dS+\delta\dot{\mathbf{U}}^{\mathrm{T}}\int_V(\mathbf{N}^{\mathrm{T}}\mathbf{NX})dV$$

So we have:

$$\Rightarrow\int\mathbf{B}^T a_{ij}^{-1}\mathbf{D}^{\mathrm{p}}a_{ij}^{-1}\mathbf{B}\dot{\mathbf{U}}dv=-\mu\left(\int_{S_\sigma}(\mathbf{T}^{\mathrm{T}}\mathbf{N}^{\mathrm{T}}\mathbf{N}\dot{\mathbf{U}})dS-1\right)\int_{S_\sigma}(\mathbf{N}^{\mathrm{T}}\mathbf{N}^{\mathrm{T}})dS+\delta\dot{\mathbf{U}}^{\mathrm{T}}\int_V(\mathbf{N}^{\mathrm{T}}\mathbf{NX})dV$$

$$\Rightarrow\int\mathbf{B}^T a_{ij}^{-1}\mathbf{D}^{\mathrm{p}}a_{ij}^{-1}\mathbf{B}\dot{\mathbf{U}}dv=-\mu\left(\int_{S_\sigma}(\mathbf{T}^{\mathrm{T}}\mathbf{N}^{\mathrm{T}}\mathbf{N}\dot{\mathbf{U}})dS-1\right)\int_{S_\sigma}(\mathbf{N}^{\mathrm{T}}\mathbf{N}^{\mathrm{T}})dS+\delta\dot{\mathbf{U}}^{\mathrm{T}}\int_V(\mathbf{N}^{\mathrm{T}}\mathbf{NX})dV \qquad (7.22)$$

Here, replace as below to above part of governing equation.

$$\int_V\mathbf{B}^T a_{ij}^{-1}\mathbf{D}^{\mathrm{p}}a_{ij}^{-1}\mathbf{B}dv\dot{\mathbf{U}}=K\dot{\mathbf{U}}$$

$$\int_{S_\sigma}(\mathbf{N}^{\mathrm{T}}\mathbf{NT})dS=F$$

$$\int_V(\mathbf{N}^{\mathrm{T}}\mathbf{NX})dV=X$$

Therefore,

$$\int\mathbf{B}^T a_{ij}^{-1}\mathbf{D}^{\mathrm{p}}a_{ij}^{-1}\mathbf{B}\dot{\mathbf{U}}dv=-\mu\left(\int_{S_\sigma}(\mathbf{T}^{\mathrm{T}}\mathbf{N}^{\mathrm{T}}\mathbf{N}\dot{\mathbf{U}})dS-1\right)\int_{S_\sigma}(\mathbf{N}^{\mathrm{T}}\mathbf{N}^{\mathrm{T}})dS+\delta\dot{\mathbf{U}}^{\mathrm{T}}\int_V(\mathbf{N}^{\mathrm{T}}\mathbf{NX})dV$$

$$\Rightarrow\mathrm{K}\dot{\mathbf{U}}=-\mu(\mathrm{F}^{\mathrm{T}}\dot{\mathbf{U}}-1)\mathrm{F}+\mathrm{X}$$
$$\Rightarrow\mathrm{K}\dot{\mathbf{U}}+\mu\mathrm{F}(\mathrm{F}^{\mathrm{T}}\dot{\mathbf{U}}-1)=\mathrm{X}$$
$$\Rightarrow\mathrm{K}\dot{\mathbf{U}}+(\mu\mathrm{F}\mathrm{F}^{\mathrm{T}}\dot{\mathbf{U}}-\mu\mathrm{F})=\mathrm{X}$$
$$\Rightarrow\mathrm{K}\dot{\mathbf{U}}+\mu\mathrm{F}\mathrm{F}^{\mathrm{T}}\dot{\mathbf{U}}=\mu\mathrm{F}+\mathrm{X}$$
$$\Rightarrow(\mathrm{K}+\mu\mathrm{F}\mathrm{F}^{\mathrm{T}})\dot{\mathbf{U}}=\mu\mathrm{F}+\mathrm{X} \qquad (7.23)$$
$$\Rightarrow\overline{\mathrm{K}}\dot{\mathbf{U}}=\mu\mathrm{F}+\mathrm{X}$$

Here, $\overline{\mathrm{K}}$ is all stiffness matrix.

B. Hibino - Hayashi yield function

$$f(\mathbf{t})=\alpha t_N-(t_s)^n+k=0 \qquad (7.24)$$

$$\Rightarrow t_s = \left(\alpha t_N + k\right)^{\frac{1}{n}} \qquad \text{or} \qquad f(\mathbf{t}) = \left(\alpha t_N + k\right)^{\frac{1}{n}} - t_s = 0 \tag{7.25}$$

$$\dot{\varepsilon}_{SMP} = \Lambda \frac{\partial f(\mathbf{t})}{\partial \mathbf{t}} = \Lambda \left(\frac{\partial f(\mathbf{t})}{\partial t_N} \frac{\partial t_N}{\partial \mathbf{t}_{ij}} + \frac{\partial f(\mathbf{t})}{\partial t_S} \frac{\partial t_S}{\partial \mathbf{t}_{ij}} \right) \tag{7.26}$$

- $\dfrac{\partial f(\mathbf{t})}{\partial \mathbf{t}_N} = \dfrac{1}{n} \alpha \left(\alpha t_N + k\right)^{\frac{1-n}{n}}$
- $\dfrac{\partial \mathbf{t}_N}{\partial \mathbf{t}_{ij}} = \dfrac{\partial \left(\mathbf{t}_{kl} a_{kl}\right)}{\partial \mathbf{t}_{ij}} = a_{ij}$
- $\dfrac{\partial f(\mathbf{t})}{\partial \mathbf{t}_S} = -1$
- $\dfrac{\partial \mathbf{t}_S}{\partial \mathbf{t}_{kl}} = \dfrac{\partial \mathbf{t}_S}{\partial \mathbf{t}'_{ij}} . \dfrac{\partial \mathbf{t}'_{ij}}{\partial \mathbf{t}_{kl}}$

$$\frac{\partial \mathbf{t}_S}{\partial \mathbf{t}'_{kl}} = \frac{1}{2\sqrt{\mathbf{t}'_{kl}\mathbf{t}'_{kl}}} 2\mathbf{t}'_{ikl} = \frac{\mathbf{t}'_{kl}}{\sqrt{\mathbf{t}'_{ij}\mathbf{t}'_{ij}}} = \frac{\mathbf{t}_{kl} - t_N a_{kl}}{\mathbf{t}_S}$$

$$\frac{\partial \mathbf{t}'_{kl}}{\partial \mathbf{t}_{ij}} = \frac{\partial}{\partial \mathbf{t}_{ij}} \left(\mathbf{t}_{kl} - t_N a_{kl}\right) = \frac{\partial \mathbf{t}_{ikl}}{\partial \mathbf{t}_{ij}} - \frac{\partial \left(t_N a_{kl}\right)}{\partial \mathbf{t}_{ij}} = \delta_{ik}\delta_{jl} - \frac{\partial t_N}{\partial \mathbf{t}_{ij}} a_{kl} = \delta_{ik}\delta_{jl} - a_{ij}a_{kl} \tag{7.27}$$

$$\dot{\bar{\varepsilon}} = \Lambda \frac{\partial \mathrm{f}(\mathbf{t})}{\partial \mathbf{t}} = \Lambda \left(\frac{1}{\mathrm{n}} \alpha \left(\alpha \mathrm{t}_{\mathrm{N}} + \mathrm{k}\right)^{\frac{1-\mathrm{n}}{\mathrm{n}}} \mathrm{a}_{\mathrm{ij}} - 1. \frac{\mathbf{t}_{\mathrm{kl}} - \mathrm{t}_{\mathrm{N}} \mathrm{a}_{\mathrm{kl}}}{\mathbf{t}_{\mathrm{S}}} \left(\delta_{\mathrm{ik}} \delta_{\mathrm{jl}} - \mathrm{a}_{\mathrm{ij}} \mathrm{a}_{\mathrm{kl}}\right) \right)$$

$$= \Lambda \left(\frac{1}{\mathrm{n}} \alpha \left(\alpha \mathrm{t}_{\mathrm{N}} + \mathrm{k}\right)^{\frac{1-\mathrm{n}}{\mathrm{n}}} \mathrm{a}_{\mathrm{ij}} - \frac{1}{\mathbf{t}_{\mathrm{S}}} \left(\mathbf{t}_{\mathrm{kl}} \delta_{\mathrm{ik}} \delta_{\mathrm{jl}} - \mathbf{t}_{\mathrm{kl}} \mathrm{a}_{\mathrm{ij}} \mathrm{a}_{\mathrm{kl}} - \mathrm{t}_{\mathrm{N}} \mathrm{a}_{\mathrm{kl}} \delta_{\mathrm{ik}} \delta_{\mathrm{jl}} + \mathrm{t}_{\mathrm{N}} \mathrm{a}_{\mathrm{kl}} \mathrm{a}_{\mathrm{ij}} \mathrm{a}_{\mathrm{kl}} \right) \right)$$

$$\dot{\bar{\varepsilon}} = \Lambda \left(\frac{1}{\mathrm{n}} \alpha \left(\alpha \mathrm{t}_{\mathrm{N}} + \mathrm{k}\right)^{\frac{1-\mathrm{n}}{\mathrm{n}}} \mathrm{a}_{\mathrm{ij}} - \frac{1}{\mathbf{t}_{\mathrm{S}}} \left(\mathbf{t}_{\mathrm{ij}} - \mathbf{t}_{\mathrm{N}} \mathrm{a}_{\mathrm{ij}} - \mathrm{t}_{\mathrm{N}} \mathrm{a}_{\mathrm{ij}} + \mathrm{t}_{\mathrm{N}} \mathrm{a}_{\mathrm{ij}} \mathrm{a}_{\mathrm{kl}} \mathrm{a}_{\mathrm{kl}} \right) \right)$$

$$= \Lambda \left(\frac{1}{\mathrm{n}} \alpha \left(\alpha \mathrm{t}_{\mathrm{N}} + \mathrm{k}\right)^{\frac{1-\mathrm{n}}{\mathrm{n}}} \mathrm{a}_{\mathrm{ij}} - \frac{1}{\mathbf{t}_{\mathrm{S}}} \left(\mathbf{t}_{\mathrm{ij}} - \mathrm{t}_{\mathrm{N}} \mathrm{a}_{\mathrm{ij}} \mathrm{a}_{\mathrm{kl}} \mathrm{a}_{\mathrm{kl}} \right) \right)$$

$$\dot{\bar{\varepsilon}} = \Lambda \frac{\partial f(\mathbf{t})}{\partial \mathbf{t}} = \Lambda \left(\frac{1}{n} \alpha \left(\alpha \mathbf{t}_N + k\right)^{\frac{1-n}{n}} a_{ij} - \frac{t'_{ij}}{\mathbf{t}_S} \right) \tag{7.28}$$

We have:

$$a_{11} = \frac{a_1 + a_2}{2} + \frac{a_1 - a_2}{2} \cos 2\alpha$$

$$a_{22} = \frac{a_1 + a_2}{2} - \frac{a_1 - a_2}{2} \cos 2\alpha$$

$$a_{33} = a_3$$

$$a_{12} = a_{21} = \frac{a_1 - a_2}{2} \sin 2\alpha$$

$$a_{23} = a_{13} = 0$$

$$a_1^2 + a_2^2 + a_3^2 = 1$$

Therefore

$$\begin{aligned} a_{kl}a_{kl} = a_{ll}a_{ll} &= a_{11}a_{11} + a_{21}a_{21} + a_{31}a_{31} + a_{12}a_{12} + a_{22}a_{22} + a_{32}a_{32} + a_{13}a_{13} + a_{23}a_{23} + a_{33}a_{33} \\ &= a_{11}a_{11} + a_{22}a_{22} + a_{33}a_{33} + 2a_{12}a_{12} \\ &= \left(\frac{a_1 + a_2}{2} + \frac{a_1 - a_2}{2}\cos 2\alpha\right)^2 + \left(\frac{a_1 + a_2}{2} - \frac{a_1 - a_2}{2}\cos 2\alpha\right)^2 + a_3^2 + 2\left(\frac{a_1 - a_2}{2}\sin 2\alpha\right)^2 \\ &= a_1^2 + a_2^2 + a_3^2 = 1 \end{aligned}$$

$$\Rightarrow \dot{\bar{\varepsilon}} = \Lambda\frac{\partial f(\mathbf{t})}{\partial \mathbf{t}} = \Lambda\left(\frac{1}{n}\alpha(\alpha t_N + k)^{\frac{1-n}{n}} a_{ij} - \frac{1}{\mathbf{t}_S}\left(\mathbf{t}_{ij} - t_N a_{ij}\right)\right) = \Lambda\left(\frac{1}{n}\alpha(\alpha t_N + k)^{\frac{1-n}{n}} a_{ij} - \frac{\mathbf{t}'_{ij}}{\mathbf{t}_S}\right) \tag{7.29}$$

$$\bar{\dot{e}} = \sqrt{\dot{\bar{\varepsilon}} : \dot{\bar{\varepsilon}}} = \sqrt{\Lambda\left(\frac{1}{n}\alpha(\alpha\mathbf{t}_N + k)^{\frac{1-n}{n}} a_{ij} - \frac{t'_{ij}}{\mathbf{t}_S}\right) : \Lambda\left(\frac{1}{n}\alpha(\alpha\mathbf{t}_N + k)^{\frac{1-n}{n}} a_{ij} - \frac{t'_{ij}}{\mathbf{t}_S}\right)}$$

$$= \Lambda\sqrt{\left(\frac{1}{n}\alpha(\alpha\mathbf{t}_N + k)^{\frac{1-n}{n}} a_{ij} - \frac{t'_{ij}}{\mathbf{t}_S}\right) : \left(\frac{1}{n}\alpha(\alpha\mathbf{t}_N + k)^{\frac{1-n}{n}} a_{ij} - \frac{t'_{ij}}{\mathbf{t}_S}\right)}$$

$$= \Lambda\sqrt{\frac{\alpha^2}{n^2}(\alpha\mathbf{t}_N + k)^{\frac{2-2n}{n}} + \frac{t'_{ij} : t'_{ij}}{\mathbf{t}_s^2}} = \Lambda\sqrt{\frac{\alpha^2}{n^2}(\alpha\mathbf{t}_N + k)^{\frac{2-2n}{n}} + 1}$$

$$\Rightarrow \Lambda = \frac{\bar{\dot{e}}}{\sqrt{\frac{\alpha^2}{n^2}(\alpha\mathbf{t}_N + k)^{\frac{2-2n}{n}} + 1}} \tag{7.30}$$

$$\Rightarrow \dot{\bar{\varepsilon}} = \Lambda\left(\frac{1}{n}\alpha(\alpha t_N + k)^{\frac{1-n}{n}} a_{ij} - \frac{\mathbf{t}'_{ij}}{\mathbf{t}_S}\right) = \frac{\bar{\dot{e}}}{\sqrt{\frac{\alpha^2}{n^2}(\alpha\mathbf{t}_N + k)^{\frac{2-2n}{n}} + 1}}\left(\frac{1}{n}\alpha(\alpha t_N + k)^{\frac{1-n}{n}} a_{ij} - \frac{\mathbf{t}'_{ij}}{\mathbf{t}_S}\right) \tag{7.31}$$

Where $\bar{\dot{e}}$ is called the equivalent strain rate and defined by: $\bar{\dot{e}} = \dot{\bar{\varepsilon}}\dot{\bar{\varepsilon}}$

$$\begin{aligned} I_1 = t_N = \mathrm{tr}\left\{\gamma\frac{\partial f(\mathbf{t})}{\partial \mathbf{t}}\right\} &= \mathrm{tr}\left\{\gamma\left\{\frac{1}{n}\alpha(\alpha\mathbf{t}_N + k)^{\frac{1-n}{n}} a_{ij} - \frac{t'_{ij}}{\mathbf{t}_S}\right\}\right\} \\ &= \gamma\left\{\frac{1}{n}\alpha(\alpha\mathbf{t}_N + k)^{\frac{1-n}{n}} a_{11} - \frac{t'_{11}}{\mathbf{t}_S}\right\} + \gamma\left\{\frac{1}{n}\alpha(\alpha\mathbf{t}_N + k)^{\frac{1-n}{n}} a_{22} - \frac{t'_{22}}{\mathbf{t}_S}\right\} + \gamma\left\{\frac{1}{n}\alpha(\alpha\mathbf{t}_N + k)^{\frac{1-n}{n}} a_{33} - \frac{t'_{33}}{\mathbf{t}_S}\right\} \\ &= \gamma\frac{1}{n}\alpha(\alpha\mathbf{t}_N + k)^{\frac{1-n}{n}}(a_{11} + a_{22} + a_{33}) + \frac{1}{\sqrt{3}}\frac{t'_{11} + t'_{22} + t'_{33}}{\mathbf{t}_S} \\ &= \frac{\gamma\alpha}{n}(\alpha\mathbf{t}_N + k)^{\frac{1-n}{n}} a \qquad (S_{ii} = 0 \Rightarrow t'_{ii} = 0) \end{aligned}$$

(7.32)

$$t'_{ij} = t_{ij} - \mathbf{t}_N a_{ij} = \gamma\left\{\frac{1}{n}\alpha(\alpha\mathbf{t}_N + k)^{\frac{1-n}{n}} a_{ij} - \frac{t'_{ij}}{\mathbf{t}_S}\right\} - \frac{\gamma\alpha}{n}(\alpha\mathbf{t}_N + k)^{\frac{1-n}{n}} a \tag{7.33}$$

$$\begin{aligned} t_s = \sqrt{t'_{ij} : t'_{ij}} &= \sqrt{\left(\gamma\left\{\frac{1}{n}\alpha(\alpha\mathbf{t}_N + k)^{\frac{1-n}{n}} a_{ij} - \frac{t'_{ij}}{\mathbf{t}_S}\right\} - \frac{\gamma\alpha}{n}(\alpha\mathbf{t}_N + k)^{\frac{1-n}{n}} a\right) : \left(\gamma\left\{\frac{1}{n}\alpha(\alpha\mathbf{t}_N + k)^{\frac{1-n}{n}} a_{ij} - \frac{t'_{ij}}{\mathbf{t}_S}\right\} - \frac{\gamma\alpha}{n}(\alpha\mathbf{t}_N + k)^{\frac{1-n}{n}} a\right)} \\ &= \gamma\sqrt{\left(\left\{\frac{1}{n}\alpha(\alpha\mathbf{t}_N + k)^{\frac{1-n}{n}} a_{ij} - \frac{t'_{ij}}{\mathbf{t}_S}\right\} - \frac{\alpha}{n}(\alpha\mathbf{t}_N + k)^{\frac{1-n}{n}} a\right) : \left(\left\{\frac{1}{n}\alpha(\alpha\mathbf{t}_N + k)^{\frac{1-n}{n}} a_{ij} - \frac{t'_{ij}}{\mathbf{t}_S}\right\} - \frac{\alpha}{n}(\alpha\mathbf{t}_N + k)^{\frac{1-n}{n}} a\right)} \\ &= \gamma\sqrt{\left(\begin{array}{l}\left\{\frac{1}{n}\alpha(\alpha\mathbf{t}_N + k)^{\frac{1-n}{n}} a_{ij} - \frac{t'_{ij}}{\mathbf{t}_S}\right\} : \left\{\frac{1}{n}\alpha(\alpha\mathbf{t}_N + k)^{\frac{1-n}{n}} a_{ij} - \frac{t'_{ij}}{\mathbf{t}_S}\right\} - 2\left\{\frac{1}{n}\alpha(\alpha\mathbf{t}_N + k)^{\frac{1-n}{n}} a_{ij} - \frac{t'_{ij}}{\mathbf{t}_S}\right\} : \left(\frac{\alpha}{n}(\alpha\mathbf{t}_N + k)^{\frac{1-n}{n}} a\right) \\ + \frac{\alpha^2}{n^2}(\alpha\mathbf{t}_N + k)^{\frac{2-2n}{n}} (a : a)\end{array}\right)} \end{aligned}$$

$$\begin{aligned} t_s &= \gamma\sqrt{\left(\left\{\frac{\alpha^2}{n^2}(\alpha\mathbf{t}_N + k)^{\frac{2-2n}{n}} + \frac{t'_{ij} : t'_{ij}}{\mathbf{t}_S}\right\} - 2\frac{\alpha^2}{n^2}(\alpha\mathbf{t}_N + k)^{\frac{2-2n}{n}} a_{ij} + \frac{\alpha^2}{n^2}(\alpha\mathbf{t}_N + k)^{\frac{2-2n}{n}}\right)} \\ &= \gamma \end{aligned} \tag{7.34}$$

$$f(\mathbf{t}) = \left(\alpha\frac{\gamma\alpha}{n}(\alpha\mathbf{t}_N + k)^{\frac{1-n}{n}} a + k\right)^{\frac{1}{n}} - \gamma = 0$$

$$\Rightarrow \gamma = \left(\frac{\gamma\alpha^2}{n}(\alpha\mathbf{t}_N + k)^{\frac{1-n}{n}} a + k\right)^{\frac{1}{n}}$$

$$t_{ij} = \gamma\frac{\partial f(\mathbf{t})}{\partial \mathbf{t}} = \left(\frac{\gamma\alpha^2}{n}(\alpha\mathbf{t}_N + k)^{\frac{1-n}{n}} + k\right)^{\frac{1}{n}} \sqrt{\frac{\alpha^2}{n^2}(\alpha\mathbf{t}_N + k)^{\frac{2-2n}{n}} + 1}\,\frac{\dot{\bar{\varepsilon}}}{\dot{\bar{e}}} \tag{7.35}$$

$$t_{ij} = \gamma\frac{\dot{\bar{\varepsilon}}}{\dot{\bar{e}}} = \gamma\frac{\mathbf{Q}}{\dot{\bar{e}}}\dot{\bar{\varepsilon}} = D^p\dot{\bar{\varepsilon}} \tag{7.36}$$

On the other hand:

$$\begin{aligned} \sigma_{ij} = a_{ij}^{-1} t_{ij} &= a_{ij}^{-1}\left[\gamma\frac{\mathbf{Q}}{\dot{\bar{e}}}\right]\dot{\bar{\varepsilon}} \\ &= a_{ij}^{-1} D^p\dot{\bar{\varepsilon}} \end{aligned} \tag{7.37}$$

Relationship between $\dot{\bar{\boldsymbol{\varepsilon}}}_{ij}(in\, t_{ij}$ space) and $\dot{\varepsilon}_{ij}$ $(in\, \sigma_{ij}$ space)

$$\begin{aligned} &W = \sigma_{ij}\dot{\boldsymbol{\varepsilon}}_{ij} = t_{ij}\dot{\bar{\boldsymbol{\varepsilon}}}_{ij} = a_{ik}\sigma_{kj}\dot{\bar{\boldsymbol{\varepsilon}}}_{ij} = a_{ki}\sigma_{ij}\dot{\bar{\boldsymbol{\varepsilon}}}_{kj} = \sigma_{ij}a_{ki}\dot{\bar{\boldsymbol{\varepsilon}}}_{kj} \\ &\Rightarrow \dot{\boldsymbol{\varepsilon}}_{ij} = a_{ki}\dot{\bar{\boldsymbol{\varepsilon}}}_{kj} \\ &\Rightarrow \dot{\boldsymbol{\varepsilon}} = a^T\dot{\bar{\boldsymbol{\varepsilon}}}_{kj} \\ &\Rightarrow \dot{\bar{\boldsymbol{\varepsilon}}} = a^{-T}\dot{\boldsymbol{\varepsilon}} \end{aligned} \tag{7.38}$$

We can check：

$$\begin{aligned} W = t_{ij}\bar{\dot{\varepsilon}}_{ij} &= \left(a_{ik}\sigma_{kj}\right)\left(a^{-T}\dot{\varepsilon}\right) = tr\left(\sigma^T a^T a^{-T}\dot{\varepsilon}\right) \\ &= tr\left(\sigma^T\dot{\varepsilon}\right) \\ &= \sigma:\dot{\varepsilon} \end{aligned}$$

$\Rightarrow \bar{\dot{\varepsilon}} = a^{-T}\dot{\varepsilon}$

Equilibrium equation:

$$\int_V \boldsymbol{\sigma}:\delta\bar{\boldsymbol{\varepsilon}}dV = \rho\int_{S_\sigma}\mathbf{T}\cdot\delta\mathbf{u}dS + \int_V \mathbf{X}\cdot\delta\mathbf{u}dV \tag{7.39}$$

Constraint condition： $\int_{S_\sigma}\mathbf{T}\cdot\dot{\mathbf{u}}dS = 1$

The load factor ρ instead incorporate to constraint condition by using penalty method:

$$\rho = -\mu\left(\int_{S_\sigma}\mathbf{T}\cdot\dot{\mathbf{u}}dS - 1\right)$$

So we have:

$$\int_V \boldsymbol{\sigma}:\delta\bar{\boldsymbol{\varepsilon}}dV = -\mu\left(\int_{S_\sigma}\mathbf{T}\cdot\dot{\mathbf{u}}dS - 1\right)\int_{S_\sigma}\mathbf{T}\cdot\delta\dot{\mathbf{u}}dS + \int_V \mathbf{X}\cdot\delta\dot{\mathbf{u}}dV \tag{7.40}$$

$$\int\sigma:\delta\bar{\boldsymbol{\varepsilon}}dv = \int\left(a_{ij}^{-1}\mathbf{D}\bar{\dot{\boldsymbol{\varepsilon}}}dv\right):\left(\mathbf{B}\delta\dot{\mathbf{U}}\right)dv = \left(\mathbf{B}\delta\dot{\mathbf{U}}\right)^T\int a_{ij}^{-1}\mathbf{D}\bar{\dot{\boldsymbol{\varepsilon}}}dv = \delta\dot{\mathbf{U}}^T\int\mathbf{B}^T a_{ij}^{-1}\mathbf{D}\bar{\dot{\boldsymbol{\varepsilon}}}dv = \delta\dot{\mathbf{U}}^T\int\mathbf{B}^T a_{ij}^{-1}\mathbf{D}\bar{\dot{\boldsymbol{\varepsilon}}}dv$$

$$\begin{aligned} -\mu\left(\int_{S_\sigma}\mathbf{T}\cdot\dot{\mathbf{u}}dS - 1\right)\int_{S_\sigma}\mathbf{T}\cdot\delta\dot{\mathbf{u}}dS + \int_V\mathbf{X}\cdot\delta\dot{\mathbf{u}}dV &= -\mu\left(\int_{S_\sigma}(\mathbf{NT})\cdot(\mathbf{N}\dot{\mathbf{U}})dS - 1\right)\int_{S_\sigma}(\mathbf{NT})\cdot(\mathbf{N}\delta\dot{\mathbf{U}})dS \\ &\quad + \int_V(\mathbf{NX})\cdot(\mathbf{N}\delta\dot{\mathbf{U}})dV \\ &= -\mu\left(\int_{S_\sigma}(\mathbf{NT})^T(\mathbf{N}\dot{\mathbf{U}})dS - 1\right)\int_{S_\sigma}(\mathbf{N}\delta\dot{\mathbf{U}})^T(\mathbf{NT})dS + \int_V(\mathbf{N}\delta\dot{\mathbf{U}})^T(\mathbf{NX})dV \\ &= -\mu\left(\int_{S_\sigma}(\mathbf{T}^T\mathbf{N}^T)(\mathbf{N}\dot{\mathbf{U}})dS - 1\right)\int_{S_\sigma}(\delta\dot{\mathbf{U}}^T\mathbf{N}^T)(\mathbf{Nt})dS + \int_V(\delta\dot{\mathbf{U}}^T\mathbf{N}^T)(\mathbf{NX})dV \\ &= -\delta\dot{\mathbf{U}}^T\mu\left(\int_{S_\sigma}(\mathbf{T}^T\mathbf{N}^T\mathbf{N}\dot{\mathbf{U}})dS - 1\right)\int_{S_\sigma}(\mathbf{N}^T\mathbf{NT})dS + \delta\dot{\mathbf{U}}^T\int_V(\mathbf{N}^T\mathbf{NX})dV \end{aligned}$$

So we have:

$$\Rightarrow\int\mathbf{B}^T a_{ij}^{-1}\mathbf{D}^p a_{ij}^{-1}\mathbf{B}\dot{\mathbf{U}}dv = -\mu\left(\int_{S_\sigma}(\mathbf{T}^T\mathbf{N}^T\mathbf{N}\dot{\mathbf{U}})dS - 1\right)\int_{S_\sigma}(\mathbf{N}^T\mathbf{N}^T)dS + \delta\dot{\mathbf{U}}^T\int_V(\mathbf{N}^T\mathbf{N}X)dV$$

$$\Rightarrow\int\mathbf{B}^T a_{ij}^{-1}\mathbf{D}^p a_{ij}^{-1}\mathbf{B}\dot{\mathbf{U}}dv = -\mu\left(\int_{S_\sigma}(\mathbf{T}^T\mathbf{N}^T\mathbf{N}\dot{\mathbf{U}})dS - 1\right)\int_{S_\sigma}(\mathbf{N}^T\mathbf{N}^T)dS + \delta\dot{\mathbf{U}}^T\int_V(\mathbf{N}^T\mathbf{N}X)dV$$

Here, replace as below to above part of governing equation.

$$\int_V\mathbf{B}^T a_{ij}^{-1}\mathbf{D}^p a_{ij}^{-1}\mathbf{B}dv\dot{\mathbf{U}} = K\dot{\mathbf{U}} \tag{7.41}$$

$$\int_{S_\sigma} \left(\mathbf{N}^{\mathrm{T}}\mathbf{N}\mathbf{T}\right)dS = F \tag{7.42}$$

$$\int_{V} \left(\mathbf{N}^{\mathrm{T}}\mathbf{N}X\right)dV = X \tag{7.43}$$

Therefore,

$$\int \mathbf{B}^{T} a_{ij}^{-1}\mathbf{D}^{\mathrm{p}} a_{ij}^{-1}\mathbf{B}\dot{\mathbf{U}}dv = -\mu\left(\int_{S_\sigma}\left(\mathbf{T}^{\mathrm{T}}\mathbf{N}^{\mathrm{T}}\mathbf{N}\dot{\mathbf{U}}\right)dS - 1\right)\int_{S_\sigma}\left(\mathbf{N}^{\mathrm{T}}\mathbf{N}^{\mathrm{T}}\right)dS + \delta\dot{\mathbf{U}}^{\mathrm{T}}\int_{V}\left(\mathbf{N}^{\mathrm{T}}\mathbf{N}X\right)dV$$

$$\Rightarrow \mathrm{K}\dot{\mathbf{U}} = -\mu\left(\mathrm{F}^{\mathrm{T}}\dot{\mathbf{U}} - 1\right)\mathrm{F} + \mathrm{X}$$
$$\Rightarrow \mathrm{K}\dot{\mathbf{U}} + \mu\mathrm{F}\left(\mathrm{F}^{\mathrm{T}}\dot{\mathbf{U}} - 1\right) = \mathrm{X}$$
$$\Rightarrow \mathrm{K}\dot{\mathbf{U}} + \left(\mu\mathrm{F}\mathrm{F}^{\mathrm{T}}\dot{\mathbf{U}} - \mu\mathrm{F}\right) = \mathrm{X}$$
$$\Rightarrow \mathrm{K}\dot{\mathbf{U}} + \mu\mathrm{F}\mathrm{F}^{\mathrm{T}}\dot{\mathbf{U}} = \mu\mathrm{F} + \mathrm{X}$$
$$\Rightarrow \left(\mathrm{K} + \mu\mathrm{F}\mathrm{F}^{\mathrm{T}}\right)\dot{\mathbf{U}} = \mu\mathrm{F} + \mathrm{X}$$

$$\Rightarrow \overline{\mathrm{K}}\dot{\mathbf{U}} = \mu\mathrm{F} + \mathrm{X} \tag{7.44}$$

Here, $\overline{K}$ is all stiffness matrix.

7.2.2 Numerical simulation of bearing capacity on sand consider to intermediate stress

- Bearing capacity analysis
- Effect of intermediate stress to bearing capacity of soils.

Figure 7.2 Block Diagram

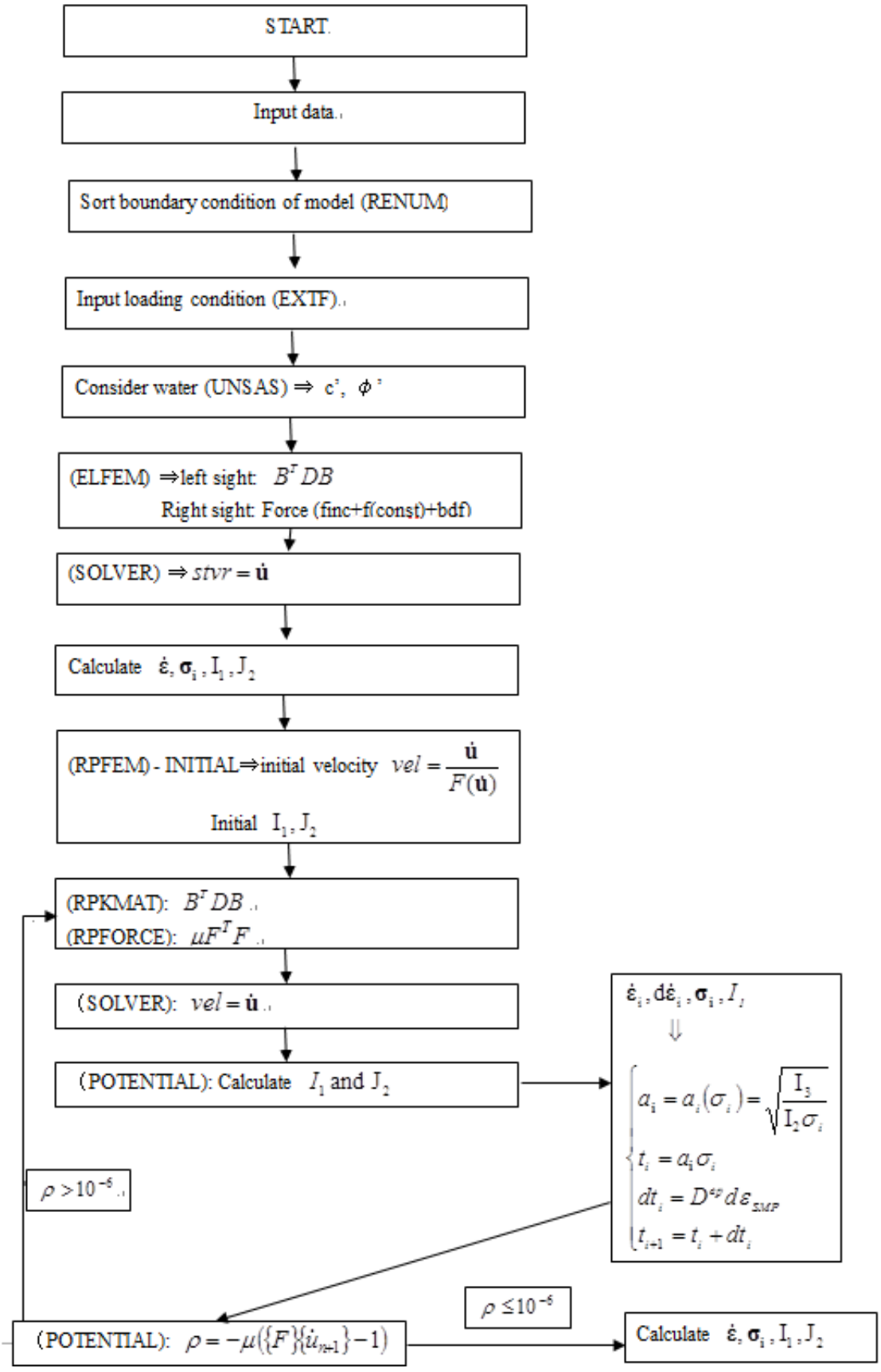

References

[1] AIJ (1988, 2001), Architectural Institute of Japan. Recommendations for design of building foundations, 430p.

[2] Georgiadis M., Butterfield, 1988. Displacements of footings on sand under eccentric and inclined loads", Can. Geotech. J., **25**(2), 199-212.

[3] Hanna A. M., Meyerhof G. G., 1981. Experimental evaluation of bearing capacity of footings subjected to inclined loads, Can. Geotech. J., **18**(4), 599-603.

[4] Houlsby G. T., Cassidy M. J., 2002. A plasticity model for the behavior of footings on sand under combined loading", Géotechnique, **52**(2), 117-129.

[5] Loukidis D., Chakraborty T., Salgado R., 2008. Bearing capacity of strip footings on purely frictional soil under eccentric and inclined loads", Can. Geotech. J., **45**(6), 768-787.

[6] Meyerhof, G. G., 1951. Ultimate bearing capacity of foundations, Geotechnique, **2**(4), 301-332

[7] Meyerhof, G. G., 1963. Some recent research on the ultimate bearing capacity of foundations", Can. Geotech. J., **1**(1), 243-256

[8] Matsuoka, H., 1974. Stress-strain relationship of sand based on the mobilized plane", Soils Found., **14**(2), 47-61.

[9] Mohammed Hjiaj, Andrei V. Lyamin, Scott W. Sloan, 2004. Bearing capacity of a cohesive-frictional soil under non-eccentric inclined loading, Computers and Geotechnics, **31**(6), 491-516.

[10] Nakai, T., 1989. An isotropic hardening elastoplastic model for sand considering the stress path dependency in three-dimensional stresses, Soils Found., **29**(1), 119-137.

[11] Takeshi Hoshina, Satoru Ohtsuka and Koichi Isobe, 2011. Ultimate bearing capacity of ground by Rigid plastic finite element method taking account of stress dependent non-linear strength property, J. Appl. Mech. **6**, 191–200 (in Japanese).

[12] Tamura, T., 1990. Rigid-plastic finite element method in geotechnical engineering. Soc. Mater. Sci., Jpn. 7, 135–164.

LIST OF PUBLICATIONS

Journal Papers

1. Ultimate bearing capacity analysis of ground against inclined load by taking account of nonlinear property of shear strength

Nguyen Le Du, Ohtsuka Satoru, Takashi Hoshina, Koichi Isobe. and Kazuhiro Kaneda

Int. J. GEOMATE **5**(2), 2013, 678-684.

2. Discussion on size effect of footing in ultimate bearing capacity of sandy soil using rigid plastic finite element method

Nguyen Le Du, Ohtsuka Satoru, Takashi Hoshina, and Koichi Isobe

Soils Found. **56** (1), 2016. (In press)

3. Ultimate bearing capacity of footing on sandy soil against combined load of vertical, horizontal and moment loads

Nguyen Le Du, Ohtsuka Satoru, and Kazuhiro Kaneda

Int. J. GEOMATE **10**(1), 2016, 1649-1655. (In press)

Conference Papers

1. Size effect of footing on the ultimate bearing capacity by considering the non-linear strength property of the ground.

Asazuma R., Nguyen Le Du, Hoshina Takashi, Ohtsuka Satoru, Isobe Koichi

Japan Society of Civil Engineers 41th Conference of Kanto Branch

Tokyo, Japan, March, 2014

2. Ultimate bearing capacity of spread foundation on sandy soils for inclined load by rigid plastic FEM

Kaneda Kazuhiro, Aoki Masamichi, Ohtsuka Satoru, Nguyen Le Du

The Proceedings of Computational Engineering Conference of JSCES, Vol. 20.

Tokyo, Japan, June, 2015

3. Ultimate bearing capacity of spread foundation on sandy soils for inclined and eccentric load by RPFEM

Kaneda Kazuhiro, Aoki Masamichi, Ohtsuka Satoru, Nguyen Le Du

Proceedings of the 12th Symposium of Kanto branch of The Japanese Geotechnical Society

Tokyo, Japan, October, 2015